The Deformation of Metallic Surfaces by Abrasion.

By

R.P.Agarwala, M.Sc.

A Thesis submitted
for the Degree of
Doctor of Philosophy
in the
University of London.

Applied Physical Chemistry Laboratories,
Imperial College of Science and Technology,
London, S.W.7.

November, 1953.

Contents.

Introduction.

Many investigations have been made on the nature of wear and lubrication of bearings in machines and of metallic surfaces in general. Although the technical literature contains descriptions of many experiments on wear, they were until recently in almost all cases made on materials which, though of industrial importance, were often of a complicated and uncertain surface nature. These tests were mainly designed to simulate specific operations in service, and could rarely serve to elucidate the nature of the wear process. The wear of a solid is a complex process which occurs under a wide range of conditions and may cause both chemical and physical changes of the surface regions. One important feature of the friction and wear of sliding surfaces is the elastic and plastic deformation of those parts which undergo stress as a result of contact between the moving surfaces. It is the nature of this deformation which is discussed below.

Initially the experiments on deformation of metals were confined to the measurement of the external strains shown by the metals as the result of application of stresses. This led to the deduction of macroscopic laws governing the elastic and plastic deformation, which were much used in the field of engineering, but gave very little information regarding the

mechanism by which the deformation took place. The deformation of metals has been increasingly studied since new techniques have become available during the last few decades to study this phenomenon.

1. The main techniques available for determining the form and nature of surfaces.

The optical microscope, now aided by optical interferometry and the electron microscope, makes possible the study of the external topography of the metallic surfaces before and after a stress or an etching treatment is applied. These techniques do not, however, provide much information about the orientation of the crystal lattice in the various parts of the specimen, except in a few favourable cases. On the other hand the technique of X-ray diffraction discovered by Laue, Friedrich and Knipping (1912) provides detailed information about crystal structure and orientation of specimens. X-rays used for diffraction purposes penetrate to a depth of the order of a few hundred thousand Angstroms before the beam intensity is reduced to half that of the incident beam. Thus most of the diffracted radiation comes from a surface layer of this order of thickness, and the diffraction pattern fails to give any clear information regarding the structure of the immediate surface regions, as distinct from that of the deeper underlying material. Recent experiments (Gay and Hirsch,

1953) have indicated that abrading or polishing a crystal disturbs (i.e. more or less fragments and disorientates) the surface to a depth of only about 10-15 μ.

Electron diffraction, discovered almost simultaneously by Davisson and Germer (1927) and by Thomson (1927) reveals the structure of matter even in exceedingly thin films. Because the scattering and adsorption is so much higher than that of X-rays, even films a few atoms thick can give strong diffraction patterns and the immediate surface region of the material can be studied without the confusing predominance of the diffraction patterns from the underlying material, such as occurs in X-ray diffraction. Thus the technique of electron diffraction is ideally suited to the study of the physical and chemical properties of surfaces and it was therefore used as the main technique of investigation in the present experiments to study the deformation caused on metallic surfaces by abrasion, though optical microscopy was also used as a subsidiary technique.

To study surface structure by the technique of electron diffraction, a voltage of 50-65 kV. is generally used. As the "reflection pattern" from a rough surface is actually obtained by the transmission of the electron beam through projections on the surface, electrons having rather higher penetration are desirable in the present case, so as to

obtain clear diffraction patterns free from undue incoherent background scattering. For this reason, 120 kV. electrons were used in this work.

2. Scope of the present experiments.

In the present study of the deformation caused on metallic surfaces by abrasion, iron crystals were used because of the simple structure, the existence of detailed knowledge about the modes of translational slip of iron, and the importance of this metal in industry. The abrasion technique used consisted mainly of unidirectional motion of the crystalline material on 0000 emery paper moistened with lubricant. A light force was applied to move the crystal in one single continuous movement for a distance of about ten inches on emery paper. The results elucidate the manner in which different directions of the abrasion influence the surface structure of the crystal.

The results on the above experiments show, as in the previous results of Evans, Layton and Wilman (1951), that due to the abrasion, parts of the crystal surface region are usually rotated through large angles about an axis which is perpendicular to a plane which lies parallel to the abrasion direction or nearly so and normal or steeply inclined to the surface. Furthermore, besides this surface fragmentation of

the crystal, flexure of the underlying layers sometimes occurs. It is also observed that due to the heating effect from the abrasion, the body-centred-cubic α-iron changed over to face-centred-cubic γ-iron, a result that had not hitherto been detected. These γ-iron crystals were twinned extensively on their densely populated planes due to the impacts resulting from the abrasion.

3. Deformation processes in crystals.

The deformation of a crystal can be contributed to by one or more types of the following processes. The main processes of deformation are:-

(i) Translation slip, including "flexural translational slip", and "kinking".

(ii) Twinning.

(iii) Rotational slip.

(iv) Deformation bands.

(i) Translational slip.

Single crystals of ductile metals require a minute force to exceed the elastic limit and to enter into the region where plastic deformation begins. The extension does not take place uniformly as the load is applied, but in discontinuous small jumps often accompanied by a noise like the ticking of a clock

(Joffé 1928) and thus forming a stepped surface. The stepped appearance caused on the previously smooth surface of the crystal during the course of the extension, is due to the slip of layers of the crystal (lamellae) over each other. From microscopic observations, this kind of slip was found to consist of a translational movement of the lamellae of the crystals over one another in the slip direction. This movement occurs in a specific (densely populated) lattice plane and a specific direction (a densely populated lattice row) depending on the particular material and the temperature.

The researches of G.I.Taylor in England, and Schmid in Germany, showed that the condition for slip to occur is that the tension generated in the slip direction on a glide plane must reach a critical shear stress which depends on the physical condition of the crystal. In all cases the slip direction is found to be the direction of a densely populated lattice row. Mathewson (1944), and Maddin, Mathewson and Hibbard (1949a) have pointed out that the slip is unlikely to be strictly linear on the atomic scale.

Mark, Polanyi and Schmid (1922) showed clearly the nature of the phenomenon of translational slip in a cylindrical zinc wire and also illustrated it by a model. They showed that the process of extension of a zinc crystal could be entirely accounted for by means of slip on the basal plane (0001) and

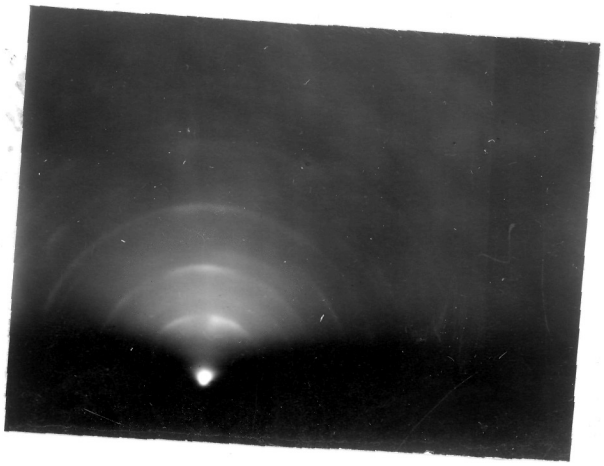

Fig 60. (110) face, abraded "[111]2, etched and electropolished, beam to abrasion direction.

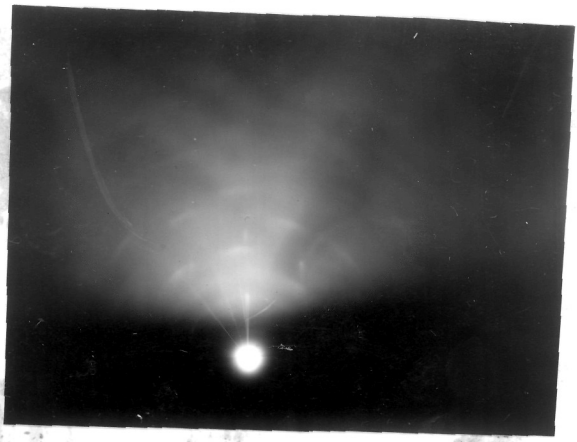

Fig 61. (110) face, abraded"[111]", etched and electropolished, beam along the abrasion direction.

in the direction of that digonal axis $\langle 100 \rangle$ which coincided most nearly with the direction of the maximum shear stress. They also observed that when the stress is applied by extending the crystal in a tensile machine, between two grips whose line of motion is fixed and along the axis of the initial wire, the glide planes are forced to change their original angle of inclination and thus the lattice planes become curved in the region of the unstretched portion of the crystal near the grips. This slip, involving cylindrical curvature of the slip lamellae, is known as "flexural translational slip" and takes place in the normal planes and directions, the flexure or curvature being about an axis normal to the translational slip direction and parallel to the slip plane. Guinier and Tennevin (1950) and Cahn (1949) reported that under specific conditions, "polygonisation" could result from the region under flexure, when recrystallised at high temperature.

Multiple slip.

In crystals where slip occurs on a type of plane and direction of which there are many such symmetrically related, e.g. in face-centred-cubic metals, which slip on $\{111\}$ along $\langle 1\bar{1}0 \rangle$, slip normally starts on a single slip system. If the tensional force continues, the slip will rotate the crystal lattice until the initial slip plane is in a less favourable

position, and as the tension still proceeds, another slip plane and slip direction of the same type becomes equally favourable for slip. In this way, extension will continue with a sequence of alternate slips on the simultaneously active slip systems. Finally, still another slip system of the possible group may share in the slip. Such slip is termed "multiple translational slip".

Clustering of slip lines.

In the deformation of cadmium, Andrade and Roscoe (1937) observed coarse slip lines which on higher resolution showed clusters of fine lines. Heidenreich and Shockley (1948) by using the electron microscope, observed in aluminium clusters of still finer slip lines, which correspond to slip lamellae about 200 A. thick and with relative displacement of about 2000 A. They also used electron diffraction, and showed that a strain-free, undistorted crystal of aluminium gave a pattern showing clear Kikuchi lines but gently tapping the crystal caused slight hardening and the disappearance of the Kikuchi lines although there was no evidence of slip lines. On removing the metal from the surface, by electropolishing, to a depth of about 200 microns, Kikuchi lines again became prominent in the diffraction pattern. Brown (1950) added to this work by showing that with increasing temperature the number of the elementary lines in a cluster and the spacing of the lines increased.

The influence of the rate of elongation on the nature of the slip lines.

In the rapid elongation of aluminium, Crussard (1945) noticed that the slip lines were fully developed when they appeared, and remained unchanged; while with slow elongation, however, some initially weak lines grew progressively stronger, and others developed from short lines and grew jerkily at both ends.

The slip plane and direction of α-iron.

Osmond and Cartaud (1906) pointed out that among the slip lines which occur in α-iron when it is strained, the curved ones predominate. Taylor and Elam (1926), Gough (1928), Andrade and others concluded that α-iron slips along the most closely packed rows $\langle 111 \rangle$, though the slip planes could be $\{110\}$ $\{112\}$, or $\{123\}$. Fahrenhost and Schmid (1932) were of the opinion that most probably α-iron slips on $\{123\}$ planes, but their experiments do not definitely establish this. Barrett, Ansel and Mehl (1937) showed that at low temperatures or with silicon contents above 4%, only $\{110\}$ planes were operative in iron-silicon alloy, whereas only $\{112\}$ would be expected according to the conclusions of Andrade and Chow (1940) summarised in Table 1 given by Barrett (1953).

The variation of slip plane with temperature.

In many metals the slip planes vary according to the temperature. Andrade and Chow (1940) summarised the results of different workers on the effects of the temperature on the slip

Table 1.

t°C.	θ	Metal	Glide plane	Reference
20	0.08	W	(112)	Goucher (1924)
20	0.10	Mo	(112)	Tsien and Chow (1937)
300	0.20	Mo	(112)	Tsien and Chow (1937)
1000	0.40	Mo	(110)	Tsien and Chow (1937)
20	0.26	β-brass	(110)	G.I.Taylor (1928)
-185	0.24	Na	(112)	Andrade and Chow (1940)
- 82	0.50	Na	(110)	Andrade and Chow (1940)
20	0.80	Na	(123)	Andrade and Tsien (1937)
20	0.87	K	(123)	Andrade and Tsien (1937).

Table 2.

Metals	T/T_m	Slip plane
W, Mo, Na	0.08 - 0.24	(112)
Mo, Na, β-brass	0.26 - 0.50	(110)
Na, K	0.80	(123)

T = absolute temp., °K. T_m = melting point °K.

planes in the body-centred-cubic metals like tungsten, molybdenum, β-brass, sodium and potassium and came to the conclusion that the operative slip plane changed from the {112} to the {110} and thence to the {123} as the ratio of the test temperature to the respective melting temperature increased through the values 0.08 to 0.87. Their results are shown in Table 1, where $\theta = T/T_m$, T is the absolute temperature at which the slip was investigated, and T_m the melting point of the substance. Barrett (1953) has more recently reviewed the results on variation of slip with temperature and summarised Andrade and Chow's (1940) results in Table 2. He points out that this correlation does not seem to apply, however, to iron and Fe-Si alloy for all the three planes, (110), (112) and (123) are active at room temperature in iron and Fe-Si alloy containing less than 4% silicon.

The above correlation fails in Fe-Si alloys when either the temperature is low or the silicon content is more than 4%. It also does not agree in Mo, for Chen and Maddin (1951) reported that at room temperature Mo slips on (110) plane along $[1\bar{1}1]$. From the above results it is quite obvious that the slip plane in body-centred-cubic metals is influenced by temperature and chemical composition but the slip direction is not so variable.

In face-centred-cubic metals, slip takes place at room

temperature along the most densely populated plane, i.e. $\{111\}$, and the direction in which it occurs is along the atom row having the greatest density of atoms, i.e. $\langle 1\bar{1}0 \rangle$. In aluminium, Boas and Schmid (1931) observed that at low temperatures slip occurs on (111) along $[10\bar{1}]$ while at high temperature (600 °C.) the slip plane changes to (100) though slip direction remains the same.

The hexagonal-close-packed metals also slip on the most densely populated basal plane (0001) along $[2\bar{1}\bar{1}0]$. According to Bakarian and Mathewson (1943), magnesium at high temperature (225°C.) slips on pyramidial planes $(10\bar{1}1)$ or $(10\bar{1}2)$ and the basal planes (0001). It was also noticed that the slip lines on the pyramidial planes were always forked and irregular in contrast to the straight continuous basal slip lines.

In the deformation of mercury, which has a rhombohedral structure, Andrade and Hutching (1935) observed straight slip lines at -50°C., but Greenland (1937) under similar conditions noticed wavy lines. Extension after slight bending of the crystal, however, produced faint but perfect lines which did not correspond to simple crystallographic planes.

Cross slip.

When short slip lines cross the main slip lines and extend from the end of a primary line to the beginning of another, they are known as "cross slips". This slip is

observed when the direction of applied stress is within the range of directions corresponding to single slip. Maddin, Mathewson and Hibbard (1948a and 1949b) established that cross slip in α-brass appeared to be in the same operative direction as that of the primary beam. During the cross slip in α-brass no appreciable hardening was observed but the deformation went on with the development of additional lines in the unslipped areas. When the additional lines were fully utilised, further slip occurred on the lines already formed and there appeared to be some noticeable overall hardening of the crystal. In the deformation of aluminium, Rosi and Mathewson (1950) observed one case in which cross slip could be resolved into components on the primary {111} plane and another {111} plane, this being the slip plane usually found in α-brass, but in 1951, Cahn, also using aluminium, reported that the cross slip plane appeared to vary between {111}, {100} and {212}.

Twist slip.

Mugge (1898), Johnsen (1914), and Buerger (1930) described a further type of slip occurring when the translational slip direction was a torsion axis, and it was called "twist slip". This slip seems to be a combination of translational and flexural slip. Some rotations may well be seen taking place, however, on the translational glide palne, and normal to its direction.

Kinking.

When the crystal is suddenly compressed with the axis of compression in the translational slip planes, a formation of "kinks" with sharp ridges takes place. Mugge (1898) referred to such deformation by the German word "Knickung" hence the English word "Kinking". The observations of Friedel (1926), Brilliantow and Obreimow (1934, 1937), Orowan (1942, 1947), Crussard (1949), and Hess and Barrett (1949) indicate that kinking is a particular type of flexural translational slip and is distinct from twinning. In 1942, Orowan first demonstrated kinking in a metal crystal, cadmium, during uniaxial compression parallel to the slip plane, and Hess and Barrett (1949) also investigated the same phenomenon in zinc crystals.

(ii) Deformation by twinning.

Deformation twins are observed under some conditions when a crystal is plastically deformed, especially when the stress is applied suddenly and the temperature is low. A crystal is said to be twinned if it is composed of two portions which are joined together in a definite mutual orientation, such that the lattice of one portion is either a mirror image of the other portion in a common plane which is called the twinning plane, or an orientation that could be derived from

that of the other by a rotation about an axis called a twinning axis. The mechanical deformation twin is formed by a shearing movement of the atomic planes over one another. An atom must surmount energy barriers in order to move into a twinned region. Since the twin and the parent lattices are of the same form, i.e. when a part of the crystal attains a new orientation having a definite crystallographic relationship to the parent matrix, the potential energy of the twinned lattices are the same before and after. At the same time, the total energy of the crystal increases and the increase is concentrated at the distorted boundary regions where the twins are in contact. Higher rates of load application and release favour twin formation. Gough and Cox (1932) consider that the deformation of a metal crystal by twinning is a function of the energy required to activate the change. Thus the low energy required for slip precludes the formation of deformation twins in face-centred-cubic metals. In hexagonal metals slight variation in the direction of the applied stress can change the active deformation process from slip to twinning.

Microscopic observations of the presence of lamellar grains in a metal do not give sufficient evidence for the existence of twins, though optical reflection from etch pits can be used to confirm this in some cases. On the other hand, X-ray and electron diffraction techniques can be quite

conclusive. Thus, when microscopic examination failed, Barrett and Haller (1947) used X-rays to show the presence of twins in magnesium crystals. The angle between twin bands and slip lines, the angular relationship of second order twins, the traces of the twins in two polished surfaces, and X-ray diffraction methods, have all been used to study twin relationships. Clark, Craig and Chalmers (1950) adopted the method proposed by Greniger (1935) to re-determine the twinning plane in tin.

The existence of a critical shear stress for twinning has been suspected for a long time, though Davidenkov, Kolesnikov and Federov (1933) showed that for zinc, as the normal force on the twinning plane increased, the resistance to twinning decreased. Miller (1936) reported that for the twinning of zinc the resolved shearing stress varied from 300 to 600 gm/mm^2. Gough and Cox (1929, 1930) observed with zinc the greatest number of twins in areas of greatest slip. In 1950, Yakoleva and Yakutovich measured the critical shear stress for the slipping and twinning of cadmium single crystals varying in diameter from 0.09 to 0.7 mm. It was found on reducing the diameter to 0.1 mm. that the stress for twinning increased ninefold but that of the gliding only twofold. The most recent work on cadmium, published by King (1952) has substantially established the presence of the critical resolved

shear stress for twinning. The strain hardening curves for slip and twinning were affected by the presence of an oxide layer.

Untwinning of a crystal occurs (Czochralski 1924, Barrett and Haller 1947) due to the application of the same stress as caused twin formation but applied in the opposite direction. Dorn and Thomsen (1943) and Carapella and Shaw (1947) suggested that untwinning takes place due to residual microtensile stresses in the test pieces, but Hess and Dietrich (1948) could find no X-ray evidence to support this.

Rapid loading (impact) favours twin formation while slow rates of stressing facilitates slip. Barrett, Ansel and Mehl (1937) suggest that the rate of application of stress is the most important factor in the formation of twins in silicon ferrite. In antimony and bismuth crystals twin bands were found by Gough and Cox (1930, 1932) to be the main results of plastic deformation. The classical work on twinning is described by Schmid and Boas (1935), while a general survey of the subject has been compiled by Barrett (1953).

The presence of twinning in a metal also influences its physical properties. Cross-rolled copper as compared with straight-rolled copper, exhibits a lower hardness and higher recrystallisation temperature. Brick and Williamson (1941) attributed this property to the formation of twins. In 1948,

Mason, McSimin and Shockley studied the twinning of tin by ultra-sonic observations.

(iii) Rotational slip.

Wilman (1950, 1951) was the first to demonstrate adequately, and define, a process of deformation which he called "rotational slip". It can be defined as the slipping of one part of a crystal on a neighbouring part, so that the two atomic sheets which slide over one another are densely populated planes, as in translational slip, but rotationally displaced about an axis normal to their plane (with or without simultaneous translational displacement) to one of a series of definable new positions where metastable equilibrium can occur. There is then only two-dimensionally periodic partial fitting together of the two crystal parts. There is evidence, e.g. Barrett's observations (see §(iv) below) of lamellar "deformation bands" parallel to {100} in Al, and {100} and {111} in Fe, that rotational slip can occur on other planes besides the normal translational slip planes.

The macroscopic effects of rotational slip were clearly shown by the torsion of potassium ferrocyanide trihydrate and gypsum, and it was also concluded that at least some "deformation bands" are bands of rotational slip, and that it may also occur in crystals which are abraded unidirectionally

(Wilman 1950, 1951). Electron diffraction results (Evans and Wilman 1950) show that when a zinc blende (110) cleavage face is abraded along [001], a lattice rotation in the surface region occurs which may be of this type, and that a similar rotation occurs in zinc oxide crystals formed epitaxially on zinc belende cleavage faces when heated in air to about 520°C.

Germer (1936) had shown that the abrasion of a cube-face cleavage surface of galena parallel to a cube edge caused rotation of the parts of the lattice about the perpendicular cube edge in the surface; and Raether (1947) found similar results for the similar case with rocksalt. Neither of these authors suggested any clear explanation of the origin of these observed rotations.

Results from the unidirectional abrasion of copper and iron (Evans, Layton and Wilman 1951) showed that the abrasion led to large rotations of parts of the surface region of the crystal about a well defined axis which was normal to densely populated net planes, usually planes parallel to the abrasion direction or nearly so.

It should be emphasised that although various authors (Osborne and Adams (1931), Collins and Mathewson (1940), Heidenreich and Shockley (1948), and Jillson (1950)) have suggested that plastic flow of crystals may involve rotation of slip lamellae about their normal, these authors did not

support their suggestions by adequate detailed quantitative tests. Thus Osborne and Adams (1931) applied pressure on a galena single crystal and then examined the crystal microscopically. They found that the galena crystal was heavily distorted and fragmented, and they suggested that there was evidence of the presence of adjacent cleavage blocks retaining contact on the common cleavage face but with rotational displacement about the normal to this face. Collins and Mathewson (1940) based their suggestions on their observations of slip in face-centred cubic metals. Heidenreich and Shockley (1948) suggested from their electron diffraction patterns, though they did not prove it, that in the tensile elongation of aluminium, some rotation of slip lamellae occurred on the operative slip plane (assumed to be {111} as usual). Jillson's (1950) evidence was slightly more convincing, since he found that zinc single crystal rods could be twisted remarkably easily about their axis when the slip plane (0001) was orientated normal to the axis or nearly so; and he found that etching then exposed prism faces which spiralled round the rod surface, about the axis of the rod.

(iv) Deformation bands.

The study of certain ill-defined bands which have been called "deformation bands" has been carried out mainly by microscopic observations. Such bands are regions in a

crystal which have taken up appreciably different orientation due to the deformation. The bands are formed in both single crystals, where their width may be a millimetre or more and grains of aggregate where they have microscopic dimensions. Barrett showed that at low deformation, these bands are not well defined microscopically like translational slip or twin bands, unless made visible by very slow etching. Barrett (1939, 1940, 1949, 1953), Barrett and Levenson (1939, 1940, 1941), Crussard (1949), Honeycombe (1950a, 1950b, 1951-52) and Calnan (1952) have studied the deformation bands in detail.

Barrett (1939,1940), Barrett and Levenson (1939, 1940 and 1941) clearly showed that some of these bands are parallel to densely populated net planes which are not always translational slip planes - e.g. they are sometimes {100} and {111} in iron and (100) and (110) in aluminium and copper. The neighbouring {100} lamellae in aluminium were observed to be rotated by up to 8° about the normal to their interface. Barrett and others have discussed these bands in terms of multiple translational slip on the system of crystallographic equivalent planes. Wilman (1951) gives a logical conclusion that at least some of the bands observed by Barrett and his collaborators originate as rotational-slip bands before translational slip has caused much orientation change, though subsequent flexure and other forms of complex translational

slip modify their form and orientation extensively at high deformation.

Honeycombe (1950) has observed deformation bands in an aluminium single crystal extending in tension. These were spaced about 0.05 mm. apart and were parallel to (110) planes; they could be seen even after one per cent elongation.

4. Previous experiments on abrasion and scratch hardness of crystals.

(i) Definition and the hardness classification.

Hardness in a metal is closely related to the plasticity and the strength of the crystal. The term "hardness" embraces different properties which are distinguished by the methods employed to determine it. The resistance of a crystal to abrasion is one of the methods of estimating the relative hardness of crystals, or of the same crystal in different directions. Hardness may be defined as a measure of the resistance which a crystal opposes to the mechanical injury of its surface layers according to the surface and direction. The experiments which have been made to estimate relative scratch hardnesses of crystals have been reviewed recently by Tertsch (1949).

It has been long desired to classify minerals and industrial materials according to their hardness. In 1774,

Werner propounded a six-membered scale for hardness, but Hauy (1801) attempted to compare the hardness of two materials by finding which one could scratch the other. Mohs (1822-24, 1832) endeavoured to make this method the basis of a practical scale, with ten minerals representing the main steps of hardness, and he also introduced the decimal system for describing the hardness of a material in terms of the chief steps and sub-divisions. His ten-membered (1.Talc; 2. Gypsum; or rocksalt; 3. Calcite; 4. Fluorspar; 5. Apatite; 6. Felspar; 7. Quartz; 8. Topaz; 9. Corundum; 10. Diamond) hardness scale is to this day in use and named after him as the Mohs hardness scale.

Soon after the introduction of the Mohs scale, it was realised that the intention to set up, in the aforesaid scale of minerals, the most equal possible hardness differences, was not strictly fulfilled, because in most minerals representing the steps of the hardness scale the hardness varied much according to the face and the direction in the face in which it was tested. This clearly shows that among the members of the scale no fixed hardness values occurred. The differences in the hardness in different directions appear especially prominent in the crystals that possess preferred cleavage planes and thus show the strongest hardness anisotropy. Thus it was indeed long known that one must not only notice on which face of the member of the scale the hardness is tested, but also in which

direction, since otherwise no comparison is possible. The strong hardness differences in different directions on the cleavage face of calcite are illustrated in figure 7.

(ii) Methods of determining the hardness in different directions on a crystal face, and typical results.

Crystallographers generally have adopted for the determination of the vectorial differences of hardness in any given crystal face, the methods involving scratching, planing or grinding either on a flat surface or locally by an abrasive wheel. On the other hand, hardness differences depending on the particular crystal face examined but involving a mean hardness over all directions in the face, can be estimated by application of such methods as piezo-electric methods or filing, as the chief technical means of investigating hardness of materials.

Frankenheim (1829) made some extensive experiments on hardeness testing of crystals in different directions in the same face by scratching with needles of different metals.

The inequality and the uncertainty in the Mohs hardness steps led to experiments which resulted in various methods of measurements. Seebeck (1833) made first the hardness measuring apparatus called by him the "Sklerometer", which for all the dynamical hardness determinations still remains adopted in its fundamentals. In this apparatus a crystal waxed to a

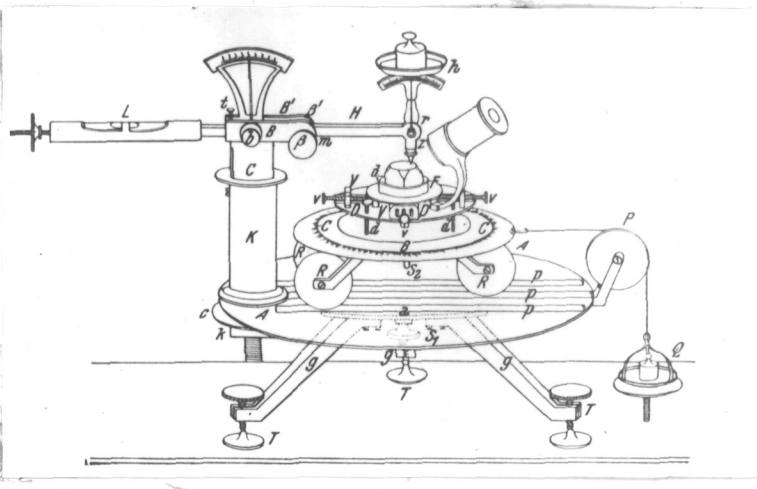

Fig 1. Redu ed reproduction of the original figure of Grailich and Pekarek. Hardness measuring app.

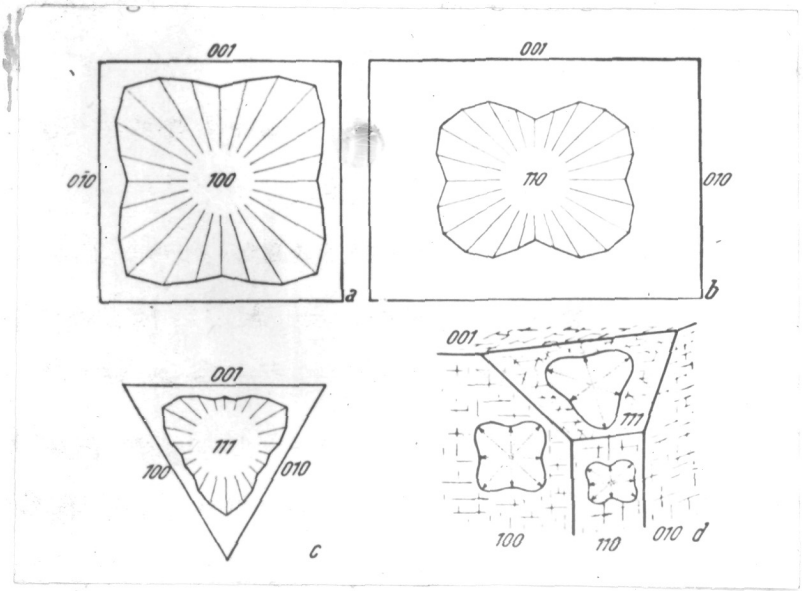

Fig 2. Hardness curve on roksalt (by Exner' a) Cube face, b) dodecahedral face, c) octahedral face, d) view on the cube face. The vectors have length proportional to the load required on the point pressing on the crystal to cause a visible scratch.

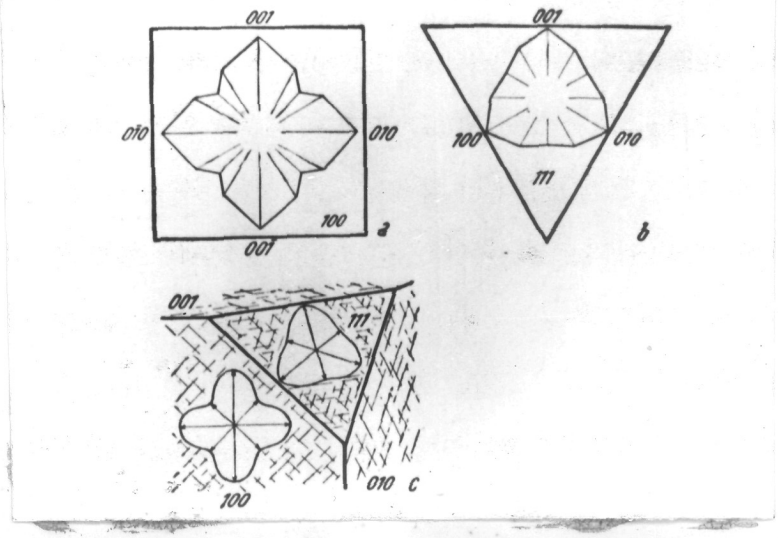

Fig 3 Hardness curve on fluorspar (by Exner) a) cube face, b) octahedral face, c) view on the cube face face corner.

rotatable supporting table with a slide arrangement, was moved sideways under a loaded point, and the load was determined when just a noticeable scratch was formed on the horizontally displaced crystal face.

In 1850, Franz improved Seebeck's apparatus by introducing a crank (winch) drive, while Grailich and Pekarck (1854) chose the drawing action of a falling weight to produce the lateral motion. Figure 1 shows the apparatus used by the latter to determine the scratch hardness. On this basis, Exner, in 1873, made his classical hardness investigations which were taken up anew by Pfaff (1883).

Figures 2 and 3 show the results obtained by Exner (1873) for the scratch hardness determination on the cube face and the octahedral planes of rocksalt and fluorspar crystals, plotted in the form of polar curves. These were obtained by connecting the terminal points of the lines which start from a point on the surface and whose lengths are proportional to the observed scratch hardness (weight on the scratching point required to cause a visible scratch) in the same directions. It is evident from these illustrations that there is a relation between the scratch hardness and the crystal symmetry, together with the cleavability. On the main cleavage face of gypsum, with the indexing based on the axial setting of Mugge, Exner (1873) obtained the hardness curve shown in figure 4, showing

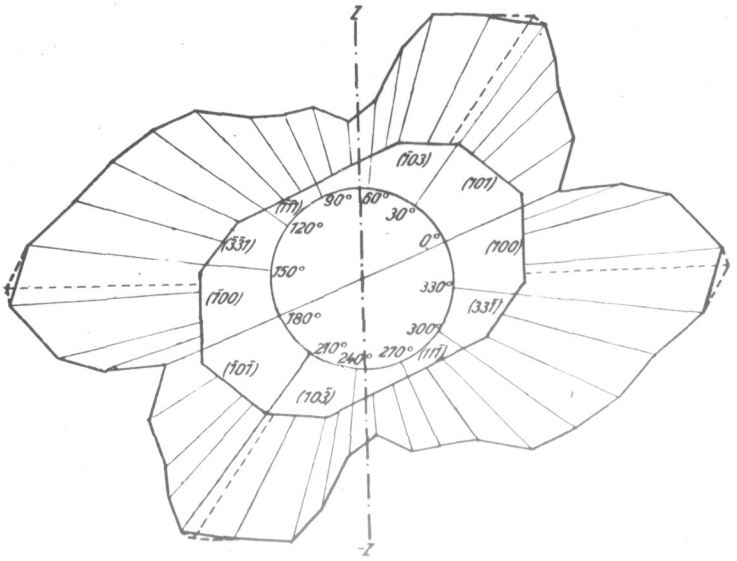

Fig 4. Exner's hardness curve on the chief cleavage face of gypsum; the indices refer to axial arrangement used by Mugge.

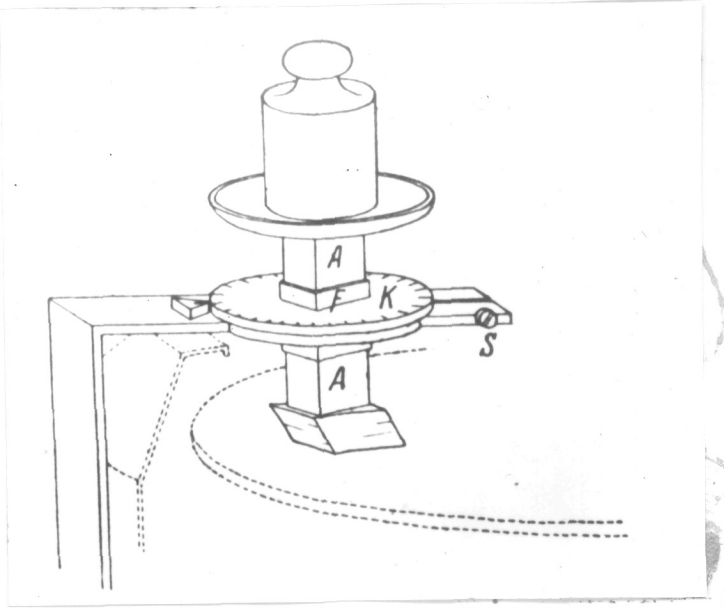

Fig 5. Apparatus for abrading crystals in any desired direction to study the abrasion direction .

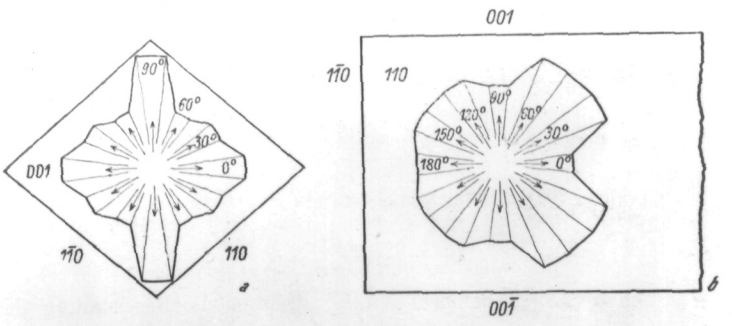

Fig 6. Tertsch's results on the azimuthal variation on abrasion hardness of barytes. a) basal-face, b) prism face.

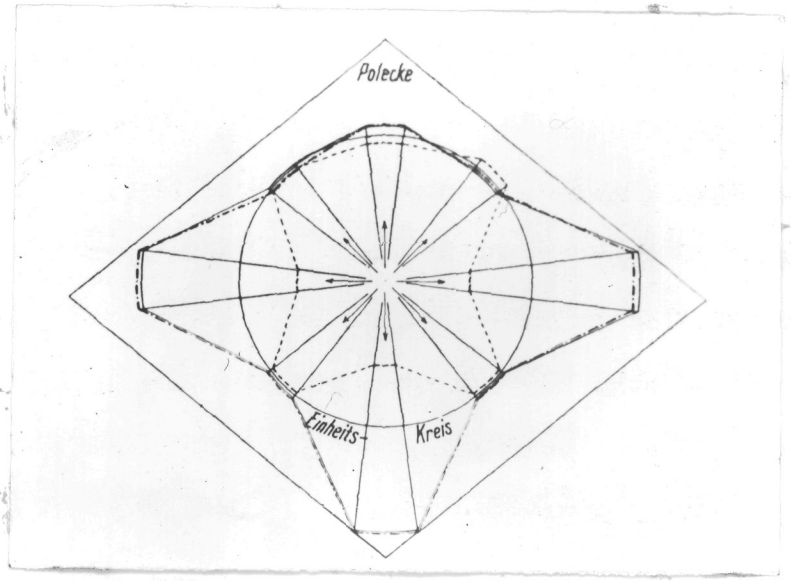

Fig7. Tertsch's results on the azimuthal variation on abrasion hardness on calcite(cleavage plane)
----- curve for 1sq cm reduced weight losses.
____ curve for relative hardness
-.-.-.- Symmetry-adjusted figure for average values of relative hardness.

the hardness variation with the direction. In general it can be said that if the surface under investigation is perpendicular to the cleavage planes, the hardness parallel to the direction of cleavage is minimum, and if the surface is inclined to the cleavage planes, the hardness is usually different in opposite directions.

(iii) Abrasion hardness.

Rosiwal (1893, 1896) carried out experiments on abrasion hardness by abrading two metallic surfaces in contact with each other and expressed abrasion hardness as inversely proportional to the obtained volume loss caused by the abrasion. Jannetaz and Goldberg (1897) designed a "Usometer" to study abrasion hardness. This apparatus was the first to be based on the principle of use of a grinding disc on which the crystal could be fixed under a load with its face lying flat against the disc. Figure 5 shows such an arrangement allowing for a rotation of the crystal. Tertsch (1934, 1936c) has discussed abrasion hardness anisotropy in crystals, and the practical details of its measurement, and has published results for calcite (1934), dolomite (1935a,b) and barytes (1936a,b) crystals. Figures 6 and 7 show the abrasion hardeness curves obtained by Tertsch for barytes on the basal and prism face, and calcite on its cleavage plane. In his experiments on

calcite, Tertsch (1934) showed that his curves for variation of abrasion hardness with direction corresponded closely to those found earlier by Pfaff (1883) for variation of scratch hardness with direction.

In 1951, Evans, Layton and Wilman also used a rotating disc covered with abrasive (emery paper) method with a little modification to that shown in figure 5, for the unidirectional abrasion of copper and iron crystals. As a load on the crystal, they applied a light hand pressure. They also noticed that in the case of an electropolished copper (110) face, it was appreciably easier to abrade along the cube face diagonal than the cube edge and $\langle \bar{1}12 \rangle$ direction, where there seemed to be a higher resistance to abrasion, thus a coarser grade of emery paper was used initially (3 followed by 0), before a final light abrasion with 0000 emery paper.

Wilks (1952), by using multiple beam interferometric technique, determined the depth of abrasion on cube, didecahedron and octahedron planes of four diamonds (two from South Africa and two from Belgian Congo) and estimated their abrasion hardness from abrasion depth per revolution of abrading wheel, in preference to length or width of abrasion. Taking the most favourable direction in each case, he came to the conclusion that dodecahedron surfaces were easier to abrade than cube surfaces, and also reported a difference of

40% in hardness of the Congo diamond as compared to that of a South African diamond. Interferograms revealed that the abrading wheel moved laterally and longitudinally while abrading, that the sides of the abraded depression were highly polished, and that there was no appreciable deformation of the surrounding surfaces.

(iv) Previous X-ray and electron diffraction experiments on the structure of abraded crystal surfaces.

Bénard and Lacombe (1946) have examined by an X-ray reflection method, iron and aluminium crystals which had been subjected to abrasion. They obtained ring patterns showing that, after abrasion, the surface of the crystal had become polycrystalline. Electropolishing of the surface to a depth of about 10 μ, resulted in the rings of the X-ray pattern being broken up into arcs, indicating an orientated texture. Further electropolishing up to 60 μ, removed this arcing and gave rise to a single-crystal Laue spot pattern. They also stated that the axis of the fibrous orientation (incomplete fibre texture) produced on each crystal varied with the crystal orientation, relative to the surface plane and the abrasion direction.

In 1936, Germer abraded a cube-face cleavage surface of galena parallel to a cube edge, and had shown that it caused rotation of the parts of the lattice about the perpendicular cube edge in the surface. Raether (1947) also

found similar results for similar cases with rocksalt. But neither of these had been able to suggest any clear explanation of these observed rotations.

Davisson (1946) took electron diffraction photographs of a quartz plate which had been lapped with emery. The photograph taken after abrasion showed the presence of a large number of small particles of quartz with random orientation. The plate was then scrubbed vigorously with soap and water, using a tooth brush, and dried. The electron diffraction pattern at this stage showed the disappearance of the rings but in their place arc-segments associated with spots due to undistorted quartz became prominent. These electron diffraction patterns show that a lapped plate has ~~been~~ randomly orientated quartz on its surface which may be removed by scrubbing, leaving a surface layer of quartz(not removed by scrubbing) with limited misorientation.

Courtel (1948) and Courtel and Leger (1948) described a device of preparation of clean metal surfaces by mechanical abrasion in vacuum with high speed wheels and simultaneously studied these surfaces by electron diffraction. A freshly polished mild steel surface showed no trace of oxide layer until air was admitted. The freshly abraded surfaces gave electron diffraction patterns showing orientation due to the polishing process.

Courtel (1949) investigated the temperature reached on the surface of metals (Fe, Al, Ni, Mg and Co) during the abrasion, including Co, which possesses a clear transition point in its crystal structure. In the case of cobalt, he noticed that a single crystal of hexagonal cobalt abraded with a peripheral speed less than 14 m./sec. gave an electron diffraction pattern showing that the surface consisted of the hexagonal variety. As the speed of the abrasive surface was increased further (20 m./sec.) a rise in the surface temperature took place, resulting in the transformation of the hexagonal Co_{β} to cubic Co_{α}. Since this transformation is known to occur at 400°C, it was concluded that at the polishing speed of 20 m./sec., the surface regions of the cobalt must have reached 400°C. or more. Courtel noted, however, that the transformation temperature of the cobalt observed in purely thermal treatment is somewhat variable (Troiano and Tokich 1948).

Courtel (1950) examined, by electron diffraction, the oxidation characteristics of metallic alloys (Co 80% - Cr 20%) at different speeds in the rarefied atmosphere in the electron diffraction camera. He also studied the preferential orientation of the oxide layers produced by grinding of carbon steel, chromium, nickel, magnesium, hexagonal cobalt (single crystal), cerium, duralumin, stainless steel (of types 80:20,

18:8, 13% Cr, 25% Cr); and the temperature produced on surfaces during grinding. He observed under these conditions the formation of cubic Ce_2O_3 in direct contact with metal. During the above study, he also noticed the adsorption of fatty vapours on the milled surfaces. Courtel (1952)in a discussion on 'Friction' summarised these electron diffraction results.

Gay (1950), showed that relatively light grinding of a lithium fluoride crystal surface produced a marked increase in the reflected intensity of X-rays. Light abrasion produced a surface fragmentation having a misorientation within the range of divergence of the incident X-ray beam, so that all the misorientated material can reflect simultaneously. Heavy working of the surface produced surface disturbances with such large misorientation that it could not all reflect the incident beam. He also pointed out the optimum grinding and etching technique of a crystal required to give the best results with the concentrating X-ray monochromator.

Gay and Hirsch (1953) summarised the results they had obtained by examination of abraded calcite crystals by X-ray and electron diffraction, and they indicated that abrading or polishing a crystal (in the case of calcite, quartz, fluorite, lithium fluoride and rocksalt) disturbs, i.e. more or less fragments and disorientates the surface appreciably to a depth of less than about 10-15 μ.

Evans, Layton and Wilman (1951) showed that the unidirectional abrasion of electropolished copper and iron crystals caused rotations of parts of the surface region of the crystal about a clearly defined axis which was normal to a densely populated plane lying parallel to the abrasion direction or nearly so or steeply inclined to the surface. They pointed out that although such rotations would be difficult to account for by known translational slip processes, they may be explained simply in terms of fragmentation involving rotational slip. Since optical and electron microscopy supplies no clear observations of the location and form of rotated regions this interpretation in terms of rotational slip is not confirmed.

II. Experimental.

1. Preparation of crystal surfaces.

a. Growing and cutting of the crystals.

In these experiments, two crystals of iron were used, which were 2.5 to 4 sq.cms. in area and about 2 mm. thick. These iron crystals were prepared in the laboratories of the British Iron and Steel Research Association by the strain and anneal method. These crystals were cut with a well lubricated jeweller's saw from strips containing several crystals. Lubricant was used to reduce the rise of temperature during the process of sawing. To keep the crystals free from any kind of distortion by bending or undue pressure, the clamping and sawing operations were carried out with great care. Then surfaces were smoothed by abrasion with a range of emery paper well lubricated with pure benzene, in the normal manner, down to No.0000.

b. Smoothing of crystals by electropolishing.

For these experiments, a perfect strain-free and smooth surface is desirable, but it was found that neither the mechanical means of polishing nor the subsequent etching in nital and in a solution of 1% picric acid in ethyl alcohol, nor annealing in vacuum, could give adequate polishing.

The technique of electropolishing developed relatively recently, mainly by Jacquet and Rocquet, was therefore applied to the crystals in the present experiments, to produce atomically smooth and strain-free surfaces and this was carried out as recommended by Jacquet and Rocquet (1939) in perchloric and acetic anhydride bath.

Various workers have tried to polish iron and steel by using different bath compositions and conditions, and have studied the factors influencing the electropolishing. Without going into great detail, the reviews of Lippert (1940), Jacquet (1943a, 1947) and Wernick (1948) may be mentioned, and these contain many other references. Young and Brytoznk (1942) used various baths for electropolishing iron and studied the optical conditions by photoelectric reflectometer and came to the conclusion that for metallographic specimens, Jacquet's method (1939a) is the best.

After considering the possible methods for electropolishing of iron, the composition of the bath and the conditions used in the following experiments were:

Perchloric acid (density 1.61 or 65%)	185 cc.
Pure acetic anhydride	765 cc.
Distilled water	50 cc.
Current density	4-6 amp per sq.dm. of anode surface.
Voltage	45-50 volts.
Temperature	15-25°C.
Time	2-4 minutes.

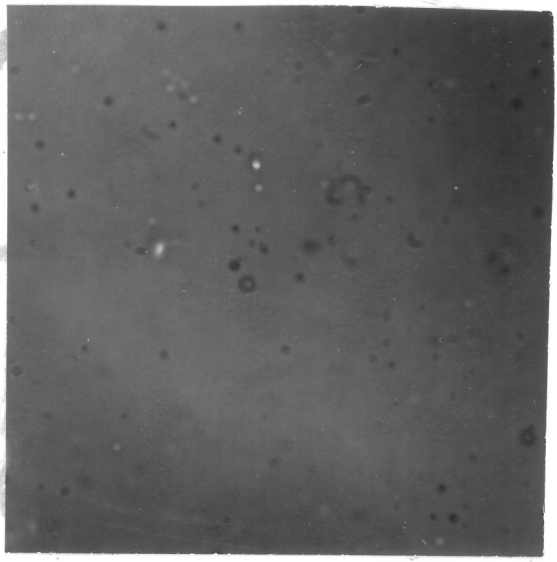

Fig8.

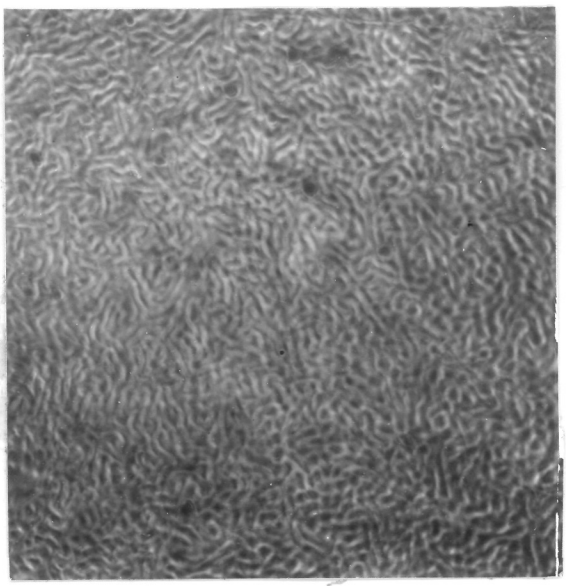

Fig 9.

Electrode arrangement	Vertical, parallel cathode about six times that of anode and 3 cms. away from anode.

By personal experience, it was found that the lower the temperature of the bath, the better the polish. Secondly, instead of polishing the iron surfaces continuously for 4 minutes, if it is done in two separate periods this helps in obtaining a good polish.

In preparing the bath, great care should be taken in mixing pure acetic anhydride in perchloric acid cooled with an ice bath, and occasionally agitated mechanically. The bath should be allowed to stand for 24 hrs. before use. Purity of the components is very essential otherwise there is always a chance of harmful explosion (Merchant 1940).

It is difficult to adjust the voltage and current density for a good polish of the iron surface, because high or low voltage or current density produces etch pits and a wavy or "lemon peel" surface form, as can be seen in figures 8 and 9.

The next important step after electropolishing is the removal of the specimen from the bath and washing. Much stress should be given to the technique of washing. A viscous brownish-red layer can be seen covering the whole of the polished surface; this is thought to be a complex salt (Jacquet 1939a) which plays an important part in the process of

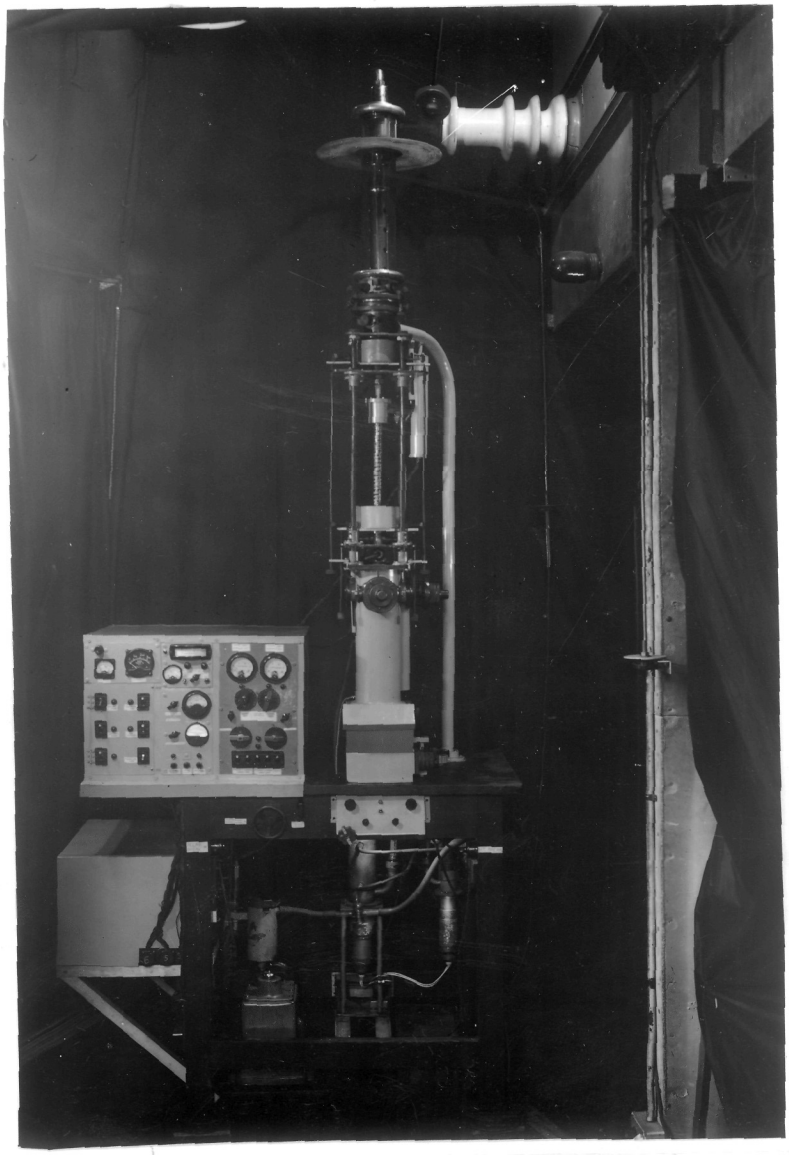

Fig 10. High Voltage Electron Diffraction Camera.

polishing. This layer can be dissolved in dilute acetic acid and also washed in water. In practice, as far possible, water should be avoided as it attacks the polished surface covering it with a thin film of oxide. It is usually washed with a jet of acetone, followed by a quick immersion of the specimen in a less volatile liquid— normal propyl alcohol, so as to avoid exposing the clean surface to the air during the few minutes which elapse from insertion of the specimen into the electron-diffraction camera until high vacuum of the order of 10^{-5} mm. of mercury is reached.

Sometimes, during the process of washing, it was noticed that a thin milky-white film of oxide was formed. To remove this film, the polished surfaces are etched for about 5 seconds (Evans, Layton and Wilman 1951) in a 1% solution of picric acid in alcohol, followed by the aforesaid procedure.

2. Investigation by electron diffraction.

The electron diffraction camera used in these experiments was of the type described by Finch and Wilman (1937) with new modifications for use at high voltages as described by Finch, Lewis and Webb (1953). Fig.10 shows a general view of the diffraction camera. Generally an accelerating voltage of 120 kV. was used so as to reduce the background scattering in the photographs from the rough surfaces. In all cases for

electron diffraction examination, the "camera length" (specimen-photographic plate) was 48 cms. For an accurate measurement of λL, its calibration was made by using graphite powder as a standard material (Finch and Wilman 1936, 1937). An extensive interpretation of electron diffraction patterns and their applications has been given by Finch and Wilman (1937) and Wilman has developed methods for interpreting Kikuchi line patterns (1948a, 1948b), patterns from crystal groupings of rotational slip type (1951) and from rotating crystal or orientated polycrystalline specimens (1952).

On examination of the iron crystal surfaces by electron diffraction, it was found from the pattern (Fig.32) that one crystal had a surface of the ($h0\bar{1}$) type, inclined $8\frac{1}{2}°$ to a (001) plane and was thus nearly (107). The other crystal was practically (110), actually inclined at 2°20' to (110) almost about the [110] lattice row, as was seen from Fig. 42 . Both the crystals, after electropolishing, yielded clear patterns of Kikuchi lines and elongated spots showing that the surfaces were atomically smooth and of high perfection, as shown in figs. 28, 32, 33, 42, 43 and 44 .

3. Technique used for abrading the crystal surfaces.

Electropolished surfaces of these crystals were abraded by a single continuous ten-inch stroke in any desired direction, at a uniform speed of about three inches per second, on 0000

emery paper well wetted with pure benzene. A light hand pressure of about 50 gms/sq.cm. was used on the crystal for abrasion. The abraded surfaces, as observedvisually, were traversed relativelyuniformly by fine scratches parallel to the direction of abrasion. To find the actual direction of abrasion, the angle between the abrasion scratches and the reference edge of the crystal could be noted by means of a protractor, and was verified in the electron diffraction camera.

4. Methods employed for progressively etching away the crystal surface.

After the examination of the abraded surfaces by electron diffraction, it was desired to remove the successive layers from the initial crystal surface to study at different depths the nature and extent of the lattice deformation by abrasion. For this, the metal was electropolished for a few seconds at a time, or an etching solution of 1% picric acid in ethyl alcohol was used. This was followed by washing in a jet of acetone and immediate transference in normal propyl alcohol to the electron diffraction camera to avoid oxidation.

In most cases, examination by optical microscopy, using a Vickers Projection Microscope, was carried out after examination in the electron diffraction camera.

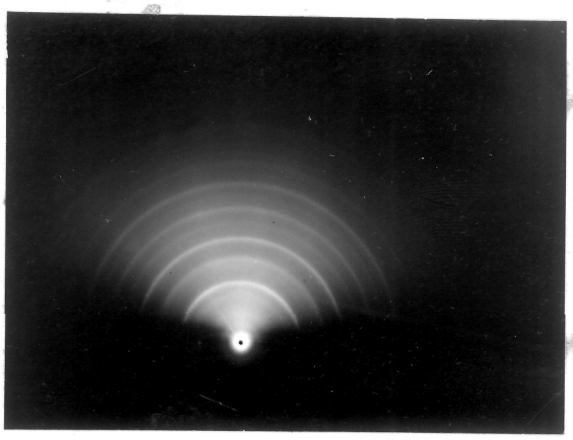

Fig 11. Freshly abraded iron.

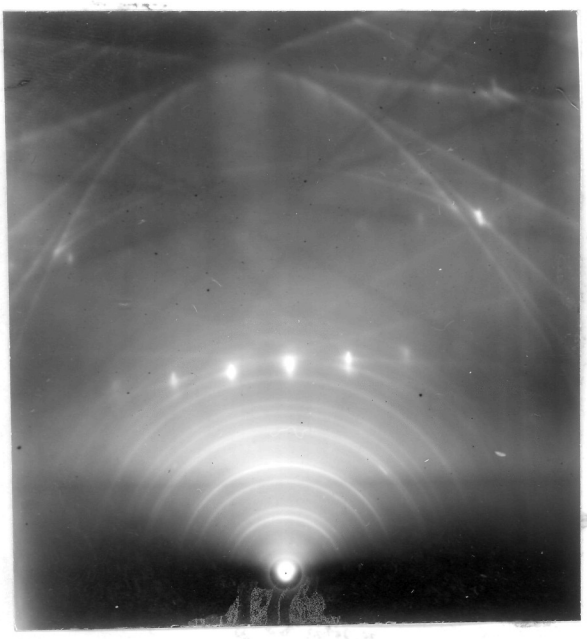

Fig 12. After etching; iron. rings.

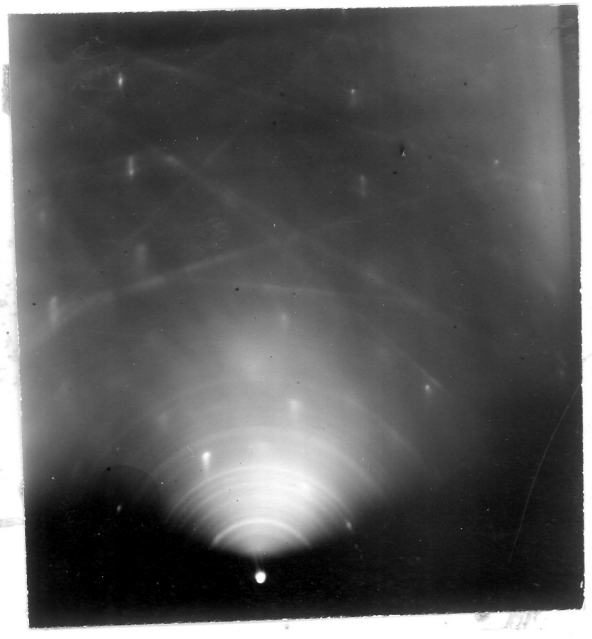

Fig 13. Mixture of b.c.c. and f.c.c. rings.

III. RESULTS.

In the following account of the present experiments on abrasion of iron crystals the "abrasion direction" is defined as the direction in which the abrasive particles moved relative to the crystal. Generally, in all the experiments on the two iron crystals used, the surfaces yielded ring patterns such as fig.11 immediately after abrasion, indicating randomly disorientated fragments of normal body-centred-cubic α-iron, with lattice dimension $\underline{a}_\alpha = 2.86$ Å. It was observed that on slight etching ($\sim$ 45 seconds) in 1% picric acid solution in alcohol, another ring pattern was obtained corresponding to a face-centred-cubic structure with a cube axis $\underline{a}_\gamma = 3.60 \pm 0.01$ Å. relative to $\underline{a}_\alpha = 2.86$ Å., either alone as in fig.12, or still with presence of some rings from the body-centred-cubic α-iron, as in fig.13. The lattice dimensions of the face-centred-cubic material, together with further evidence given in Part 2, confirms that the material consists of γ-iron. The presence of this γ-iron indicates that its formation must have taken place due to the rise in temperature of at least parts of the iron crystal surfaces up to 900°C. or more during abrasion.

After further etching (approximately two minutes) the ring patterns due to γ-iron had usually disappeared and only

rings and arcs due to α-iron remained. Roughly four to six minutes total etching removed most of these randomly disorientated α-iron fragments, and the pattern then showed some spots corresponding to the main α-iron crystal orientation and well defined arcs on the α-iron ring positions, with traces of a ring pattern due to γ-Fe_2O_3. These arcs due to α-iron indicated in almost all cases a range of rotation from the initial crystal orientation, about a well-defined axis.

The observations recorded after etching or electro-polishing down to the above region are described below. In all cases, the sense of the lattice rotations observed was the same as that of a wheel rolling on the surface along the abrasion direction, with its axis usually normal to a main lattice plane. It should be noted that for convenience in considering the relation between the various azimuths, all the diagrams showing indexing of diffractions correspond to the negative photographic plate as viewed along the beam direction, whereas the patterns illustrated are positives and thus are reversed from left to right relative to the negative or index diagram.

PART 1.

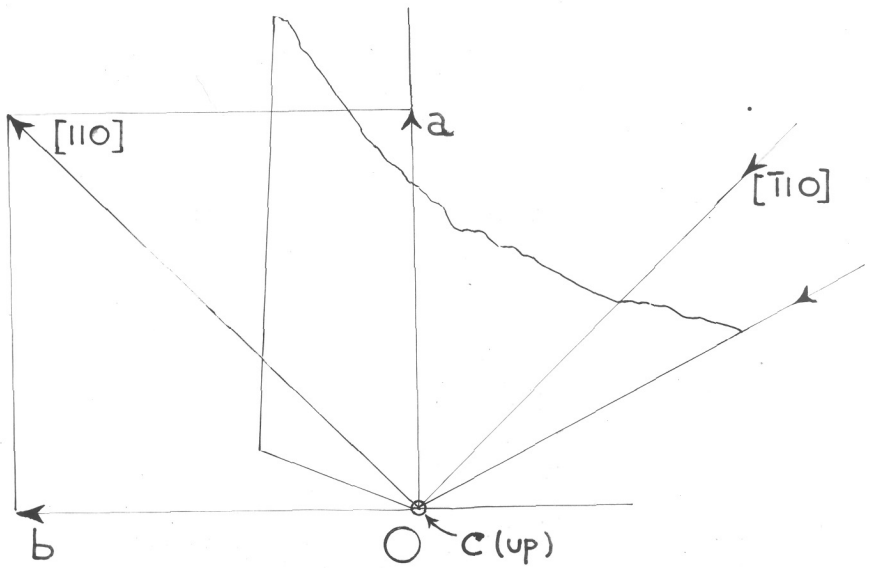

Fig14

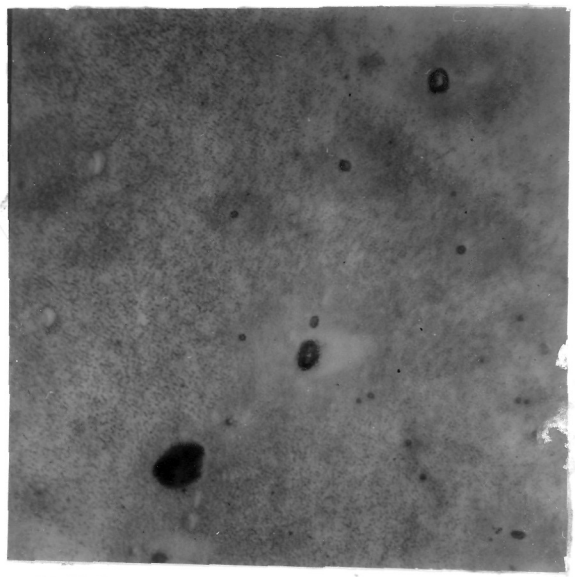

Fig 15. Optical micrograph showing electropolished surface, 600x.

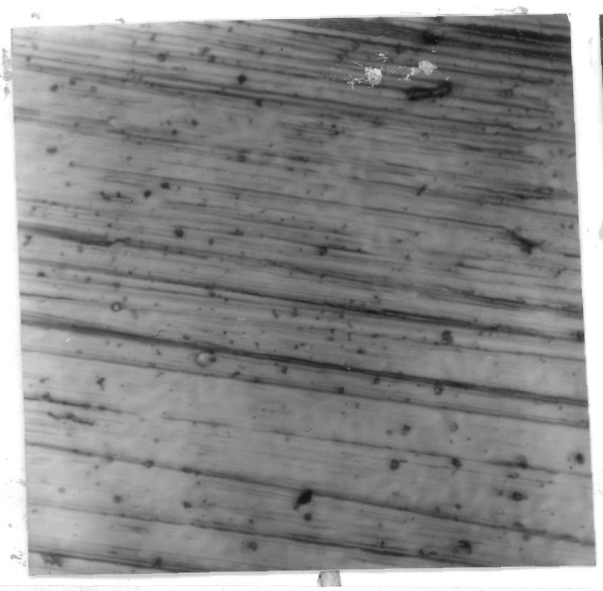

Fig 16. Optical micrograph showing the freshly abraded surface.-600x.

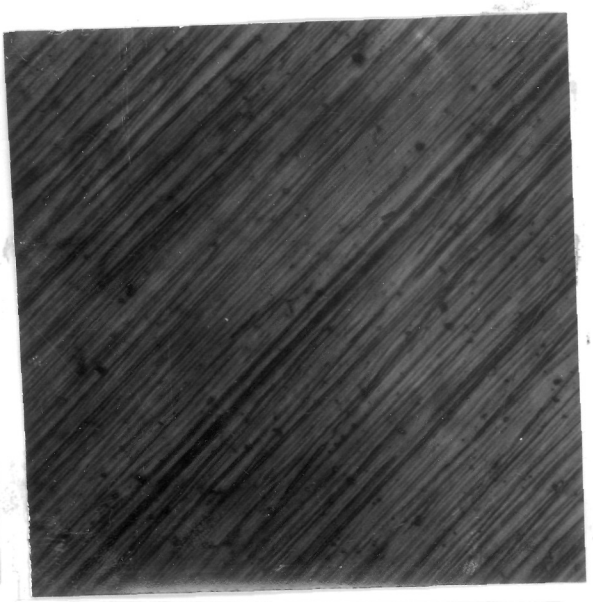

Fig 17. optical micrograph after 15sec etching from figure 16. — 600x.

A. Experiments on the ($\underline{h}$ 0 $\underline{l}$) face inclined at $8\frac{1}{2}°$ to (001).

Since the (001) plane was nearly parallel to the surface, it is most convenient to refer to the azimuths in the surface in terms of the nearest lattice-row directions in the (001) plane. Figure 14 shows the direction in which the crystal was abraded relative to the cubic axes chosen.

1. Abrasion parallel to the "[$\bar{1}$10]" direction.

Figure 15 shows the micrograph of the electropolished iron surface. Except for a few etch pits, the surface appears to be fairly smooth and perfect. After abrading the electropolished surface in the "[$\bar{1}$10]" direction, the micrograph shown in figure 16 was obtained, and, as stated above, the electron diffraction pattern then consisted of rings due to α-iron as in figure 11. The surface was etched in stages and at each stage was also examined by electron diffraction and in the microscope. After 2 minutes 15 seconds etching, the micrograph figure 17 was obtained and shows the abrasion scratches still existing on the surface though fainter than in figure 16. The surface then yielded (from roughly the same region as yielded figure 17) a clear Kikuchi-line pattern due to undistorted crystal, together with some strong spots corresponding to the initial crystal orientation. In addition, the pattern figure 18 obtained with the beam normal to the...

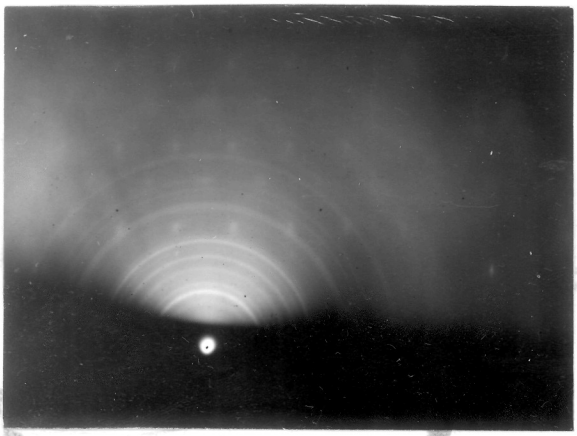

Fig 19. (107)face, abraded [$\bar{1}10$]and etched, beam along the abrasion direction.

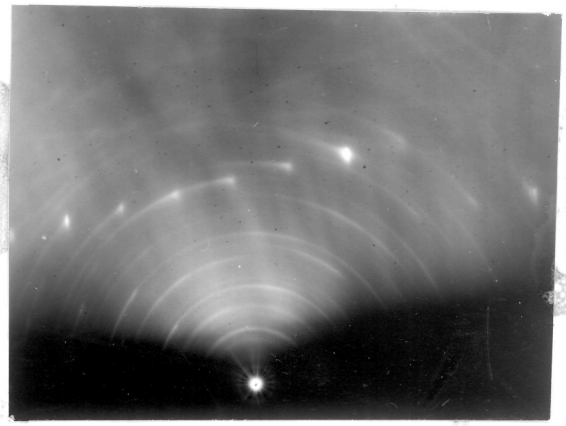

Fig18. (107) face, abraded "[$\bar{1}10$]"and etched, beam $\perp$r to the abrasion direction.

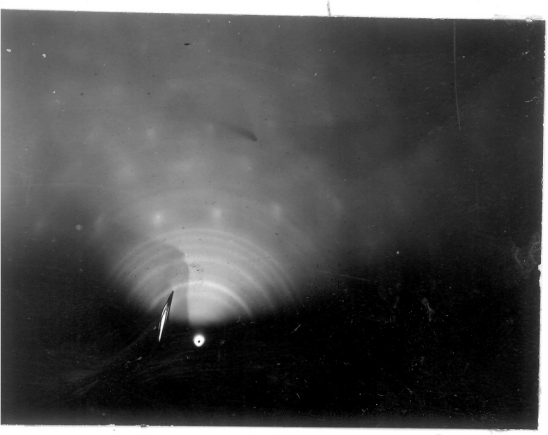

Fig 21. Same as fig 20, but beam along [$\bar{1}10$].

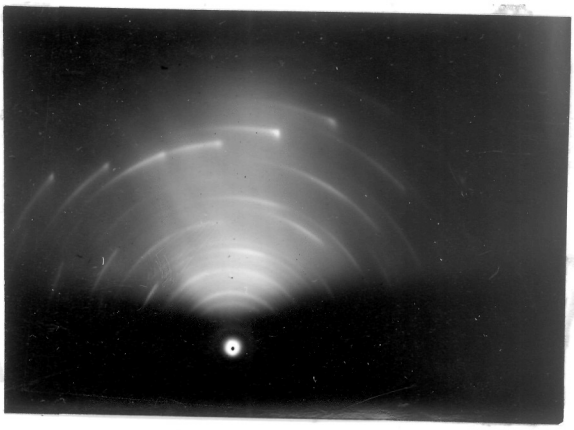

Fig20. Further etching for 1min30sec from fig18, beam $\perp$r to abrasion direction.

abrasion direction, shows strong arcs tailing off in intensity in one direction.

These asymmetric arcs became shorter when the electron beam was in an azimuth on one side or other of the above. Thus it is clear that parts of the lattice had been rotated through 40-50° about an axis which was evidently approximately [110].

Figure 19 obtained with the beam along the abrasion direction, "[$\bar{1}$10]", contains many spots corresponding to the initial crystal orientation and many additional spots or short arcs, occurring on nearly vertical "layer lines" midway between the nearly vertical rows of spots due to the initial crystal orientation. This confirms to a high accuracy that rotation had indeed occurred about the [110] axis. The presence of additional arcs corresponds to the reciprocal-lattice points crossing the Ewald sphere during the rotation. The arcs had a spread of about $\pm$ 2° from the mean, round the electron beam direction.

Further etching for 1½ minutes caused little change in the diffraction patterns as seen in figures 20 and 21, and still further etching merely reduced the angular range of the rotation progressively until practically undeformed underlying crystal surface was reached. The optical micrographs showed that the abrasion scratches have become still fainter than in

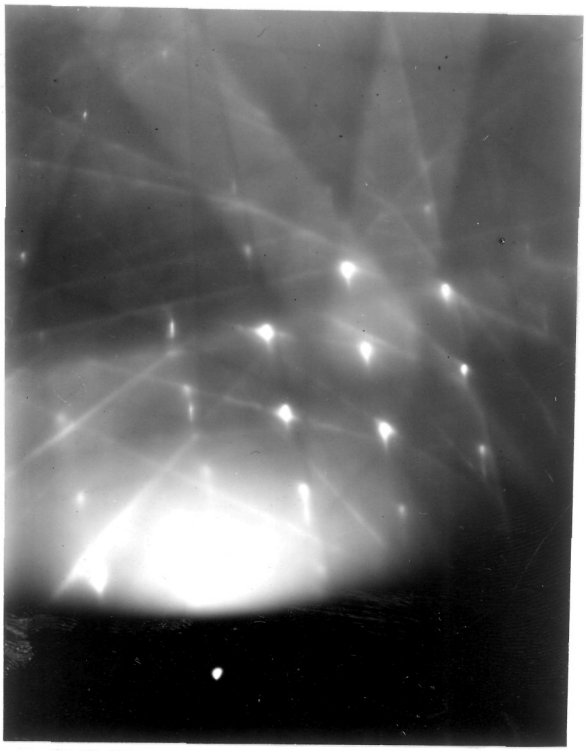

Fig 22. Electropolished (107) face, beam along [120].

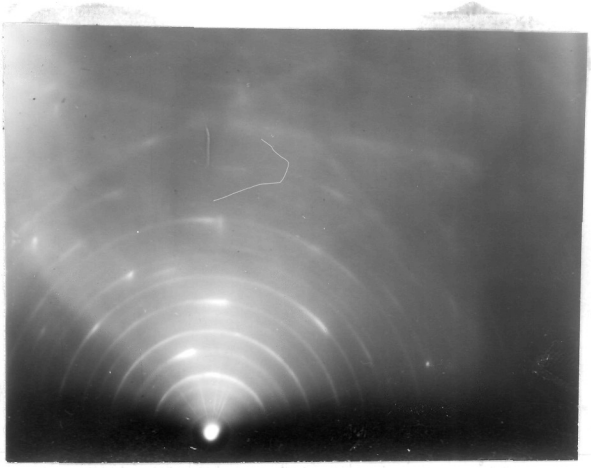

Fig23. (107)face, abraded [$\bar{2}$10], etched and electropolished, beam perpendicular to the abrasion dir.

figure 17. These results are closely similar to those found in case (iii) for iron by Evans, Layton and Wilman (1951). It may, however, be noted that in the present crystal, the surface was inclined by $8\frac{1}{2}°$ about [010] instead of by $10\frac{0}{2}$ about a $\langle 110 \rangle$ row.

2. Abrasion along "$[\bar{2}10]$".

Figure 22 shows the electron diffraction pattern obtained after re-electropolishing the surface. The sharp Kikuchi lines and elongated spots indicate that the surface was atomically smooth. The optical microscope showed a featureless surface without any trace of the scratches caused by the previous abrasion. The surface was then abraded and gradually etched in stages and examined both by electron diffraction and optical microscopy. After 4 minutes etching, it yielded electron diffraction patterns of well-defined Kikuchi lines and some strong spots corresponding to the initial crystal orientation, and also, with the beam normal to the abrasion direction, long arcs tailing off in one direction from the normal spots as seen in figure 23. The angular range of the stronger part of these arcs round the undeflected beam was about 20-25°, and the arcs extended with appreciable intensity up to 40-50°. The asymmetric arcs became progressively shorter when the crystal was displaced to

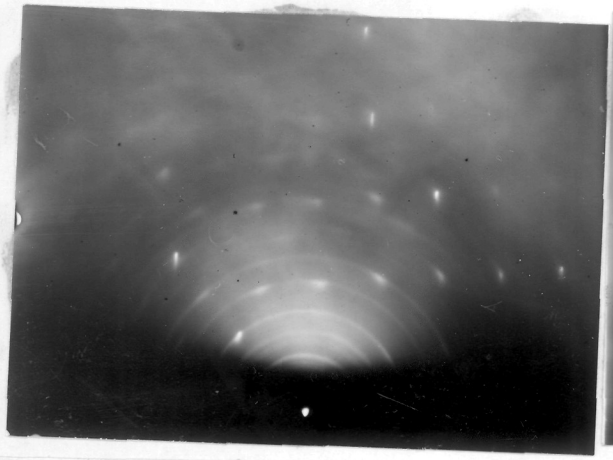

ig 24. (107) face, abraded [$\bar{2}10$], etched, beam along [$\bar{1}10$]

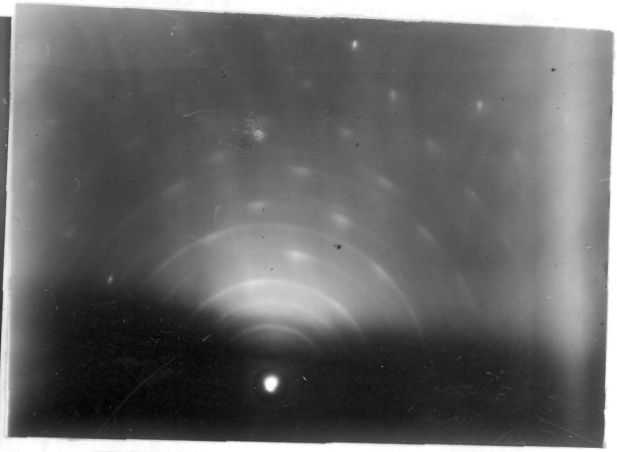

Fig 25. (107) face, abraded etched, beam along [$0\bar{1}0$].

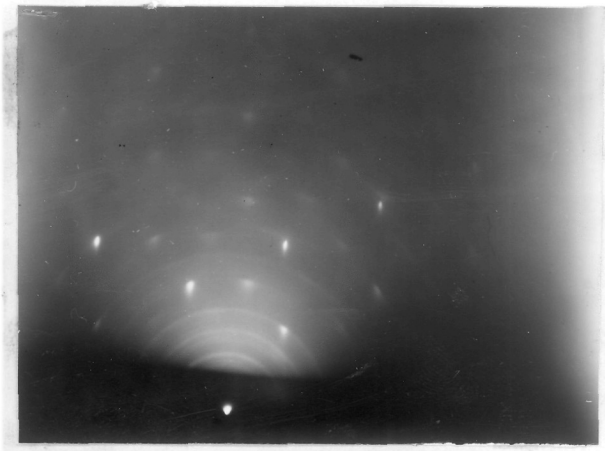

Fig 26. (107) face, abraded "[210]", etched, beam along the abrasion dir.

azimuths on one side or other of the above direction, and for example figures 24 and 25 were obtained with the beam along $[\bar{1}10]$ and $[0\bar{1}0]$ respectively.

It was thus evident that parts of the lattice near the surface had thus rotated by up to 50° about an axis approximately parallel to the "[120]" lattice row, which was practically normal to the abrasion direction.

Figure 26, obtained with the electron beam along the abrasion direction, agreed fully with this conclusion, and here the diffraction arcs were shortest and showed no asymmetric tailing off in intensity to one side or the other. The pattern at this azimuth shows clearly (to within two or three degrees accuracy) that the rotation axis was the [120] row in the (001) plane, not the direction lying in the crystal surface normal to the abrasion direction. The strong and vertically elongated spots in figure 26 correspond to smooth parts of the surface which had been unaffected and still retained the initial crystal orientation. These strong spots lie in a centred $\sqrt{6}$-rectangle pattern with the long side inclined at about 5° to the (horizontal) shadow edge.

The indexing of the normal spots and the additional short arcs in the above figure 26 is shown in figure 27, which was constructed from a reciprocal-lattice plan on (001), in the same way as described by Evans, Layton and Wilman (1951). For

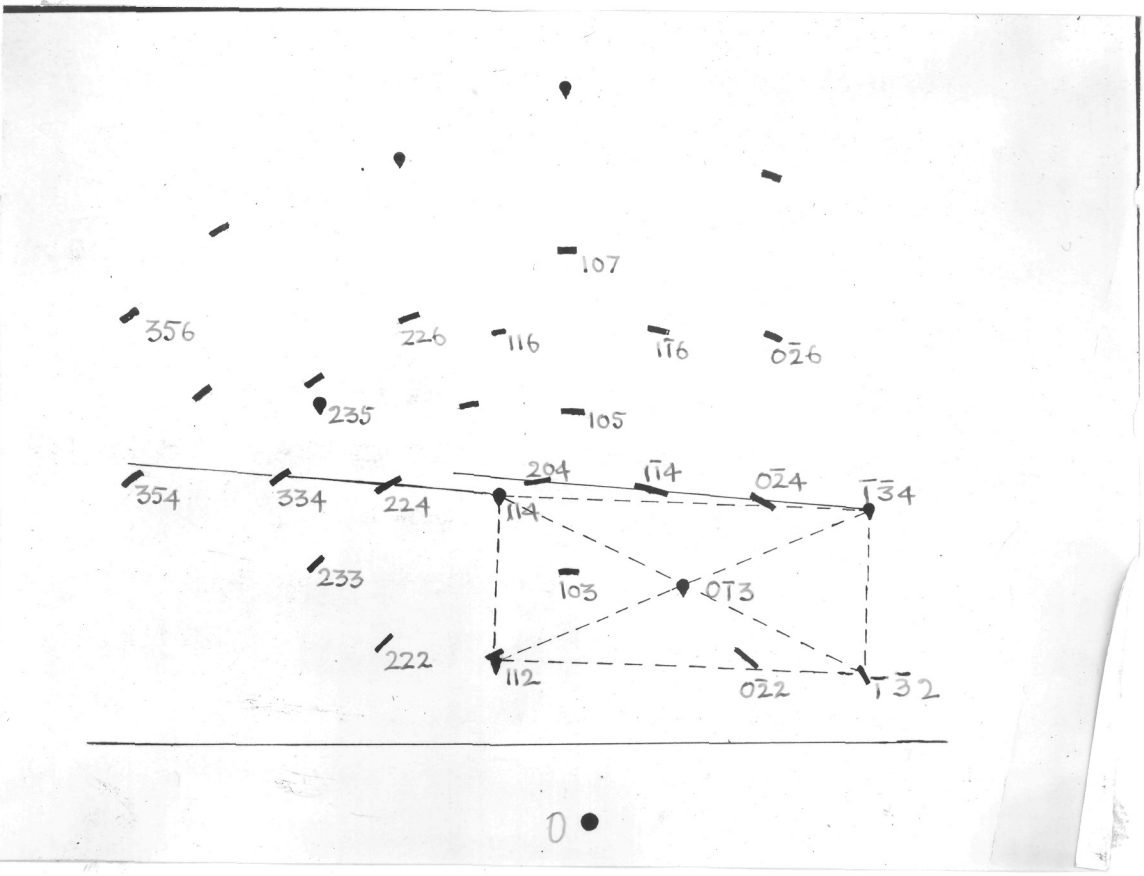

Fig 27. Indexing of figure 26.

example, the diffraction points $0\bar{2}4$, $1\bar{1}4$ and 204 occurring at distances 0.3, 0.6 and 0.9 times the long side of $\sqrt{6}$ rectangle from the strong $\bar{1}\bar{3}4$ spot fully stand in evidence that the rotation axis was [120]. The extent of arcing of these additional diffractions in figure 26 is only about $\pm 1\frac{1}{2}$ to 2° about the abrasion direction in the case of those diffractions which occur as a result of lattice rotation attaining 12° from the initial orientation about the [120] axis normal to the abrasion direction.

On further etching the crystal in stages, the electron diffraction patterns obtained were of similar type to the above except a progressively smaller range of rotation of the lattice at the then exposed lower levels. The crystal was therefore electropolished far enough to remove the disturbed layer caused by abrasion. At this stage, it yielded electron diffraction patterns similar to figure 22, showing the surface to be highly perfect and atomically smooth.

The above experiment was repeated, i.e. the crystal was abraded along $[\bar{2}10]$, and again the results were in agreement with the above conclusion.

3. Abrasion along 17° off $[\bar{1}10]$ towards $[0\bar{1}0]$, i.e. very close to $[\bar{2}10]$.

After re-electropolishing the (107) iron surface, figure 28 was obtained by electron diffraction. The smooth-

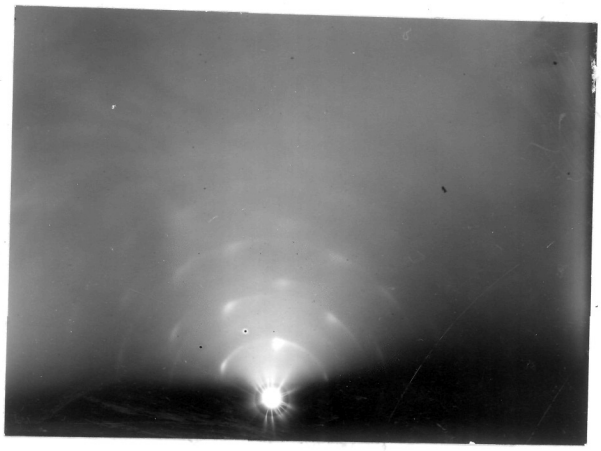

Fig 28. electropolished (107) face, beam along [$\bar{1}$10].

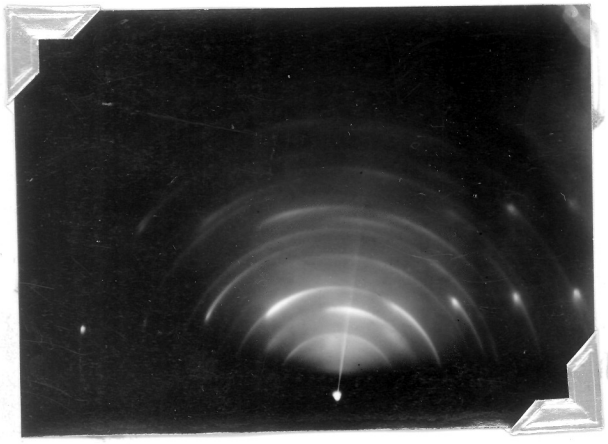

Fig 29. Abrasion along 17° off [$\bar{1}$10] on (107), etched, beam perp to abrasion dir.

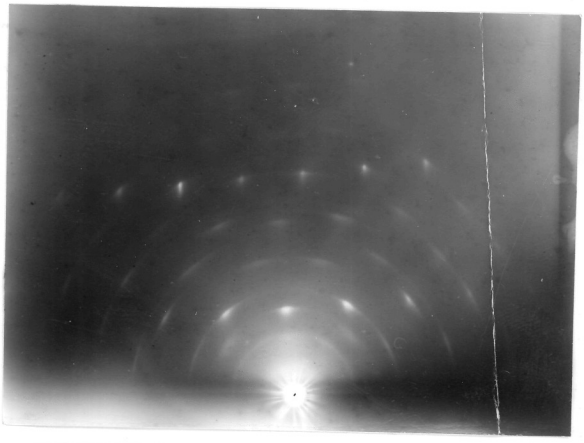

Fig 30. Abrasion along 17° off [$\bar{1}$10] on (107), etched, beam along abrasion dir.

-ness and perfection of the crystal surface could be seen by sharpness of Kikuchi lines. After etching the abraded surface for a total of 6 minutes 45 seconds, electron diffraction examination of this etched surface showed Kikuchi lines and some of the normal spots corresponding to the initial orientation and with the beam normal to the abrasion direction, long arcs tailing off in one direction from the nromal spots were also present, as shown in figure 29. The angular range of the strong part of these arcs, round the undeflected beam spot, was 35° with appreciable intensity of the aforesaid arcs up to 65°. On grazing the crystal surface with the beam on either side from this position, unsymmetrical arcs were obtained, showing that the rotation axis was practically normal to the abrasion direction.

With the beam parallel to the abrasion direction, figure 30 was obtained, which contains short arcs lying on vertical layer lines, together with normal (slightly elongated) spots corresponding to the initial crystal orientation. The extent of arcing of these additional diffractions in figure 30 is only about $\pm$ 6° about the electron beam, i.e. the abrasion direction.

This fully conforms that the rotation axis in this case was practically normal to the abrasion direction, which was 17° off $[\bar{1}10]$, i.e. very near to the direction of $[\bar{2}10]$. This

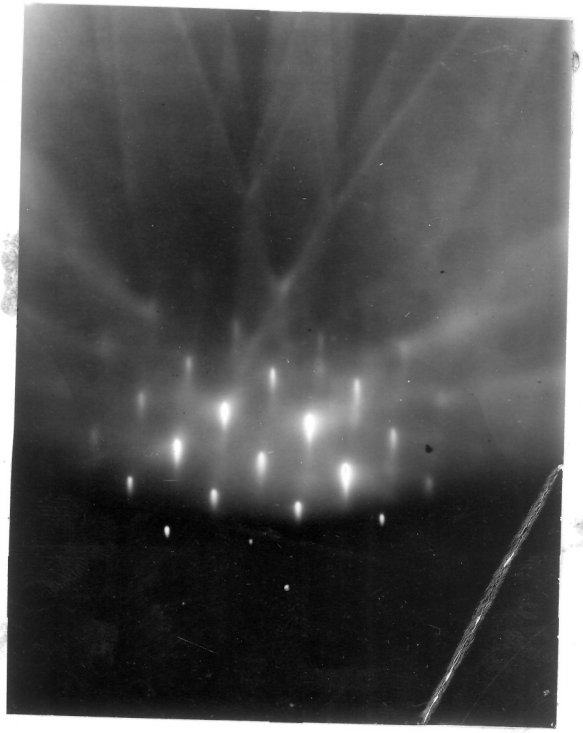

Fig 31. Optical micrograph. 600x.

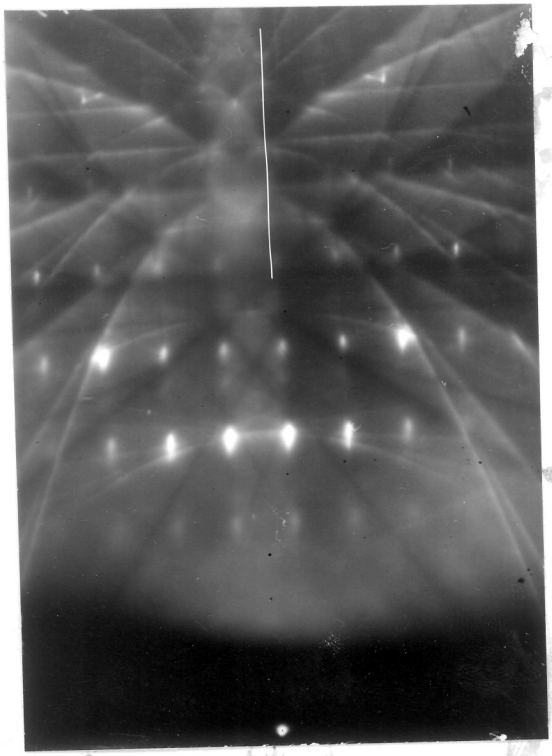

Fig 32. Electropolished (107) beam along [100].

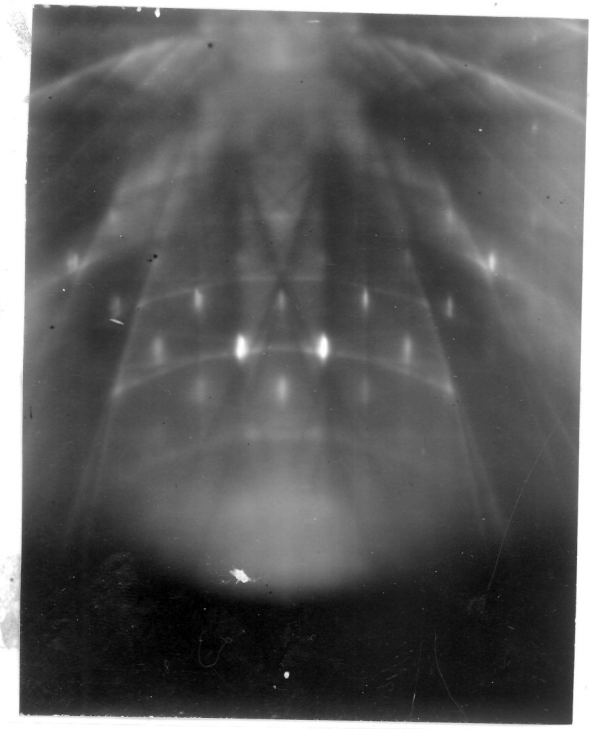

Fig 33. Electropolished(107) face, beam along [010].

conclusion thus also supports the previous results in §2 of Part 1A.

Figure 31 shows the channel-shaped parallel scratches obtained after abrasion in the above direction, at this stage of etching. Some sratches initially present immediately after abrasion, have disappeared, but the deeper ones are still present. Apart from this, the microscope does not indicate in any way the nature of the deformation of the surface region.

On further electropolishing and etching the crystal surface, the arcs became shorter until there was no trace of any disturbance of the crystal lattice at the surface. The electron-diffraction pattern yielded at this stage showed clear Kikuchi lines and elongated spots indicating the smoothness of the surface and its high perfection.

4. Abrasion along "[100]".

After re-surfacing the crystal face by electropolishing, it was examined by electron diffraction, which once again showed sharp Kikuchi lines and elongated spots as seen in figure 32 and 33, confirming the undistorted and atomically smooth nature of the surface. It was then abraded in the "[100]" direction and etched for 45 seconds in 1% picric acid in alcohol. The patterns obtained with the beam perpendicular

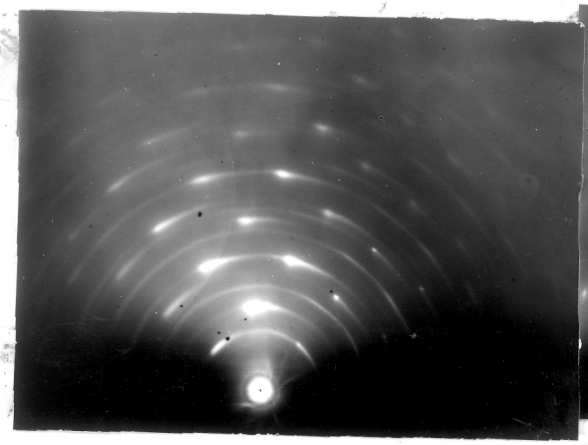

Fig 34. (107) face, beam perpendicular to abrasion direction.

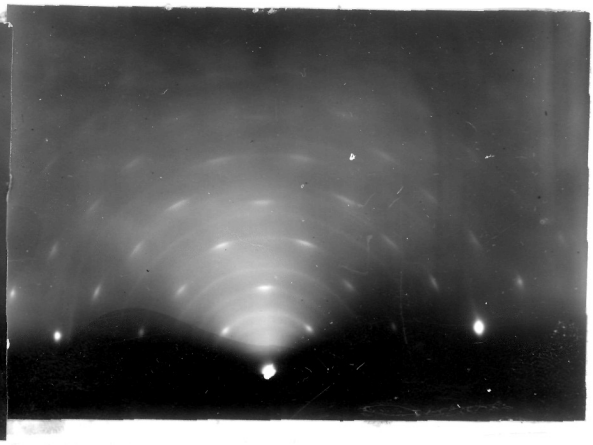

Fig 35. (107) face, beam parallel to abrasion.

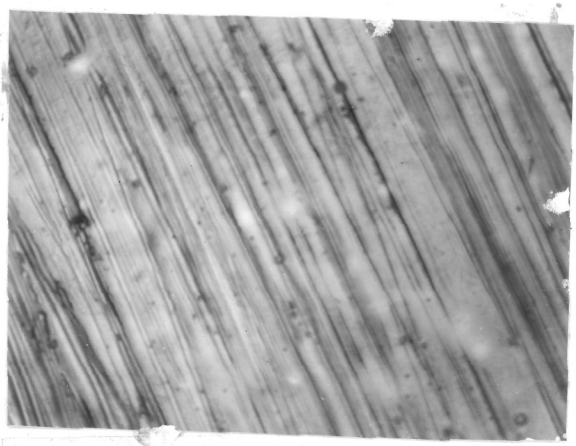

Fig 36. Optical micrograph 600x.

and along the abrasion direction are shown in figures 34 and 35 respectively. Figure 34 mainly consisted of the normal square spot pattern associated with the initial crystal orientation, rotated round the undeflected beam spot through about 50-60° of arc, the arcs tailing off in intensity continuously in one direction along each arc. Thus, parts of the lattice had been rotated about 50-60° about an axis parallel to or very close to the beam direction i.e. [010].

Short symmetrical arcs are present in figure 35 which was obtained with the beam parallel to the abrasion direction, i.e. [100]. These arcs correspond to the square array of lattice points in the (001)* plane through the origin in the reciprocal lattice, and these reciprocal lattice points cross the Ewald sphere almost simultaneously after a rotation of $8\frac{1}{2}°$ from the initial crystal orientation. As compared with this main rotation of $8\frac{1}{2}°$ about [010], it was also observed that the amount of arcing of these diffractions corresponded to a spread of about $\pm$ 3° of rotation about the abrasion direction, i.e. [100]. The presence of other fainter additional diffraction arcs is associated with the rotation of parts of the lattice through angles larger than $8\frac{1}{2}°$ about [010]

Figure 36 shows the ...ph of the surface after 45 seconds etching in 1% picric acid and alcohol, corresponding to the electron diffraction patterns of figures 34 and 35.

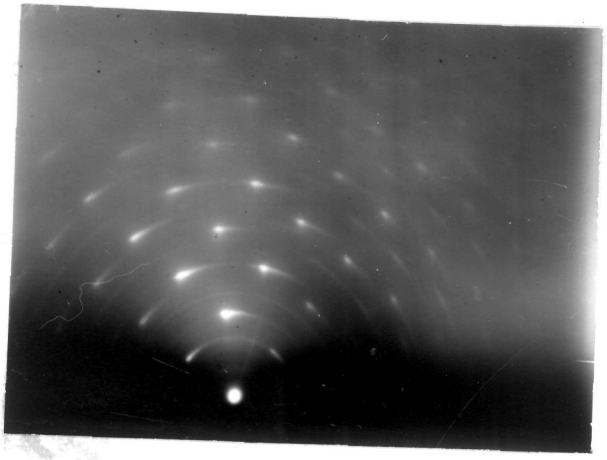

Fig 37. Further etching from fig 34, beam ⊥r to abrasion.

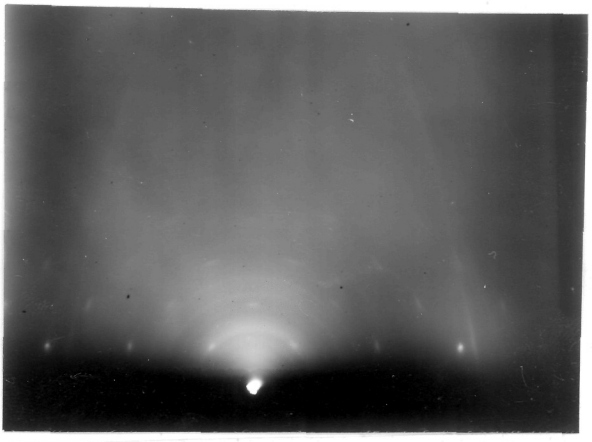

Fig 38. As fig 37but beam parallel to abrasion.

Some of the channel shaped scratches have become fainter from the stage when the surface was abraded. Apart from this the micrograph does not show any other sign of deformation.

Further etching for 1½ minutes practically reduced the angular range of arcing by about half the amount, as seen in figures 37 and 38, obtained with the beam normal to and along the abrasion direction, respectively. Further etching for 45 seconds, reduced the range of arcing almost to nothing and the electron diffraction patterns showed undeformed single crystal structure.

The crystal surface was next smoothed by electropolishing to prepare again a smooth and perfect surface and the above experiment was then repeated with practically similar results.

5. Abrasion along "[$\bar{1}$00]".

Another abrasion experiment was carried out on the crystal after freshly resurfacing it by electropolishing, but this time the abrasive motion was along [$\bar{1}$00], opposite to that of §4. After several minutes of etching the surface yielded electron diffraction patterns similar to figure 34, when the beam grazed the surface in a direction perpendicular to the abrasion direction. The angular array of the arcs, which tailed off in intensity in one direction, indicates that the

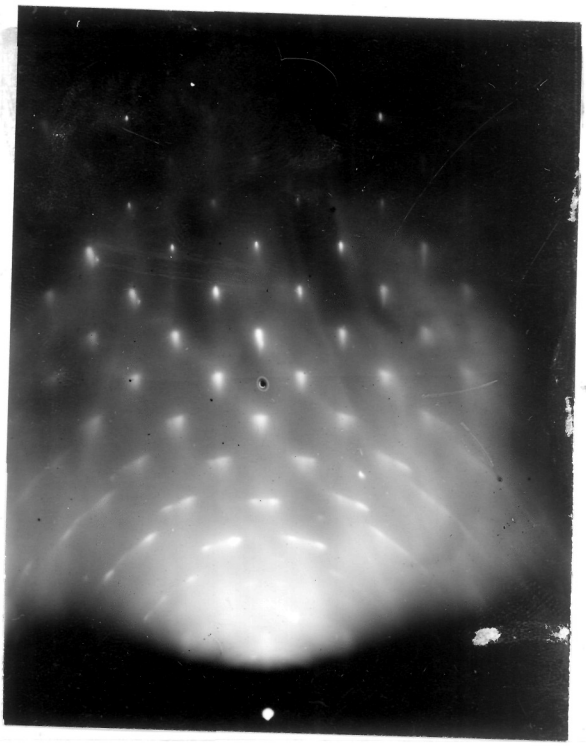

Fig39. As fig32 after abrasion "[$\bar{1}$00]" and etched ; beam along [100].

parts of the crystal had rotated by up to 40-50° about an axis roughly in the surface and normal to the abrasion direction. At this stage, when the beam was along the abrasion direction, the patterns yielded consisted mainly of rings due to body-centred-cubic ∝-iron.

The etching of the crystal was carried out in stages up to 12 minutes and at each stage the surface was examined by electron diffraction and by optical microscopy. The diffraction patterns obtained with the beam along the abrasion direction still did not show any well defined vertical layer lines. On the other hand, the angular range of asymmetric arcing was progressively reduced to only 10°, when the electron beam was normal to the abrasion direction. After 45 seconds subsequent electropolishing of the crystal surface, the arcing was still more reduced to only about 5° range extending from the strong spots which corresponded to parts of the crystal which still had the initial crystal orientation. Figure 39 shows the interesting pattern obtained with the beam along [100], i.e. opposite to the abrasion direction.

In the upper part of figure 39, in the region of the circular zone of stronger spots round the point where the [100] cube edge met the plate, there are sharp strong and elongated spots in an array of squares whose sides are at 45° to the shadow edge. These spots correspond to the initial

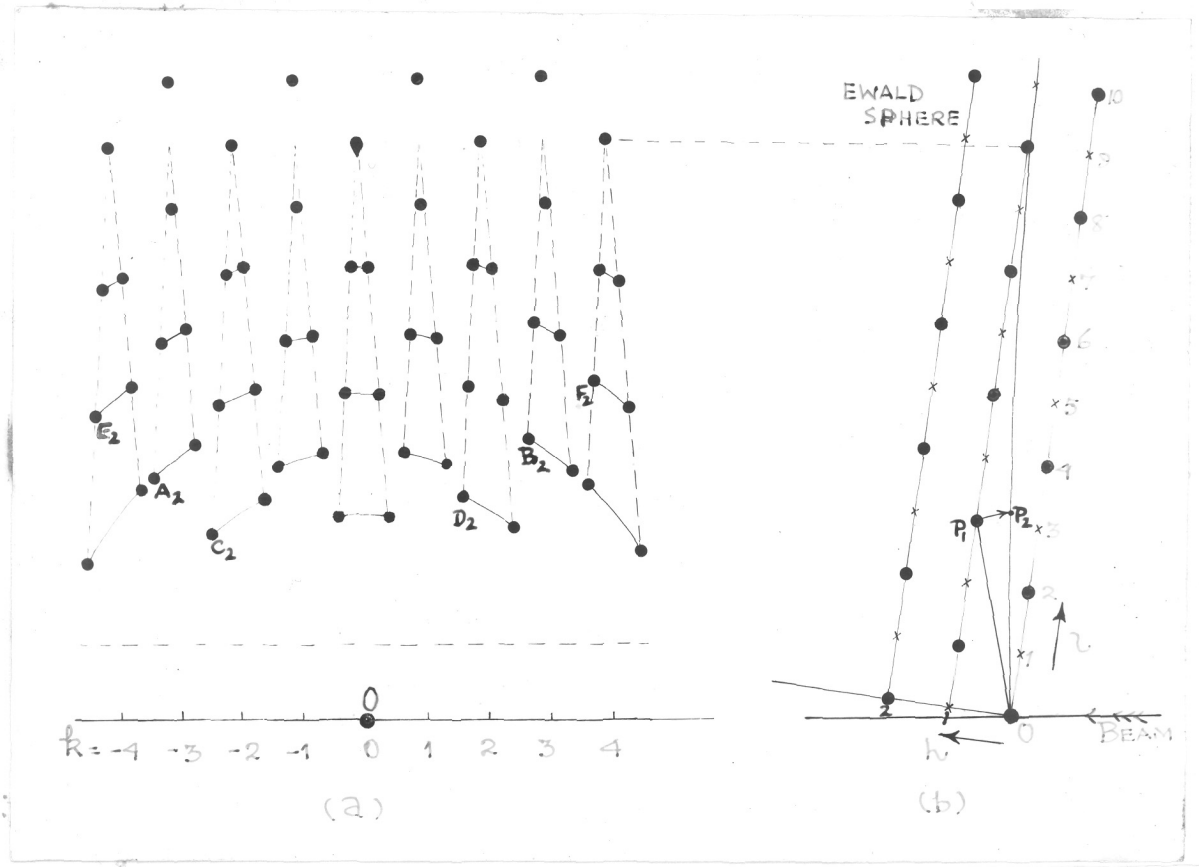

Fig 40. Diagram for indexing of figure 39 :- (a) spotpositions; (b) side view (along rotation axis [010]) of part of reciprocal lattice in initial orientation.

crystal orientation and can be compared with figure 32, obtained from the freshly polished surface, at the same azimuth, before any abrasion was carried out. Some additional short arcs are seen in the lower parts of figure 39, which at first sight appear to be the continuation of the pattern of spots due to the initial crystal orientation, along vertical layer lines, as seemed indicated by the tailed arcs obtained from the perpendicular azimuth. If the additional diffractions are carefully inspected, it is seenthat these are not single short arcs but pairs of spots joined together by a faint continuous arcs, as in figure 40(a). Both spots of each pair lie at the same radial distance from the undeflected-beam spot but are practically equally displaced to one side or the other from the appropriate vertical rows of spots corresponding to the initial crystal orientation.

These characteristics, together with the regular increase in the distance apart of the spots of these pairs, towards the lower region of the pattern (see figure 39), suggest that parts of the lattice had rotated about one axis and others about another. These two axes are symmetrically disposed relative to the (010) plane (which is the plane of incidence of the electron beam in figure 39) but are inclined away from the [010] axis. The spots corresponding to these rotations suggest that the extent of rotation at this stage of etching

was nearly 5°, which agreed with the extent of the asymmetrical arcing in patterns at the perpendicular azimuth.

Using a method based on Ewald's reciprocal lattice construction, the directions of these rotations axes were estimated. The positions of the strong spots corresponding to the initial crystal orientation were used to define the location of the Ewald sphere relative to the reciprocal lattice, as shown in section on the (010)* plane in figure 40(b). Next the co-ordinates [[hkl]]* of points such as P_2 corresponding to the observed additional spots, were found relative to the axes $\underline{a}^*$, $\underline{b}^*$, $\underline{c}^*$ of the initial reciprocal lattice. The h_2 and l_2 co-ordinates relative to $\underline{a}^*$ and $\underline{c}^*$, were obtained sufficiently accurately from the diagram as in figure 40(b), drawn to a scale such that the Ewald sphere radius was 480 cms. (i.e. 10 times the camera length). Then k_2 was estimated directly from figure 39, by considering the spot positions relative to the vertical rows of normal spots present in the upper region of the pattern. The direction of these vertical rows of spots was precisely determined by the row which passed through the undeflected-beam spot. Each point such as P_2 on the Ewald sphere in figure 40(b), corresponding to an additional spot in the pattern, is brought into the position P_2 by the rotation from the initial point P_1 whose co-ordinates are $[[h_1 k_1 l_1]]^*$ relative to the initial reciprocal lattice axes.

The line joining P_1 and P_2 has thus indices $[\underline{u}\underline{v}\underline{w}]^*$ given by $[\underline{h}_2-\underline{h}_1, \underline{k}_2-\underline{k}_1, \underline{l}_2-\underline{l}_1]^*$ and is perpendicular to the rotation axis. Thus the indices $[\underline{U}\underline{V}\underline{W}]^*$ of the rotation axis are related to $[\underline{u}\underline{v}\underline{w}]^*$ by the zone relation:-

$$\underline{u}\underline{U} + \underline{v}\underline{V} + \underline{w}\underline{W} = 0 \quad \ldots\ldots\ldots\ldots\ldots\ldots \quad (1)$$

The co-ordinates $[[\underline{h}\underline{k}\underline{l}]]^*$ of the initial reciprocal lattice points $A_1, B_1, C_1 \ldots$, and of the points $A_2, B_2, C_2 \ldots$ where, during the rotation, they cross the Ewald sphere as shown in figure 40(b), are tabulated in Table 3. The points $A_2, B_2, C_2 \ldots$ etc. were all associated with the same rotation axis of the symmetrical pair. The indices $[\underline{u}\underline{v}\underline{w}]^*$ of the lines A_1A_2, B_1B_2, etc. are shown in Table 4.

To find directly the ratio $\underline{U}:\underline{V}$, the co-ordinates of $[\underline{u}'\underline{v}'1]^*$ and suitable pairs of equations of type (1) were then combined as shown in Table 5(a). The nine most accurate determinations of $\underline{V}/\underline{U}$ were 1.35, 1.57, 1.41, 1.44, 1.61, 1.50, 1.31, 1.51 and 1.31; and the mean of these values gave $\underline{U}:\underline{V}$ as 1:1.44. Similarly as shown in Table 5(b), the most precise estimates of $\underline{W}/\underline{U}$ were 0.08, 0.33, 0.19, 0.00, 0.29, 0.15, 0.14, 0.38 and 0.23, giving a mean value of $\underline{U}:\underline{W}$ = 1:0.20. In this way, six diffraction spots, A, B, C, D, E and F gave a combined mean estimate of $\underline{U}:\underline{V}:\underline{W}$ as 1 : 1.44 : 0.20. Within the obtainable accuracy, it seems most probable that the axis of rotation in this case corresponds to the [451] axis, which

Table 3. Coordinates [[hkl]]*, relative to the reciprocal lattice of the initial crystal, of initial lattice points $A_1, B_1, C_1 \ldots$ and of the points $A_2, B_2, C_2 \ldots$ where, during the rotation, they cross the Ewald sphere, in the case of abrasion of (107) along [$\bar{1}$00].

	A_1	A_2	B_1	B_2	C_1	C_2	D_1	D_2
h	-1	-0.49	-1	-0.57	-1	-0.38	-1	-0.44
k	-3	-3.40	3	2.70	-2	-2.43	2	1.71
l	-4	-3.65	-4	-4.35	-3	-2.77	-3	-3.31

	E_1	E_2	F_1	F_2
h	-1	-0.60	-1	-0.66
k	-4	-4.35	4	3.81
l	-5	-4.67	-5	-5.37

Table 4. Indices [uvw]* of the lines joining pairs of points such as A_2 and A_1 of Table 3.

	A_2-A_1	B_2-B_1	C_2-C_1	D_2-D_1	E_2-E_1	F_2-F_1
u	0.51	0.43	0.62	0.56	0.40	0.34
v	-0.40	-0.30	-0.43	-0.29	-0.35	-0.19
w	0.35	-0.35	0.23	-0.31	0.33	-0.37

Table 5a(i). To find directly the ratio of U:V, the coordinates of [uvw]* as in Table 4 were modified to take up a form [u'v'1]*.

	1 A_2-A_1	2 B_2-B_1	3 C_2-C_1	4 D_2-D_1	5 E_2-E_1	6 F_2-F_1
u'*	1.47	-1.24	2.71	-1.80	1.218	-0.930
v'*	-1.14	0.86	-1.87	0.94	-1.061	0.514
w'*	-1.00	-1.00	-1.00	-1.00	-1.00	-1.00

Table 5a(ii). Suitable pairs of equations of the type (1) were combined to give directly the ratio of U:V.

Suitable pairs from Table 5a(i)	U : V	Suitable pairs from Table 5a(i)	U : V
1 - 2	1:1.35	3 - 6	1:1.50
1 - 4	1:1.57	5 - 2	1:1.31
1 - 6	1:1.41	5 - 4	1:1.51
3 - 2	1:1.44	5 - 6	1:1.31
3 - 4	1:1.61		

Mean value of U:V = 1 : 1.44

Table 5b(i). To find directly the ratio of U:W, the coordinates of [uvw]* as in Table 4 were modified to take up a form [u'1 w']*

	1 A_2-A_1	2 B_2-B_1	3 C_2-C_1	4 D_2-D_1	5 E_2-E_1	6 F_2-F_1
u'*	1.28	1.44	1.45	1.92	1.49	1.81
v'*	-1.00	-1.00	-1.00	-1.00	-1.00	-1.00
w'*	-0.88	1.17	-0.54	1.07	-0.94	1.95

Table 5b(ii). Suitable pairs of equations of the type (1) were combined to give directly the ratio of U:W

Suitable pairs from Table 5b(i)	U : W	Suitable pairs from Table 5b(i)	U : W
1 - 2	1:0.08	3 - 6	1:0.15
1 - 4	1:0.33	5 - 2	1:0.14
1 - 6	1:0.19	5 - 4	1:0.38
3 - 2	1:0.00	5 - 6	1:0.23
3 - 4	1:0.29		

Mean value of U:W = 1 : 0.198

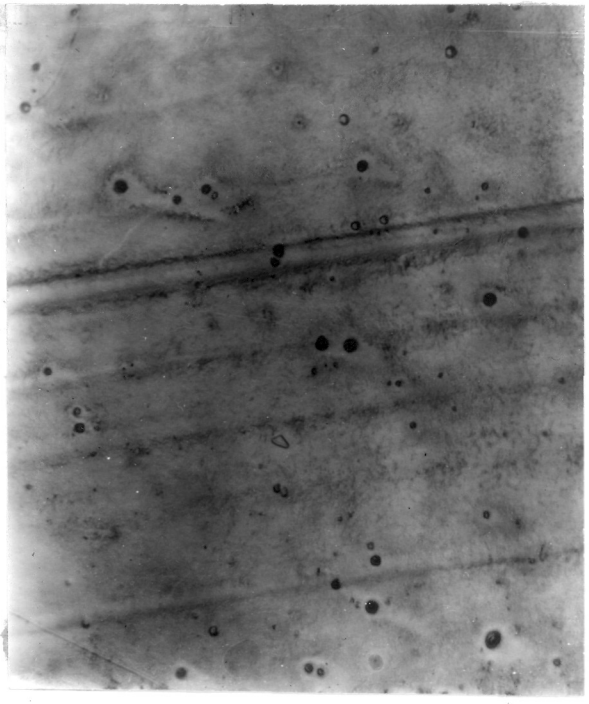

Fig 41. Optical micrograph from the area from where fig 39 was obtained. - 600x.

is the axis of flexure of $(\bar{2}13)$ slip lamellae, since [451] is perpendicular to the slip direction $[1\bar{1}1]$ in the $(\bar{2}13)$ plane. The other axis of rotation, symmetrically disposed to (010), is $[4\bar{5}1]$ direction, which lies in the $(2\bar{1}3)$ plane and is normal to [111].

The micrograph (Figure 41) taken at this stage of etching still shows some parallel scratches remaining, together with etch pits. The black lines represent the still visible depressions where the deepest scratches occurred, while the white lines suggest raised regions at the side of the scratch depressions. The hazy lines correspond to scratches which are on the verge ofdisappearance. No information regarding the fragmentation of the crystal surface could be recognised from the micrograph, to supplement that yielded by the electron diffraction pattern.

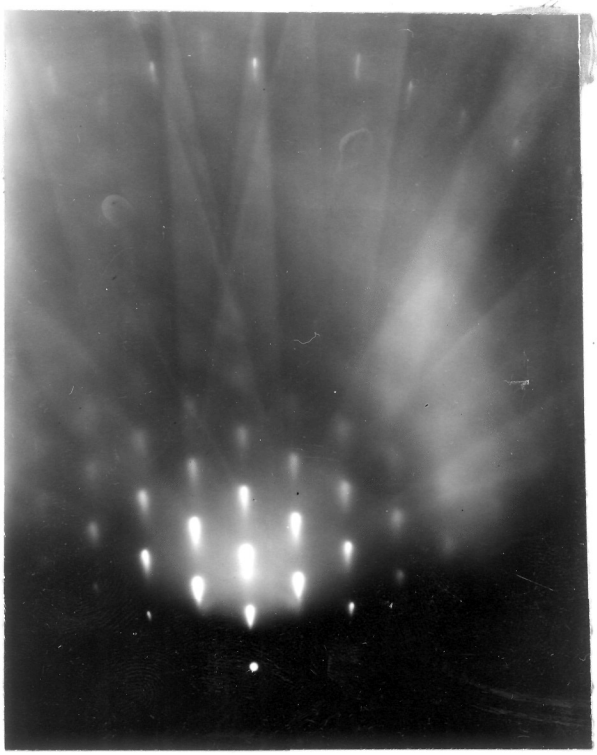

Fig 42. Electropolished (110) face, beam along [1$\bar{1}$0].

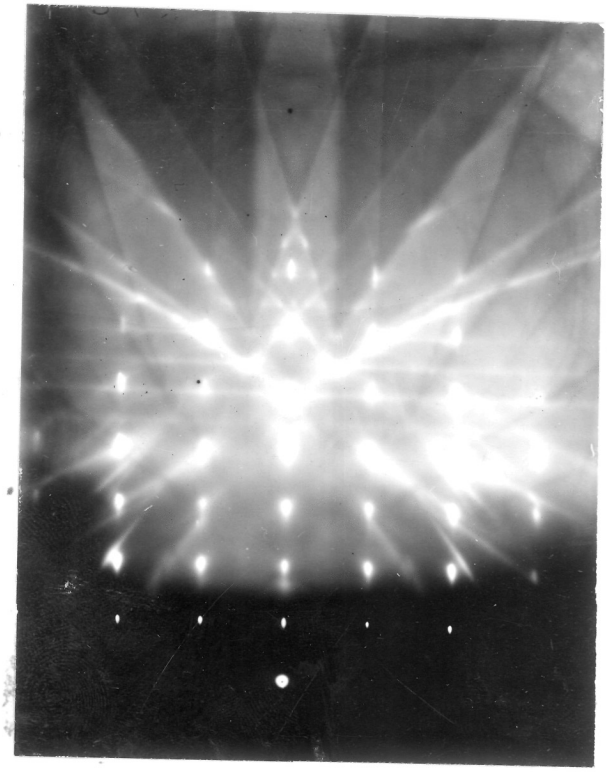

Fig 43. Electropolished (110) face, beam along [11$\bar{1}$].

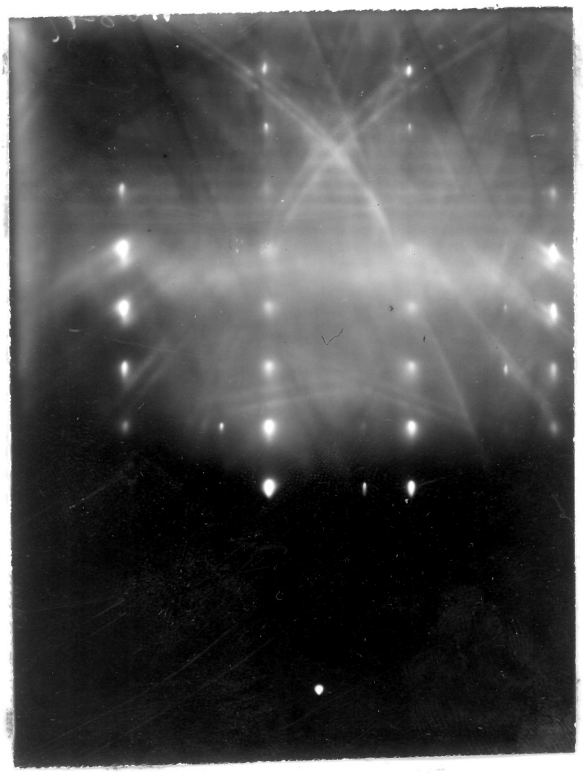

Fig 44a. Electropolished (110) face, beam along [11$\bar{2}$].

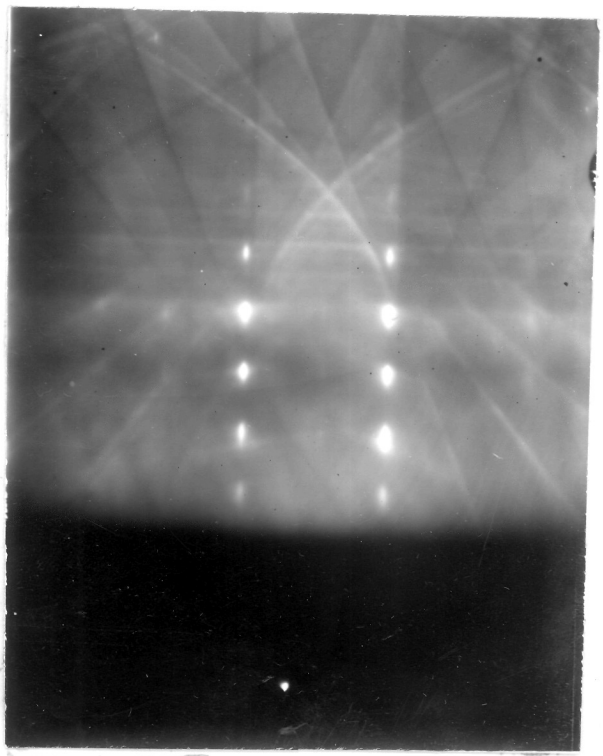

Fig 44b. Electropolished(110) face, beam alomg [11$\bar{2}$].

B. Experiments on the approximately (110) face.

The crystal face was carefully smoothed first with emery paper of different grades in succession and then by electropolishing to remove the work hardened surface layer. Examination of the surface by electron diffraction then yielded the patterns of figures 42, 43 and 44(a), and enabled the direction of main lattice rows to be determined relative to the surface. The sharp and strong Kikuchi lines together with the elongated spots normal to the shadow edge show that the surface was atomically smooth and that the crystal was highly perfect.

One region of the (110) iron surface yielded patterns which showed presence of some {211} twinning. Fig.44(b), obtained in the $[1\bar{1}2]$ azimuth, shows the normal pattern of spots in the $\sqrt{6}$-rectangle arrangement as in figure 44(a), but there are in addition spots forming a similar pattern which is displaced to the left (in the positive shown in figure 44(b)) from the normal pattern by a distance of one third of the horizontal rectangle side. This is clearly the reflection of the normal pattern in the plane of incidence, which is the (111) plane of the main crystal, thus the additional spots correspond to the (111) reflection twin of the main crystal. In the body-centred-cubic structure, however, it is usual to designate this as of the equivalent {211} type of twinning.

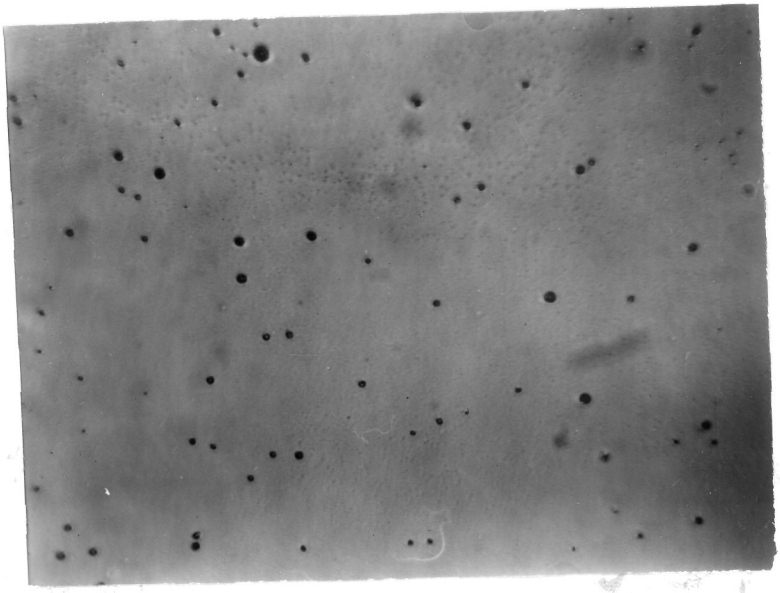

Fig 45. Optical micrograph showing electropolished surface. 600 x

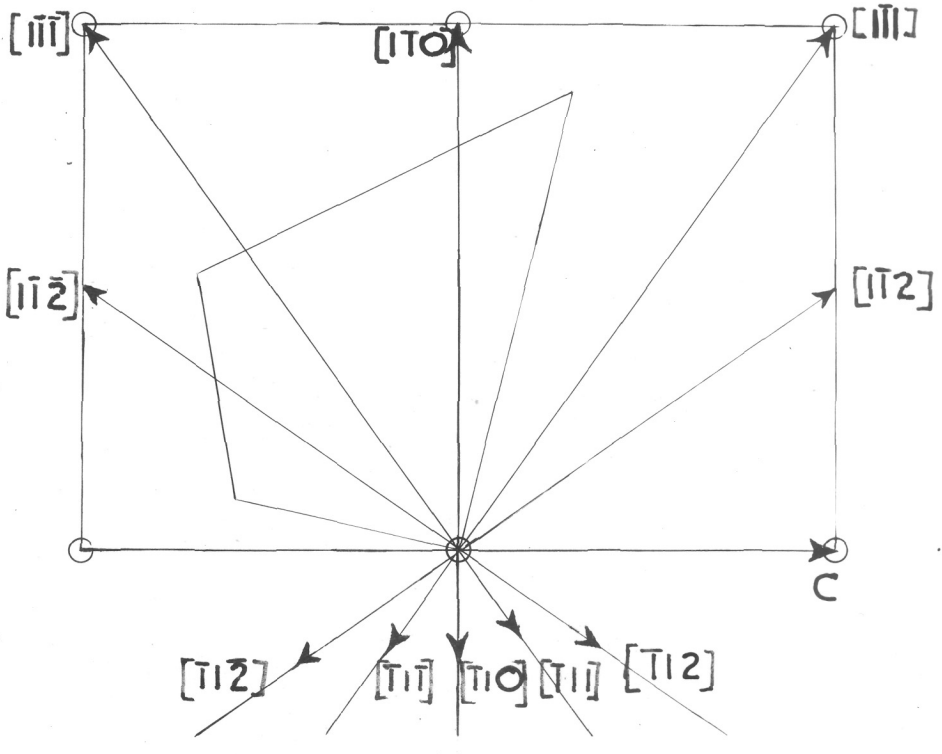

Fig 46.

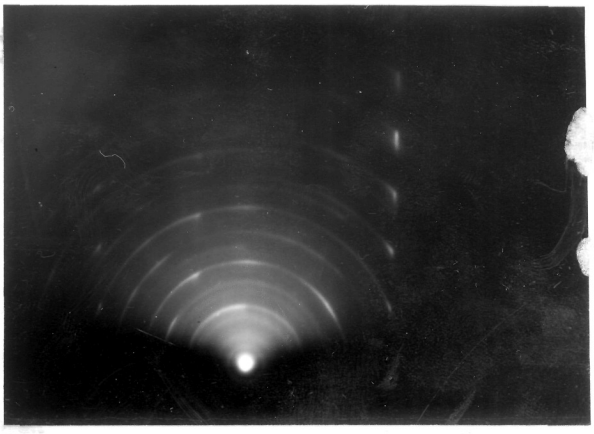

Fig 47. beam perpendicular to abrasion.

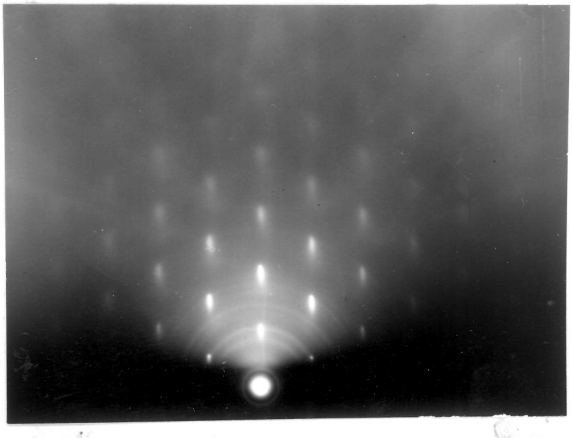

Fig 48. Beam parallelto abrasion.

The optical microscopic examination of the crystal surface also gave almost featureless micrograph (Fig.45). Figure 46 shows the direction in which the crystal was abraded relative to the axes chosen.

1. Abrasion along $[\bar{1}11]$.

After the abrasion along $[\bar{1}11]$ and etching for 3 minutes 40 seconds, the electron diffraction pattern, figure 47, with the beam normal to the abrasion direction, yielded some spots forming a $\sqrt{6}$-rectangle due to the still undistorted parts of the crystal surface, and long arcs tailing off in one direction from such normal spots. The range of such arcing varies from 40-45° showing that the rotation of parts of the surface region of the lattice had thus evidently taken place about $[1\bar{1}2]$ or some neighbouring direction. However, with the beam along the abrasion direction, only ring patterns such as figure 48 were observed, showing randomly disorientated fragments, together with some spots from the still undistorted regions, and no clear groups of arcs along vertical layer lines were visible. even after much further etching up to nearly 4 minutes down to the practically undisturbed lower region of the crystal. Although the rotation axis was thus not identifiable more closely, it is clear that it corresponded to that described *below in §4 of Part 1(B).*

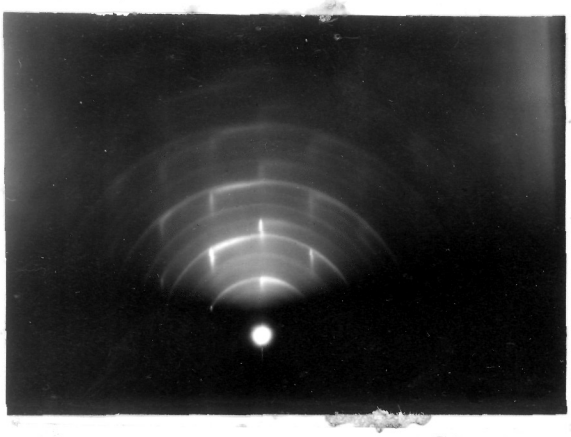

Fig49. Beam along [1$\bar{1}\bar{1}$]

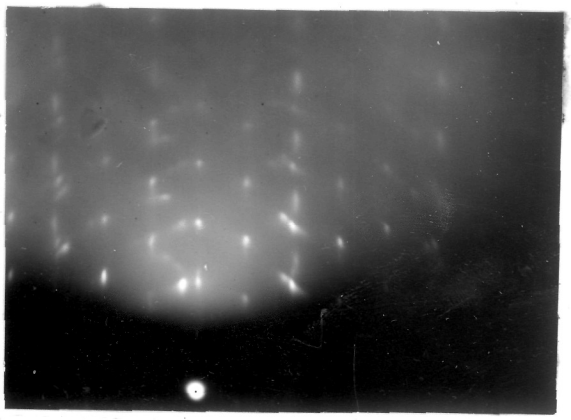

Fig 50. (110) face abraded 8° off[$\bar{1}$1$\bar{2}$], etched and electropolished, beam along [1$\bar{1}$2].

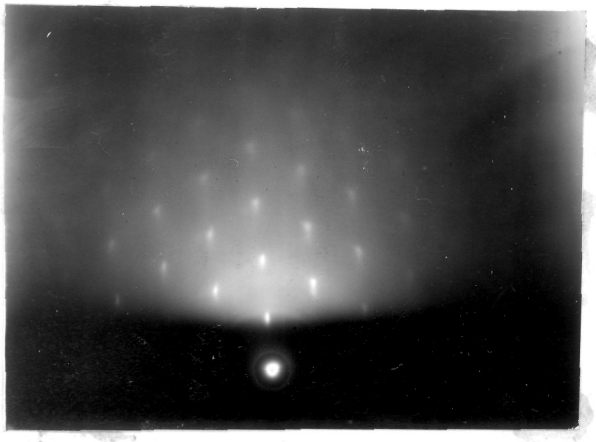

Fig 51. As fig 50, but beam along [1$\bar{1}$1].

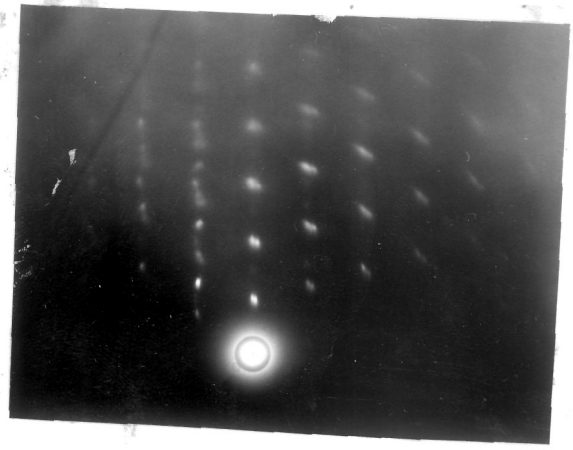

Fig 52. As fig 50, but beam along [00$\bar{1}$].

Fig 53. As fig 50, beam parallel to abrasion.

2. Abrasion along a direction 8° from [$\bar{1}1\bar{2}$], on the side towards [$00\bar{1}$].

This time also, the electropolished iron surface after being abraded in the above direction, yielded after etching in 1% picric acid in alcohol, the electron diffraction pattern of figure 49 showing long arcs tailing off in one direction from the spots of the normal pattern, when the beam was normal to the abrasion direction. The angular arcing in the pattern suggests that the fragments had rotated by up to 30° from the initial crystal orientation about an axis parallel to [$\bar{1}11$] or nearly so. Even after gradual etching and slight electropolishing, when the beam was along [$\bar{1}1\bar{2}$] (i.e. 8° away from the abrasion direction), the electron diffraction patterns mainly consisted of rings from randomly disorientated iron fragments. The optical micrograph at this stage showed nothing except parallel channel-shaped abrasion scratches. The continuous rings when the beam was in the [$\bar{1}1\bar{2}$] direction made it impossible to specify the rotation axis more closely.

After ten seconds total electropolishing an etching in 1% picric acid in alcohol, the crystal yielded clear spot patterns in practically all the azimuths. These spot patterns, figures 50, 51, 52, and 53 obtained respectively with the beam along [$1\bar{1}2$], [$1\bar{1}\bar{1}$], [$00\bar{1}$] and the abrasion direction, i.e. (8° from [$\bar{1}1\bar{2}$] on the side towards [$00\bar{1}$]), are similar to those described in Part 1 (B) §§3 and 4. The main diffraction spots in these patterns are

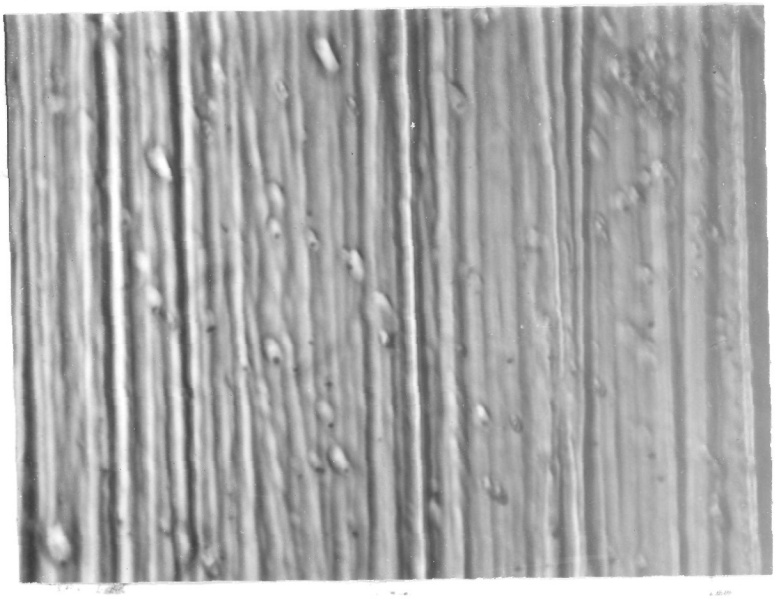

Fig 54. Optical micrograph 600x.

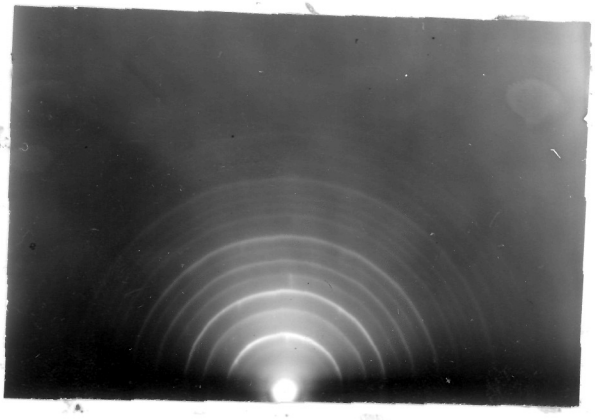

Fig 55. Beam perpendicular to abrasion.

due to epitaxially orientated γ-iron and are dicussed in detail in Part 2.

The micrograph (figure 54) taken at this stage, shows parallel channel-shaped abrasion scratches together with some etch pits having a parallel orientation. Some of the deeper scratches are still clearly visible, illustrating the extent to which the surface is not homogeneous. In between the main remaining scratches, there are some obscure traces of shallower scratches on the verge of disappearance. Nothing else can be recognised which might be attributed to the orientated γ-iron crystals.

3. Abrasion along $[\bar{1}1\bar{2}]$.

To remove all the traces of previous abrasions, the crystal was resurfaced by five to six minutes' electropolishing till the electron diffraction patterns showed clear and sharp Kikuchi lines and elongated spots, indicating the high perfection of the crystal and high smoothness of the surface to an atomic scale. It was then abraded along $[\bar{1}1\bar{2}]$ by the standard single stroke. On examination in the electron diffraction camera, the pattern figure 55 was obtained when the beam was perpendicular to the abrasion direction, which shows practically randomly disorientated iron fragments together with slight traces of spots due to normal crystal orientation. After etching for four minutes, the electron diffraction pattern

contained arcs tailing off in one direction from the normal spots, when the beam was normal to the abrasion direction; but the patterns showed only rings when the beam was along the abrasion direction. At this stage, the crystal surface was next electropolished very slightly, i.e. for only 5 seconds and this resulted in a large part of the surface yielding the usual patterns of arcs tailing off in one direction.

However, the remaining part of the surface, which had evidently undergone much lighter abrasion as compared to that described above, yielded at various azimuths patterns consisting mainly of sharp strong spots with faint Kikuchi lines. These spot patterns are due to orientated γ-iron and are described in Part 2, §1. The Kikuchi lines, together with a few faint spots, correspond to the main undistorted α-iron substrate. Microscopic and visual examination showed that the surface, though highly smooth after the initial electropolishing, must have been not perfectly flat and hence it had not been uniformly abraded. The thin surface layer of disorientated material from the less abraded regions had been more extensively removed by progressive etching and electropolishing, while the thicker layers from the heavily abraded parts had been proportionally less removed.

When the beam was grazing the heavily abraded region of the crystal along $[1\bar{1}\bar{1}]$, i.e. normal to the abrasion direction,

Fig 56. (110)abraded "$[\bar{1}1\bar{2}]$" and etched; beam ⊥r to abrasion

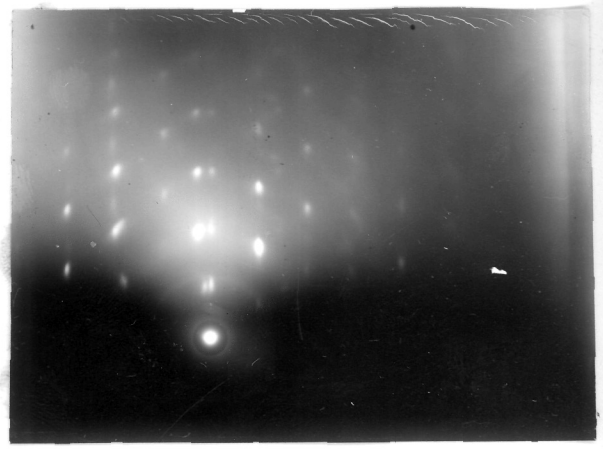

Fig 57. As fig 56, but beam parallel to abrasion.

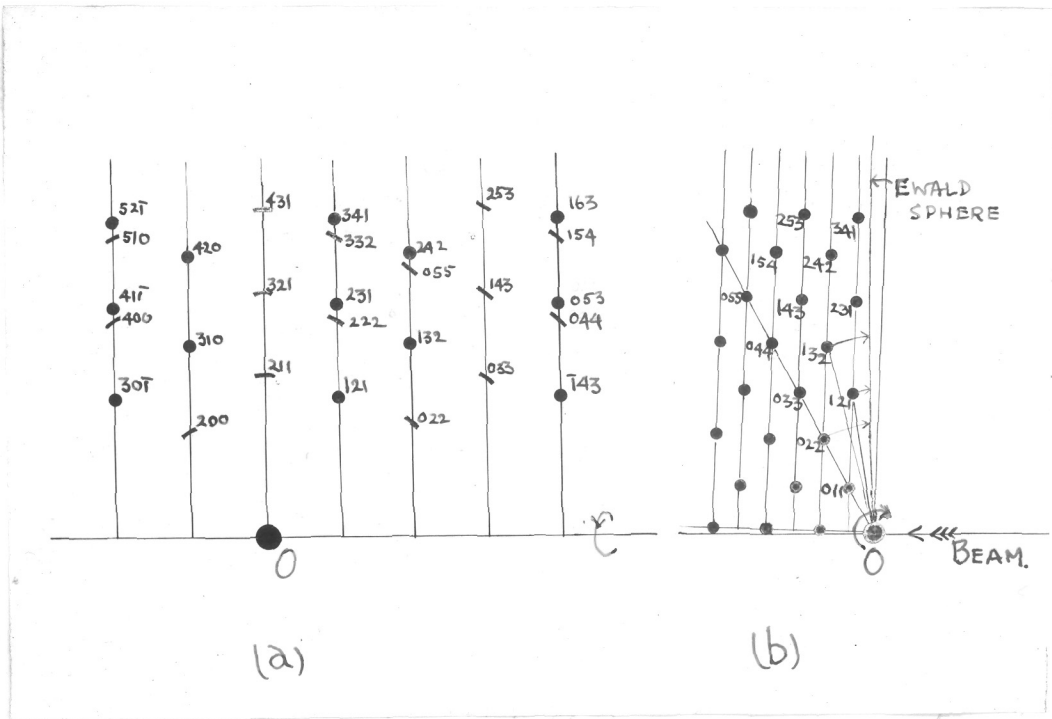

Fig58. Indexing of figure 57:- (a) diffraction positions and indices; (b) side view along rotation axis of part of reciprocal lattice.

figure 56 was obtained. This pattern contains the normal hexagonal pattern of spots due to undistorted normal crystals together with arcs extending in one direction from these spots round the ring positions. The strongest parts of each arc subtend an angle of 30° at the undeflected beam spot, while the arcs extend with weaker intensity up to 60° extent. This arcing suggests that the axis about which the fragments had been rotated from the initial crystal orientation was approximately $[1\bar{1}\bar{1}]$, i.e. normal to the $(1\bar{1}\bar{1})$ planes. Figure 57 was obtained from the same region but with the beam along the abrasion direction, i.e. $[\bar{1}1\bar{2}]$, the pattern again showing some spots from the normal crystal orientation and also very short arcs lying on the corresponding roughly vertical layer lines.

From the reciprocal-lattice construction shown in figure 58 for the above pattern, a detailed analysis was carried out which confirms the rotation axis as $[1\bar{1}\bar{1}]$ within an accuracy of estimation of two or three degrees. By comparing figure 57 with the indexed diagram of the diffraction positions, together with the side view along the rotation axis of the parts of the reciprocal lattice (figure58), it is seen that the spread of diffractions is quite small relative to the angle of rotation from the initial crystal lattice orientation. The diffractions 321 and 211, for example, have a spread of

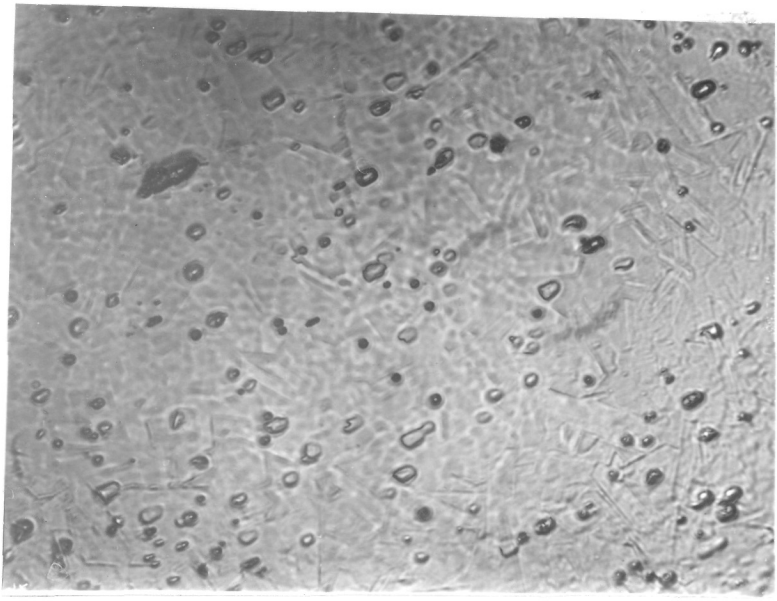

Fig59a. Optical micrograph with phase contrast, 600x.

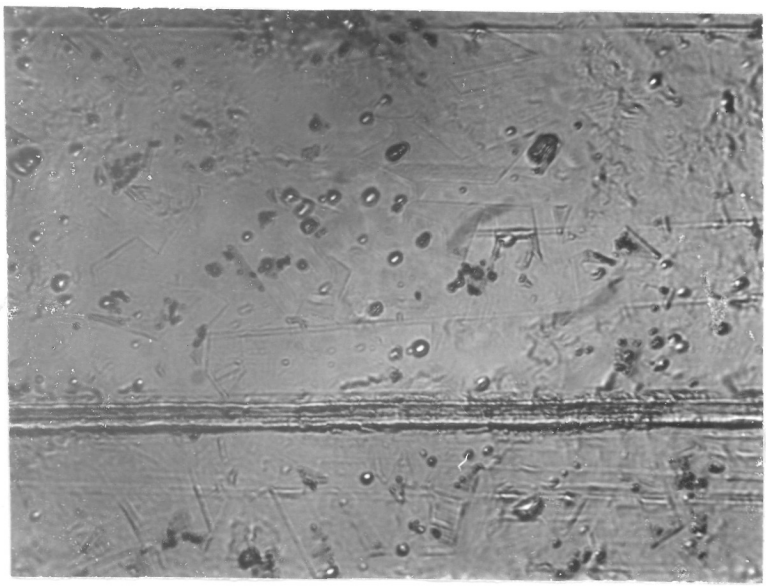

Fig 59b. Optical micrograph with phase contrast, 600x.

only about ± 2° and ± 3° respectively from the mean position, although they occur as a result of a lattice rotation of roughly 16° and 27½° respectively round the $[1\bar{1}\bar{1}]$ rotation axis (cf. figure 58).

On electropolishing the crystal for a further 5 seconds, the electron diffraction patterns obtained with the beam perpendicular to the abrasion direction showed Kikchi bands and elongated spots due to the main α-iron crystal orientation, with only negligible arcing of the spots. Five seconds additional electropolishing removed all the remaining disturbed surface layer and left a highly perfect and smooth crystal surface as shown by the electron diffraction patterns of sharp Kikuchi lines and elongated spots in all the azimuths.

The micrograph, figure 59(a) and (b), were obtained from the less heavily abraded part of the crystal, at the stage of etching where the electron diffraction patterns of spots due to orientated γ-iron were obtained, as described in Part 2, §1. These micrographs show that the abrasion scratches have mostly disappeared, leaving a few traces of abrasion here and there. Many long narrow rectangles can be seen in figures 59(a) and (b), scattered all over the region under examination, but their orientation is not sufficiently clear-cut to permit their interpretation reliably, thus it is at present uncertain whether these could correspond to the γ-iron crystals or their $\{111\}$ twins.

4. Abrasion along $[\bar{1}11]$.

The iron crystal was again electropolished for 5 to 6 minutes to remove all traces of previous abrasion and to obtain a smooth surface. Optical microscopic examination then showed an almost featureless (110) surface. It was then abraded along $[\bar{1}11]$, which yielded ring patterns indicating randomly disorientated α-iron. Etching for 2 minutes in 1% picric acid in alcohol, followed by 2 seconds electropolishing, removed the layer of randomly disorientated α and γ-iron and exposed a region which yielded figures 60 and 61, when the electron beam was perpendicular to and along the abrasion direction, respectively.

Figure 60 shows the usual long arcs, tailing off in one direction from the normal diffraction-spot positions associated with the initial crystal orientation. It is obvious that parts of the lattice had thus rotated about an axis which was not far from the beam direction $[\bar{1}1\bar{2}]$. Figure 61 (beam along the abrasion direction) confirms this conclusion by the positions of the arcs and the fact that they are short and not tailing off asymmetrically. Here, however, it is clear that the rotation had not been about $[\bar{1}1\bar{2}]$, which would have caused the main diffraction arcs to be in the positions shown in figure 63 which was constructed from the reciprocal-lattice

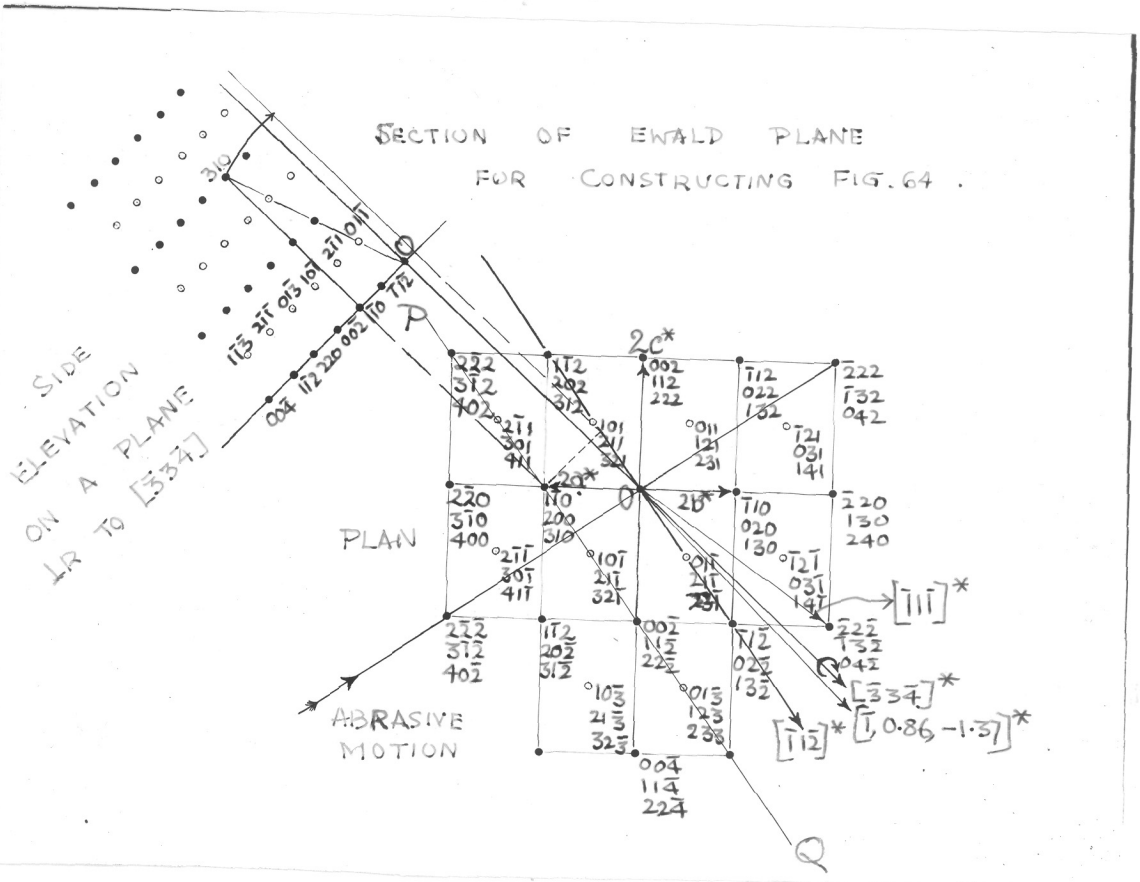

Fig 62. Ewalds reciprocal lattice construction for figure 61.

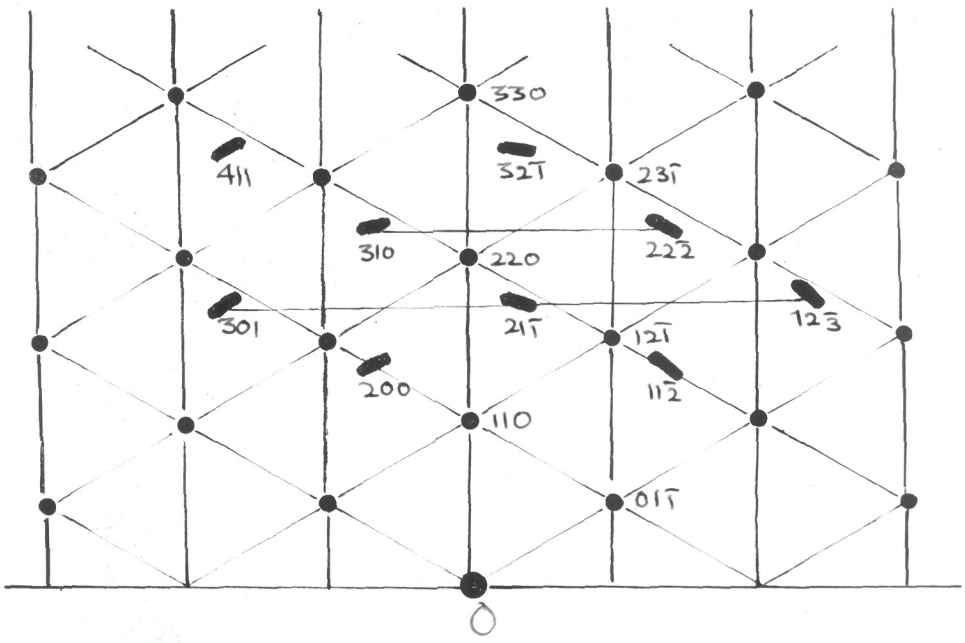

Fig 63. The position of main diffraction arcs when the rotation axis was [$\bar{1}$12].

plan shown in figure 62. For example, the line joining the 301, $21\bar{1}$ and $12\bar{3}$ arcs, and the line joining the 310 and $22\bar{2}$ arcs, would then be horizontal and parallel to each other, and normal to the 110 radius vector in figure 63, instead of being inclined at $3\frac{1}{2}°$ to the horizontal as in figure 61. These arcs would also then be displaced too far to the right in the negative (i.e. to the left in the positive, figure 61). On the other hand, the rotation cannot have taken place about the $[\bar{1}1\bar{1}]$ row which was in the surface (110) plane but at 21° to $[\bar{1}1\bar{2}]$, because this would have resulted in the $21\bar{1}$ and $32\bar{1}$ arcs being centred on the plane of incidence, which is not the case.

The method based on Ewald's reciprocal-lattice construction, as used in Part 1(A) §4, was therefore applied to estimate the rotation axis directly from the observed arc positions. Table 6 shows the indices of reciprocal-lattice points lying in the $(1\bar{1}\bar{1})^*$ plane next to that through the origin, seen in the plan in figure 62 as the line PQ. The indices (relative to the axes of the reciprocal lattice corresponding to the initial crystal) are also given for the points where these lattice points cross the Ewald sphere during the rotation. These indices were calculated from the observed arc positions relative to the faint sharp spots which correspond tothe initial crystal orientation (marked by small

Table 6. Coordinates [[hkl]]*, relative to the reciprocal lattice of the initial crystal, of initial points $A_1, B_1, C_1 \ldots$ and of the points $A_2, B_2, C_2 \ldots$ where, during the rotation, they cross the Ewald sphere, in the case of abrasion of (110) along $[\bar{1}11]$.

	A_1	A_2	B_1	B_2	C_1	C_2	D_1	D_2
h	2	1.64	3	2.52	1	0.75	2	1.64
k	1	1.81	2	2.76	1	1.97	2	2.83
l	-1	-0.17	-1	-0.23	-2	-1.22	-2	-1.19

	E_1	E_2	F_1	F_2	G_1	G_2
h	1	0.76	3	2.50	3	2.52
k	2	2.94	0	0.70	1	1.65
l	-3	-2.18	1	1.80	0	0.87

Table 7. Indices [uvw]* of the lines joining pairs of points such as A_2 and A_1 of Table 6.

	A_2-A_1	B_2-B_1	C_2-C_1	D_2-D_1	E_2-E_1	F_2-F_1	G_2-G_1
u	0.37	0.48	0.26	0.36	0.24	0.50	0.49
v	-0.81	-0.76	-0.97	-0.83	-0.94	-0.70	-0.65
w	-0.83	-0.77	-0.78	-0.81	-0.82	-0.80	-0.87

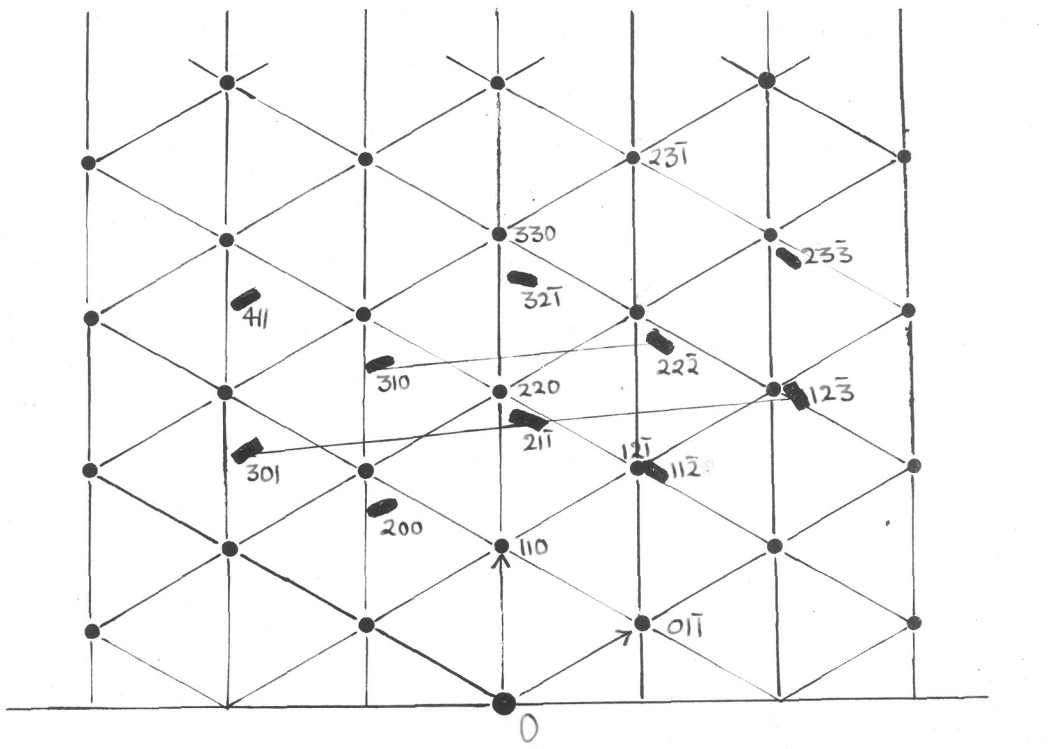

Fig 64. the position of main diffraction arcs, when the rotation axis was [$\bar{3}3\bar{4}$].

filled in circles in figures 63 and 64). The differences between the two sets of indices, given in Table 7, represent the indices of lines which are normal to the rotation axis $[\underline{U}\underline{V}\underline{W}]$*. They lead as before (taking the most accurate combinations) to the following determinations of the ratio $\underline{V}/\underline{U}$: 0.37, -1.07, -0.77, -0.43, -0.52, -2.13, -1.12, -0.37, -0.83, -1.27, -0.65, -1.12 and -0.51; and to the following estimates of ratio $\underline{W}/\underline{U}$: 0.86, 1.72, 1.39, 0.89, 1.03, 2.65, 1.71, 0.83, 1.28, 1.77, 1.03, 1.77 and 0.92.

The mean estimate of the above values thus gives $\underline{U} : \underline{V} : \underline{W} = -1 : 0.86 : -1.37$, defining $[\underline{U}\underline{V}\underline{W}]$ to an accuracy of the order of 2-3°. This axis is shown in the plan in figure 62 and is inclined downward about 4° from the hroizontal plane (110) on which the plan is made. A diagram was then constructed, showing the pattern of arcs which would result from rotation of the initial crystal lattice about this axis, and this still showed some appreciable discrepancies relative to the observed pattern, figure 61.

Figure 64 shows the positions of the arcs (301, $21\bar{1}$, $12\bar{3}$ etc.) resulting from a rotation of roughly 30° about an axis $[\bar{3}3\bar{4}]$, which lies in the (110) plane near the above estimated direction of the rotation axis. The main discrepancy still present is that the rows of arcs such as that on which lie 301, $21\bar{1}$ and $12\bar{3}$, are at 5° to the horizontal

(i.e. the normal to the 110 radius vector in figure 64) instead of $3\frac{1}{2}°$ observed, and this suggests that the rotation axis is at about this azimuth in the (110) plane but inclined down about 1° and thus slightly more inclined away from the actual crystal surface than was the (110) plane.

Thus the symmetrical arcs seen in figure 61 are accounted for as being due to a rotation about an axis very close to $[\bar{3}3\bar{4}]$. In figure 62, those arcs which tail off in one direction from the spots associated with the initial crystal orientation also correspond well to this rotation axis. There are, however, other prominent arcs still not explained in figure 61, for example on the 110, 211, 321 and 310 ring positions. At first sight it appeared as if parts of the lattice had rotated about an axis near $[\bar{1}10]$, which would account quite well for the positions of the arcs concerned on the 110, 211, 321 and 310 ring positions. It would also account largely for their relative intensities except, however, the marked absence of a $2\bar{2}\bar{2}$ diffraction centred on or near the plane of incidence, although the $1\bar{1}\bar{2}$ arc was moderately strong.

The true explanation, however, for the presence of all these additional arcs is evidently that they result also from the above $[\bar{3}3\bar{4}]$ rotation, but appear only because the surface projections through which the electron beam can pass, and which therefore contribute to the pattern, are thin (i.e. of

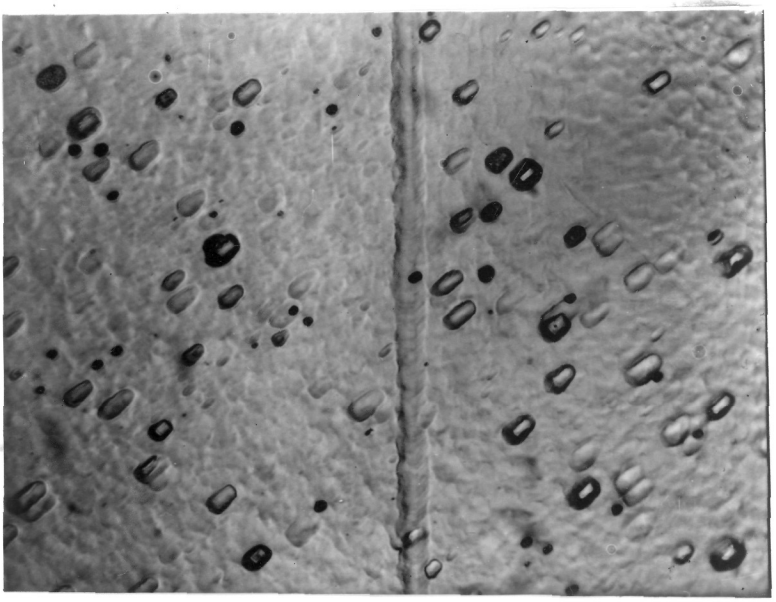

Fig 65. Optical micrograph.

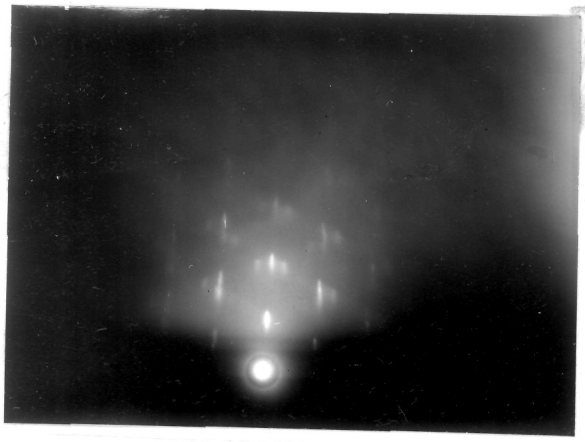

Fig 66. Beam along [1$\bar{1}$1] γ-iron spots mainly.

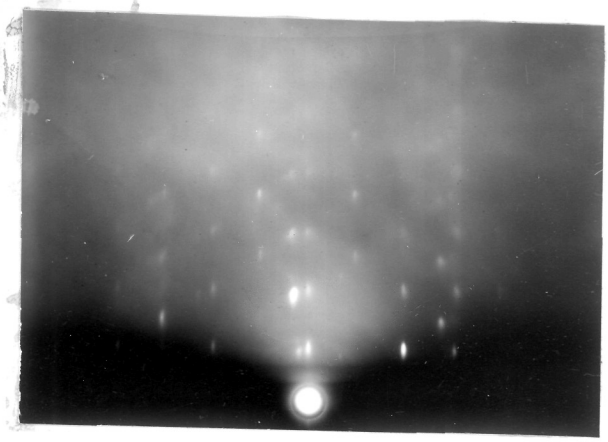

Fig 67. Beam along [1$\bar{1}$2] γ-iron spots mainly -, α-iron Kikuchi bands.

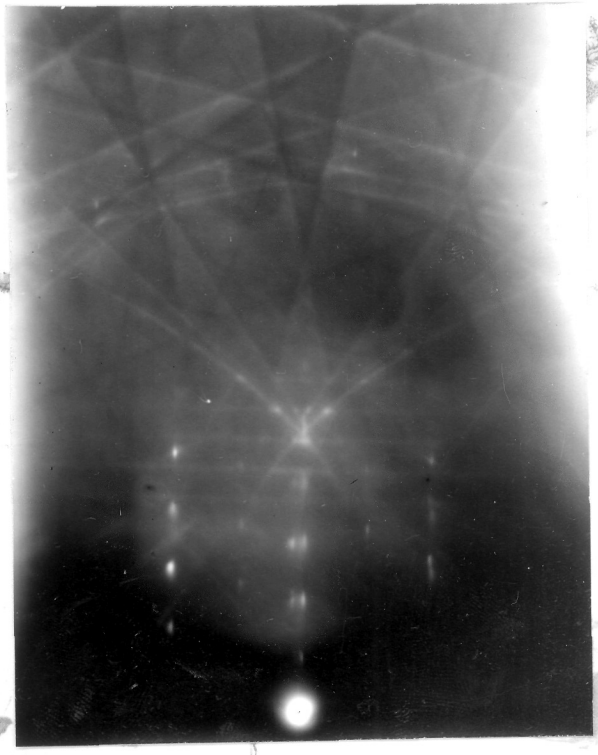

Fig 68. Beam along [1$\bar{1}$0]. Fe pattern with spot groups due to {11?} facets.

limited extent) in the beam direction. The optical micrograph, figure 65, shows the appearance of the surface. The presence of the additional arcs corresponds, in terms of Ewald's reciprocal-lattice construction, to an extension in (or near) the beam direction, of the reciprocal-lattice intensity regions surrounding the lattice points, so that these extensions cross the Ewald sphere even though the lattice points themselves do not cross the sphere. In the present case such extensions, together with the established $[\bar{3}3\bar{4}]$ rotation would indeed give rise to the observed arcs. The correspondingly similar pattern figure 47, described in Part 1(B), § 1 and obtained with the beam normal to the same $[\bar{1}11]$ abrasion direction but with the beam in the opposite sense, shows more clearly the correctness of this interpretation.

After electropolishing for a further 5 seconds (i.e. a total of 2 mins. of etching, followed by 7 secs. electropolishing) part of the crystal which was evidently more lightly abraded than the part which still yielded arc patterns, gave figures 66 and 67. These spot patterns show the presence of γ-iron strongly orientated relative to the main α-iron crystal. Similar patterns obtained in Part 1(B), § 3 are discussed in detail in Part 2, § 1.

Figure 68 taken at the same stage shows the presence of iron diffractions but with groups of four spots in the plane of incidence region, indicating the development of $\{110\}$ facets on the α-iron surface left after etching away the orientated γ-iron. Similar patterns are discussed in Part 2, § 2.

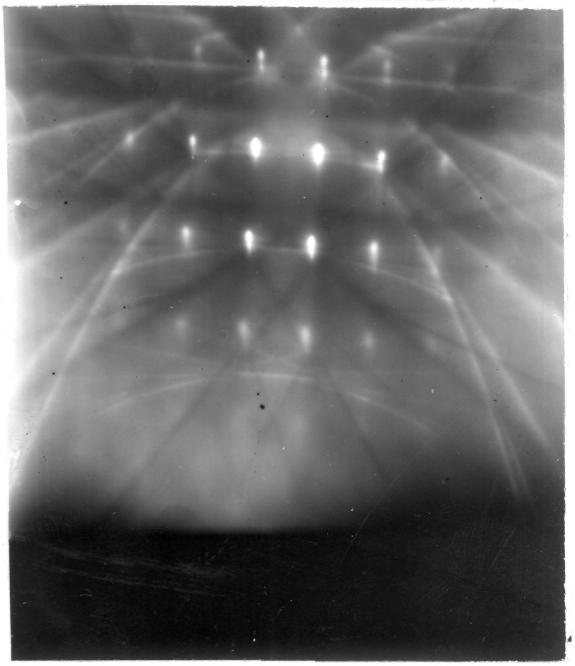

Fig 69. Electropolished (107) face after pressing on emery. beam along [$\bar{1}$10].

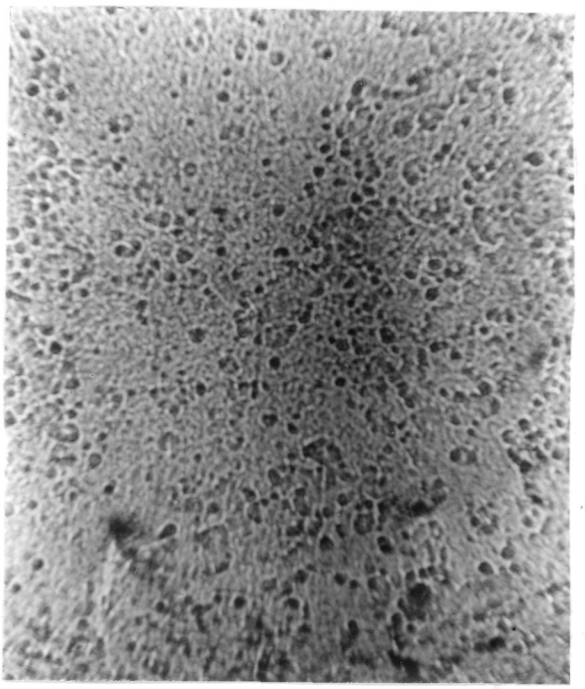

Fig 70. Optical micrograph after pressing against emery. 120x.

C. Experiments on the effect of pressing the (107) and (110) iron single-crystal surface against 0000 emery paper, without any lateral motion.

1. The effect of pressing the electropolished (107) iron crystal surface against 0000 emery.

The iron crystal was electropolished in the usual way and yielded electron diffraction patterns as in figure 31, consisting of clear Kikuchi lines and elongated spots, which showed that the crystal surface was highly smooth and perfect. The optical micrographs also showed an almost featureless smooth surface.

The (107) iron crystal face was then pressed against 0000 emery paper wetted with benzene, using a light hand pressure of about 50 gm./sq.cm., as applied when abrading the iron crystals. The electron diffraction examination then showed no recognisable change in the pattern (figure 69) while the optical microscope yielded figure 70, which suggests some minute indentations on the crystal surface due to the protruding particles of emery. Subsequent gradual etching or electropolishing revealed no other change.

2. The effect of pressing the (110) iron surface against 0000 emery.

The iron crystal surface was smoothed by electropolishing to remove any marks of previous abrasion and the optical

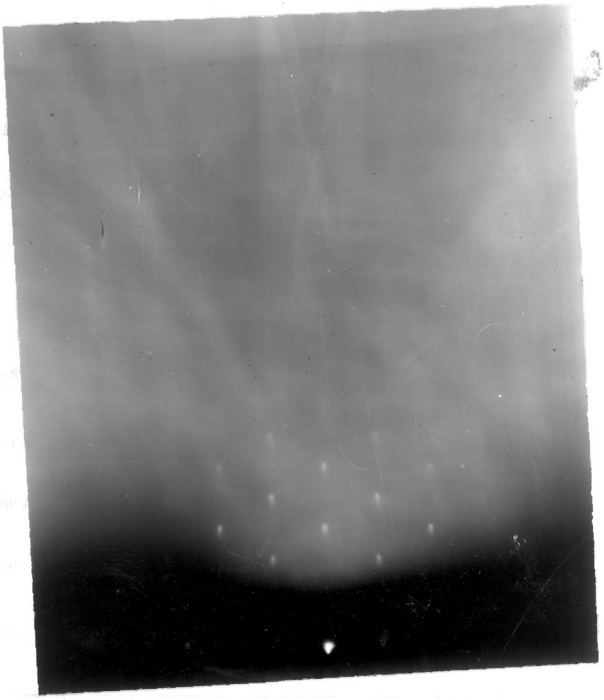

Fig 71. Electropolished (110) face after pressing against emery, beam along [11$\bar{1}$].

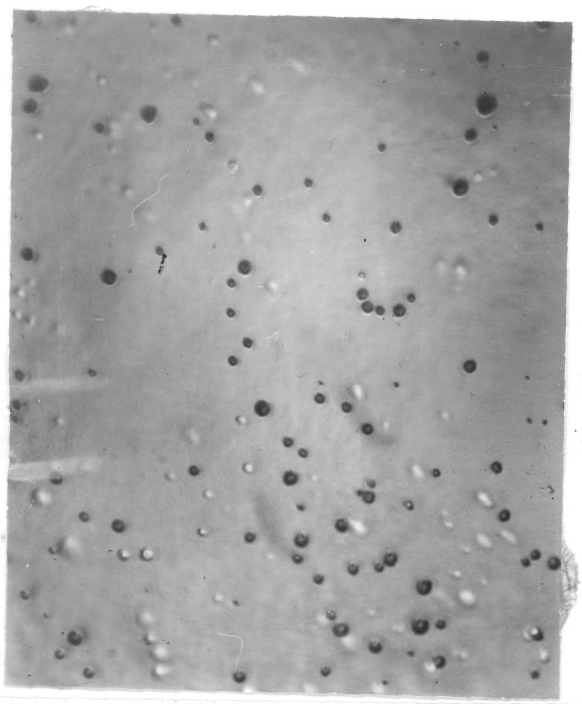

Fig 72. Optical micrograph after pressing the crystal against emery, with $\perp$r illumination. 600×

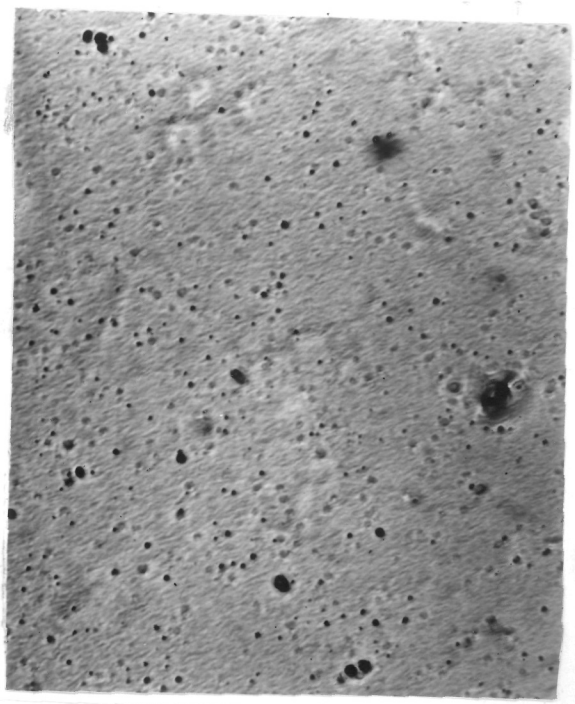

Fig 73. Same as figure 72, but with oblique illumination.

200×

microscope also showed no trace of deformation or scratches. The electron diffraction patterns were similar to figure 46, which showed that the surface was highly perfect and atomically smooth. The optical microscope showed a smooth, almost featureless surface.

The crystal face was then pressed on 0000 emery paper wetted with benzene to produce the same conditions as were used in the abrasion experiments. A light hand pressure equivalent to 50 gms/sq.cm. was used, without any lateral movement. Figure 71 shows the electron diffraction pattern taken at this stage. It shows no features suggestive of any appreciable deformation. The optical micrographs, figures 72 and 73, showed very many minute indentations on the crystal, but fail to show any other features of deformation on the crystal surface. Etching of the surface did not reveal any further indications.

D. Experiments on abrasion of polycrystalline mild steel.

The mild steel was polished mechanically first on 0000 emery and then with alumina. The optical microscope shows an almost featureless surface, while electron diffraction yielded figure 74 showing that the surface is fairly smooth on the atomic scale.

It was then abraded unidirectionally by a single stroke

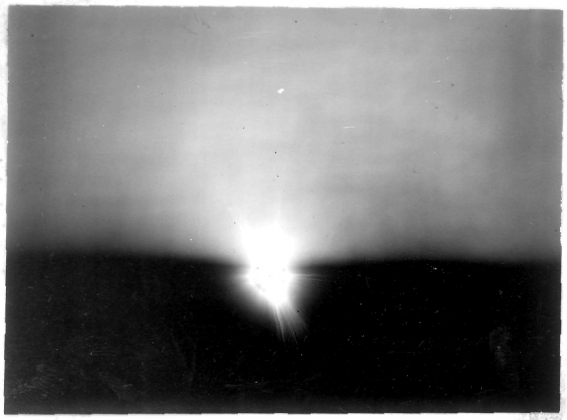

Fig 74. Electron diffraction patterns after mechanical polishing polycrystalline mild steel.

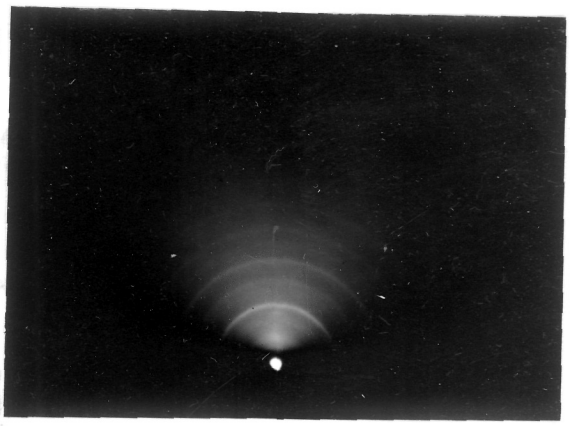

Fig 75. After abrasion on 0000 emery, beam parallel to abrasion.

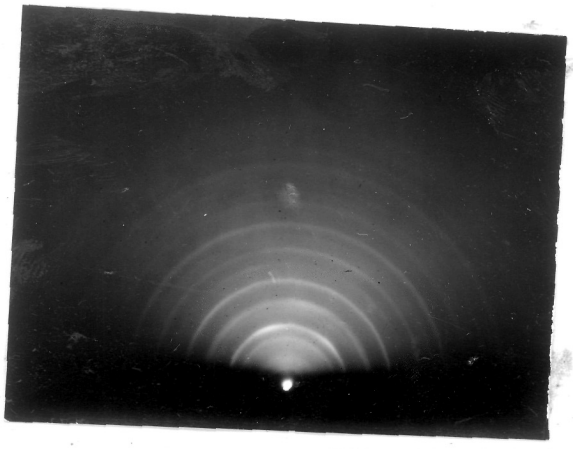

Fig 76. After total etching 3min 45sec, beam ⊥r to abrasion.

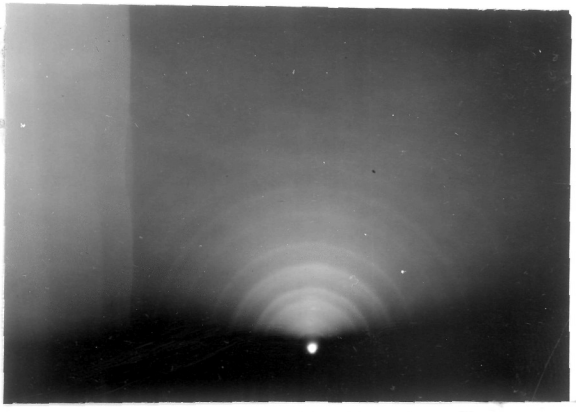

Fig 76b. As figure 76, but beam parallel to abrasion.

Fig77. Optical micrograph 200x

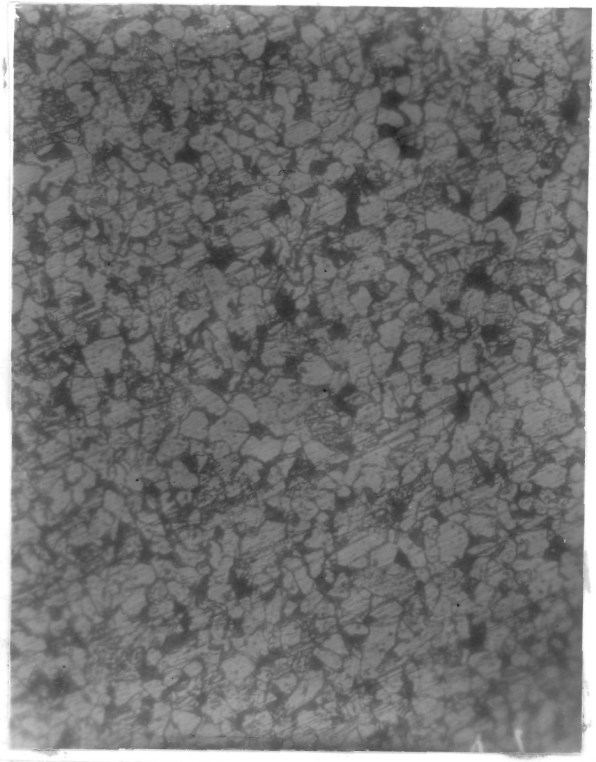

Fig 78a. Optical micrograph showing grain boundaries and very faint scratches. 120x.

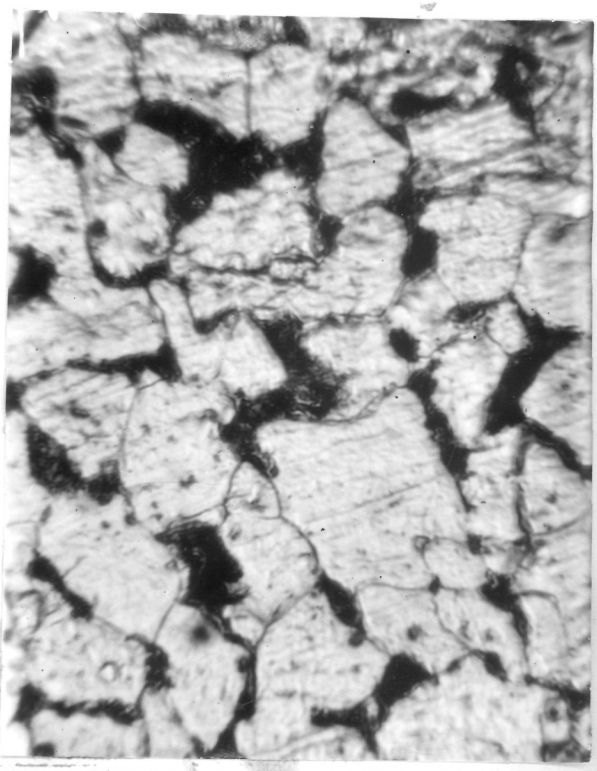

Fig 78b. Same as figure 78a, but 500x.

(10 inch) on 0000 emery paper wetted with benzene (as in Part A) A light hand pressure of 50 grams per square centimetre was used during this abrasion of the crystal. The electron diffraction examination at all azimuths showed patterns such as figure 75, consisting of randomly disorientated rings. The iron surface was etched in stages and at each stage it was examined by electron diffraction as well as in the optical microscope.

After a total etching of 3 minutes 45 seconds, the electron diffraction figure 76 was obtained, with no change from that of figure 75. The optical micrograph, figure 77, also showed no change except the abrasion scratches had become fainter.

The surface was then further etched in 2% nitric acid in alcohol and examined in the optical microscope, which yielded figures 78a and b, showing grain boundaries with very faint scratches. Electron diffraction also showed only slight change from the initial ring pattern to a pattern of weakly arced continuous rings (figure 76), when the beam was normal to the abrasion direction. On the other hand, when the beam was along the abrasion direction, it yielded continuous rings, patterns showing γ-Fe_2O_3 and also α-iron.

Thus it was found that no γ-iron was detectable on the abraded polycrystalline α-iron. The arc pattern such as in

figure 76 indicate that the α-iron near the surface had developed a preferred orientation as a result of abrasion, though further experiments would be required to check whether this is typical of these conditions of abrasions and what is its relation to the deformation process.

Part 2.

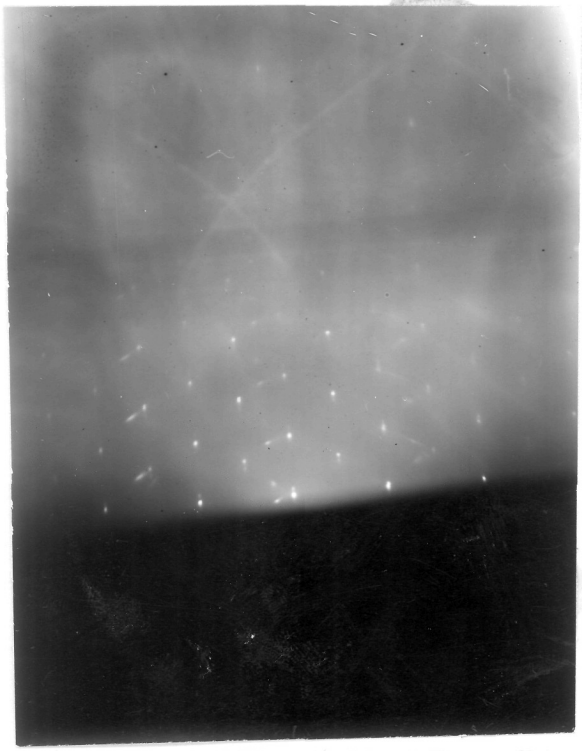

Fig 79. Beam practically along [$11\bar{1}$] of (110) face; γ iron spots (mainly), α iron Kikuchi bands.

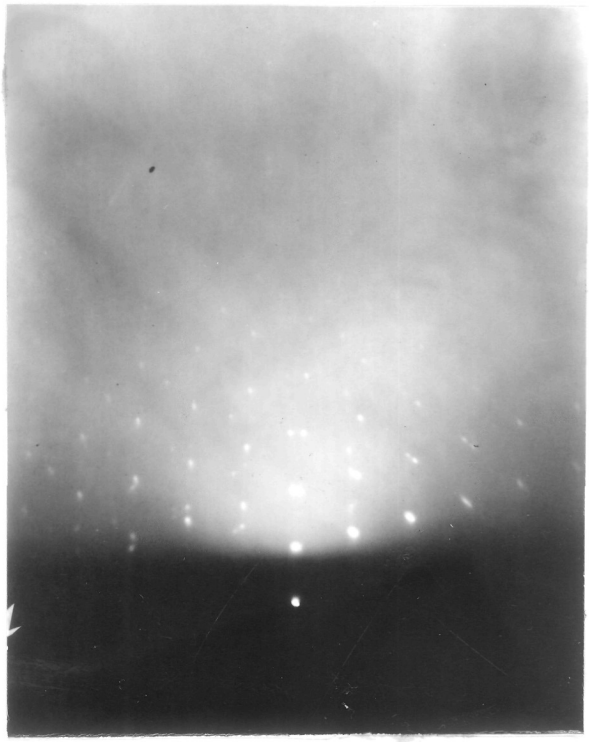

Fig 80. Beam about 2° from [$00\bar{1}$] γ-iron spot pattern.

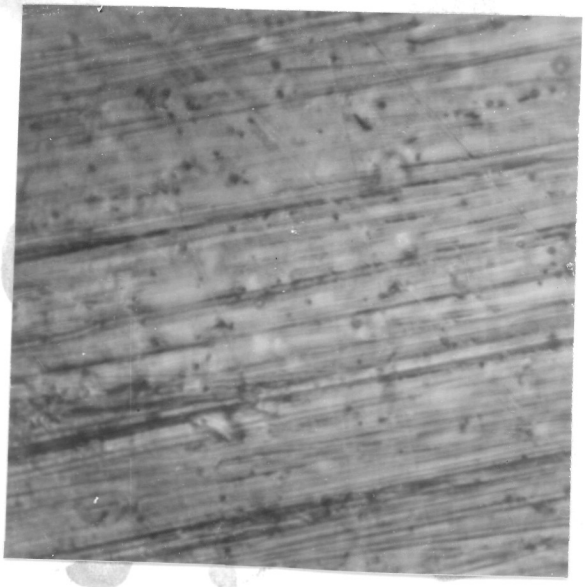

Fig 81. Beam nearly [$1\bar{1}2$]; γ-iron spots, α- iron Kikuchi bands.

The spot patterns described below were obtained after the (110) iron crystal surface had been abraded (as described in Part 1(B) §3) along $[\bar{1}1\bar{2}]$ and then etched for 4 minutes in a 1% solution of picric acid in alcohol, followed by 5 seconds electropolishing. These patterns show the presence of a γ-iron layer orientated in a definite way relative to the main underlying α-iron crystal, and meeting it at plane interfaces parallel to $\{110\}$ planes of the α-iron. Abrasion of the (110) iron surface (freshly resurfaced by electropolishing) along a direction 8° from $[\bar{1}1\bar{2}]$, on the side towards $[00\bar{1}]$, and $[\bar{1}11]$ respectively, yielded essentially identical patterns to those obtained after the $[\bar{1}1\bar{2}]$ abrasion, when the electron beam was along the same azimuth. Thus the orientation of the γ-iron, and the form of boundary separating it from the underlying α-iron, were related only to the main iron lattice, and were independent of the direction of the abrasion.

1. <u>The spot patterns from the orientated γ-iron.</u>

The characteristic spot patterns representing the structure in the region below the rotationally disorientated layer, clearly correspond to face-centred-cubic γ-iron having an estimated cube axis dimension $a_\gamma = 3.60 \pm 0.01$ Å., relative to $a_\alpha = 2.86$ Å. the iron being orientated in several ways relative to the underlying practically undisturbed α-iron crystal.

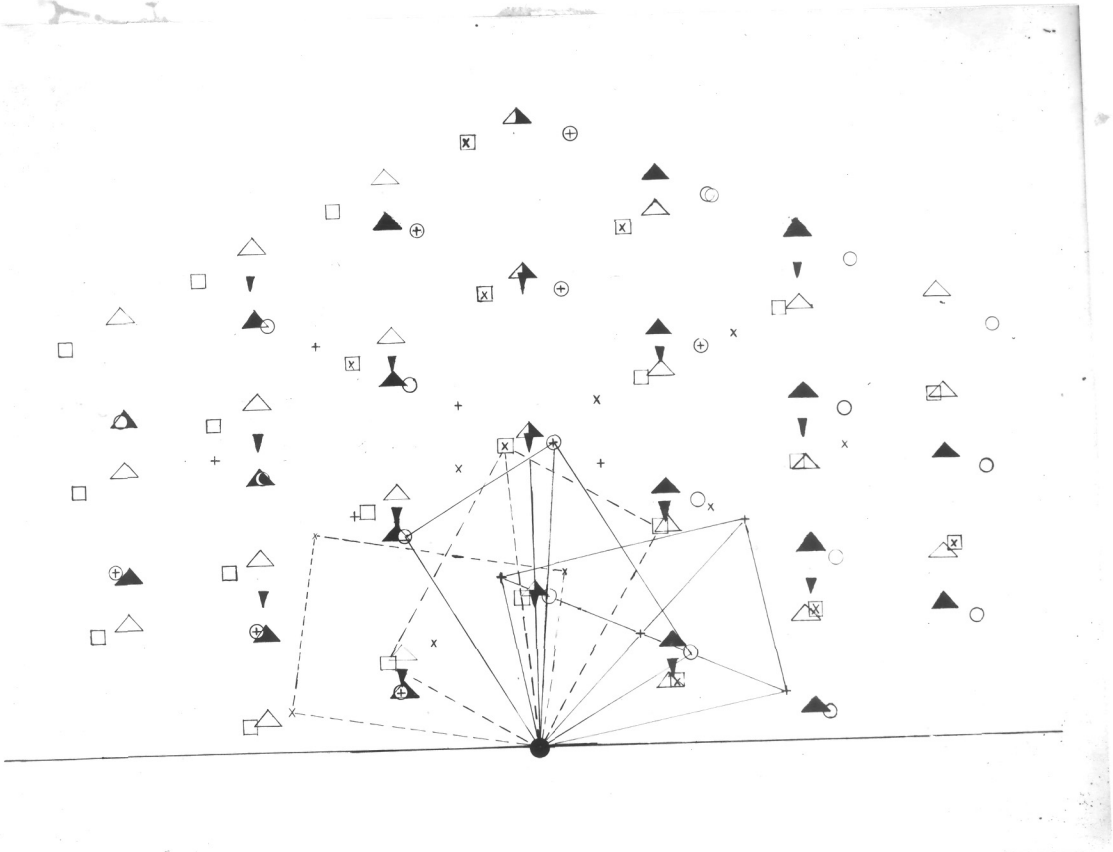

Fig 82. Spot positions in figure 79, showing component patterns. (▼ = ∝- iron diffractions; other symbols γ- iron diffractions with + and x = spots due to {111} twins of main orientations which give spots shown by ○ and □ respectively .)

In the case of the (110) iron surface abraded along $[\bar{1}1\bar{2}]$ (Part 1(B) §3), figures 79, 80 and 81 were obtained when the beam was along directions 0.18° from $[1\bar{1}\bar{1}]$, about 2° from $[00\bar{1}]$, and nearly $[1\bar{1}2]$ respectively.

The relative positions of the diffraction spots in figure 79 are shown in figure 82, where the various component patterns are distinguished by different symbols. There are several component patterns of centred-$\sqrt{2}$-rectangular type, the two main ones (which show a 3° arcing with one-sided tailing-off of intensity) being symmetrically disposed relative to a vertical line through the undeflected-beam spot in figure 79. This vertical line of symmetry is perpendicular to the line where the α-iron (110) plane (produced) met the photographic plate. These two main patterns have one diagonal of the rectangles inclined by 5° to the vertical line. From the lengths of the sides of the $\sqrt{2}$-rectangle unit, in relation to the distance apart of the vertically elongated fainter spots (in a regular hexagon pattern) from the normal α-iron, it is clear that these main $\sqrt{2}$-rectangle patterns correspond to γ-iron crystals orientated with a $\{1\bar{1}0\}$ type of plane normal to the beam (i.e. to $[1\bar{1}\bar{1}]\alpha$). The perpendicular $[1\bar{1}0]\gamma$ row was thus parallel to the $[1\bar{1}\bar{1}]$ cube diagonal of the α-iron, but a $(111)\gamma$ plane through this $[1\bar{1}0]\gamma$ row was clearly inclined by 5° to the initial $(110)\alpha$ crystal plane which approximated to

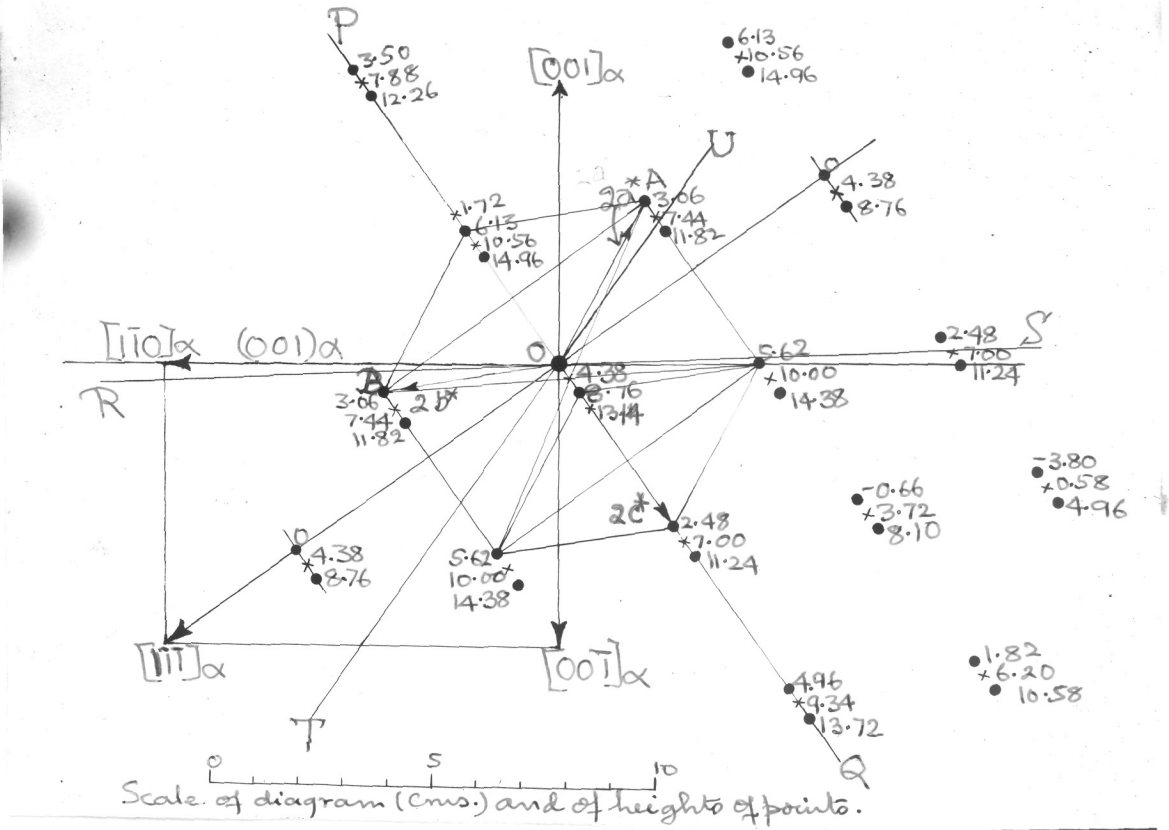

Fig 83. Plan of one of the γ iron face centred cubic reciprocal lattices, on (110)α ; corners of unit cells represented by • , cell centred by x.

the surface. This orientation is more clearly specified as such that a cube face (for example (001) in figure 83) of the γ-lattice was parallel to a $\{110\}$ type of plane of the α-iron ($(01\bar{1})\alpha$ in figure 83, at 60° to the horizontal $(110)\alpha$ plane), with a cube face diagonal ($[\bar{1}10]\gamma$ in figure 83), in this cube face parallel to a cube diagonal ($[\bar{1}11]\alpha$ in figure 83) of the above $(110)\alpha$ plane.

Next, a reciprocal lattice of one of the γ crystals was constructed from the spot pattern of figure 79 in the following way. Thus, if the above $(1\bar{1}0)\gamma$ plane was exactly normal to $[1\bar{1}\bar{1}]\alpha$ it would be represented by the line PQ in the reciprocal-lattice plan, figure 83, on the (110) surface plane of the initial α-crystal. In that case the above centred-$\sqrt{2}$-rectangle spot pattern must correspond to a similar arrangement of reciprocal lattice points in the $(1\bar{1}0)^*\gamma$ plane through the origin O, because for figure 79 the part of the Ewald sphere concerned is closely approximated by the plane through PQ normal to the diagram. The positions of these reciprocal-lattice points are therefore defined in the reciprocal-lattice plan (figure 83), by the points lying on PQ, together with their corresponding heights (obtained from figure 79 and marked nearby) above the $(110)\alpha$ plane through O on which the plan is projected. On this basis other reciprocal-lattice points of this face-centred-cubic reciprocal lattice of the γ-iron were then constructed as in figure 83.

It is noted that there are other component centred-$\sqrt{2}$-rectangular spot patterns in figure 79, as marked in figure 82, showing that the above main γ-iron crystals were twinned extensively on their $\{111\}$ planes. Figure 79 also shows continuous diffraction lines normal to those twin lamellae which were parallel to the beam or nearly so. These diffraction lines are associated with this twinning and also indicate the extreme thinness of some of the twin lamellae. These lines correspond to extensions of the reciprocal-lattice intensity regions in directions normal to the planes of these lamellae, and for two twins, the extensions are tangential to the Ewald spheres in certain regions near the origin ofthe lattice, hence the presence of the lines in the pattern.

It will now be seen that owing to these $\langle 111 \rangle^*$ extensions of the reciprocal-lattice intensity regions, then if the $(110)\gamma$ type of plane had not been exactly normal to the $[1\bar{1}\bar{1}]\alpha$ row, as stated above, there would have been a pair of spots one above the other, instead of each spot of the centred $\sqrt{2}$-rectangle pattern, but this is not seen in the pattern. Again, the plan of the γ-iron reciprocal lattice in figure 83 can also be used to construct the patterns which are contributed to figure 79, by γ-iron lattices orientated in some of the other ways of the set, of the above type, which are geometrically equivalent relative to the initial α-iron crystal.

In this way, most of the remaining spots in the pattern

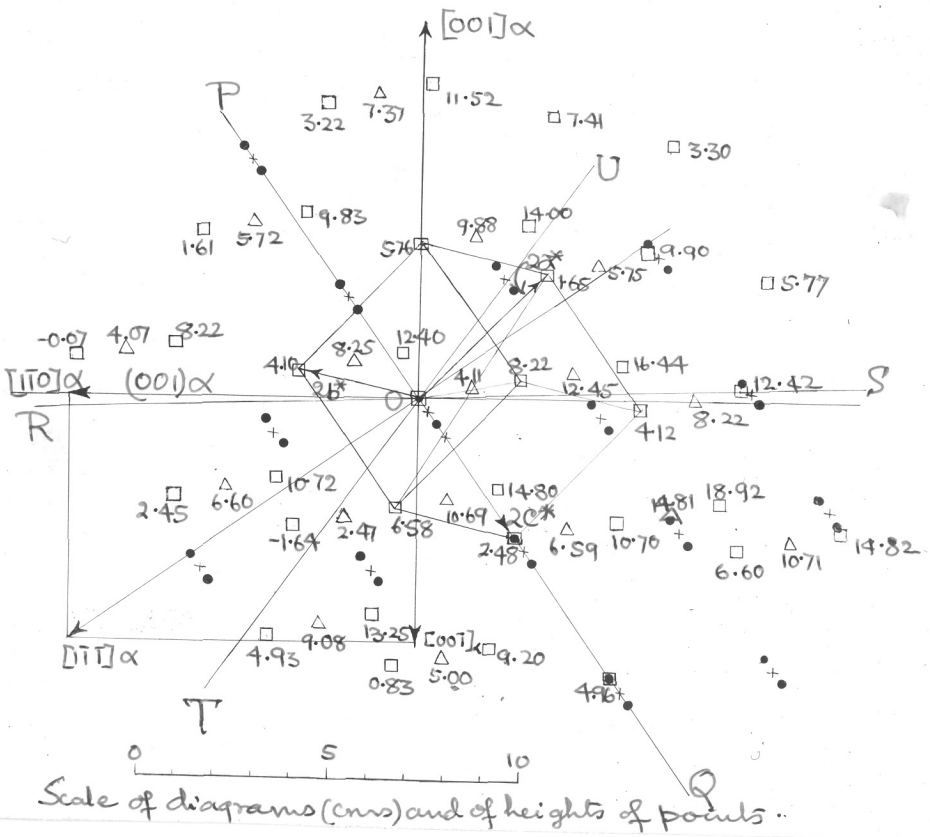

Fig 84. Plan of a γ iron reciprocal lattice (on (110)α)obtained from fig 83 by rotating the lattice round C^*_γ until the [110]γ row is parallel to [111]α ; corners of cells represented by □ , cell centres by △ . For comparision the points marked in fig 83 are also superposed.

are accounted for, particularly the strong spots denoted by the triangles in figure 82. These spots, and in particular the spots lying on the vertical symmetry line through the undeflected beam spot in figure 79, are seen to be single sharp spots lying on the continuous diffraction lines which are associated with the twinning as described above. They correspond to intersections of the $\langle 111 \rangle^*$ elongated intensity regions with the Ewald sphere and their position further confirm clearly, with high precision (to a small fraction of a degree), the γ-iron orientation stated above.

Although some of the γ-iron reciprocal lattices which are symmetrically equivalent relative to the α-iron substrate can be derived from that shown in figure 83, by reflection in the $(001)^*$ and $(1\bar{1}0)^*$ planes of symmetry passing through the origin O, the remaining set of lattices are similarly related to that shown in plan on $(110)\alpha$ in figure 84. This was derived from figure 83 by the normal methods of geometry, and shows the lattice obtained from that of figure 83 by a rotation about the $[001]^*$ axis, to a position where a $(001)^*\gamma$ face diagonal is parallel to the other diagonal $[111]^*\alpha$ of the α-iron $(01\bar{1})$ plane. However, no spots were found in figure 79 which could correspond to any of this second group of γ-iron lattices, which therefore appear to have been not present.

Now consider figure 81, obtained when the electron beam was along the $[1\bar{1}2]$ direction, i.e. normal to the direction

used for figure 79. The sharp spots in a practically $\sqrt{8}/3$ rectangle arrangement are immediately seen to correspond to γ-lattice orientations of the type already described above, having a $\{111\}\gamma$ plane inclined from the horizontal $(110)\alpha$ surface by 5°, about an axis which is now normal to the electron beam for two of the γ-lattices. The presence of (among others) the $(110)\alpha$ Kikuchi-line system in figure 81, nearly horizontal and a few centimetres above the shadow edge, enables close confirmation that the smaller (vertical) side of the spot rectangles in figure 81 is indeed normal to the $(110)\alpha$ Kikuchi lines to within a small fraction of a degree. This shows that the $(1\bar{1}0)\gamma$ plane was normal to the $[1\bar{1}\bar{1}]\alpha$ row in $(110)\alpha$, as already concluded from figure 79.

The fact that the spots occur in close pairs, a weak spot above a strong spot of each pair in the zero-order circular zone, is completely explained as due to the 4° inclination of the electron beam to the $(110)\alpha$ plane, so that the Ewald sphere is (near the origin) approximately a plane through TU in figure 83, but 4° inclined from normal to the $(110)\alpha$ plane. This causes one set of $\langle 111\rangle^*\gamma$ intensity-region extensions to meet the sphere much further from the reciprocal lattice points than do the corresponding extensions of the other γ lattice of the symmetrical pair concerned, leading to the faint upper spot and the strong lower spot respectively, in each pair in the lower part of the pattern.

The nature and location of the pairs of streaks diverging from certain of the spots of this pattern are also found to correspond to $\langle 111 \rangle^*_\gamma$ extensions of intensity regions of others of the lattices of the above type, the extensions in this case intersecting the Ewald sphere very obliquely.

Finally, the spot positions in figure 80, obtained with the beam in an azimuth 2° from $[00\bar{1}]_\alpha$, were also found to be completely explained by the above γ-iron orientations. The $[00\bar{1}]_\alpha$ cube edge, produced, met the photographic plate at a point corresponding in the positive figure 80 to a point 1.8 cm. to the right of the plane of incidence and 1.8 cm. below the level of the undeflected-beam spot, as was shown by Kikuchi-line patterns obtained from the fresh electropolished surface. Relative to figure 83, therefore, the Ewald sphere near the origin is approximated by a plane through RS inclined 2° away from normal to $(110)_\alpha$. This inclination causes $\langle 111 \rangle^*_\gamma$ extensions of the intensity-regions of two of the γ-iron reciprocal lattices to meet the Ewald sphere correspondingly nearer to the lattice points and therefore at slightly lower level and more to the left and right respectively. While those of two others met the sphere further from the lattice points and are, therefore, at much weaker intensity and at a slightly higher level and more to the left and the right, at points vertically above the lower pair of spots. Instead of single spots in the plane of incidence there are thus the groups of

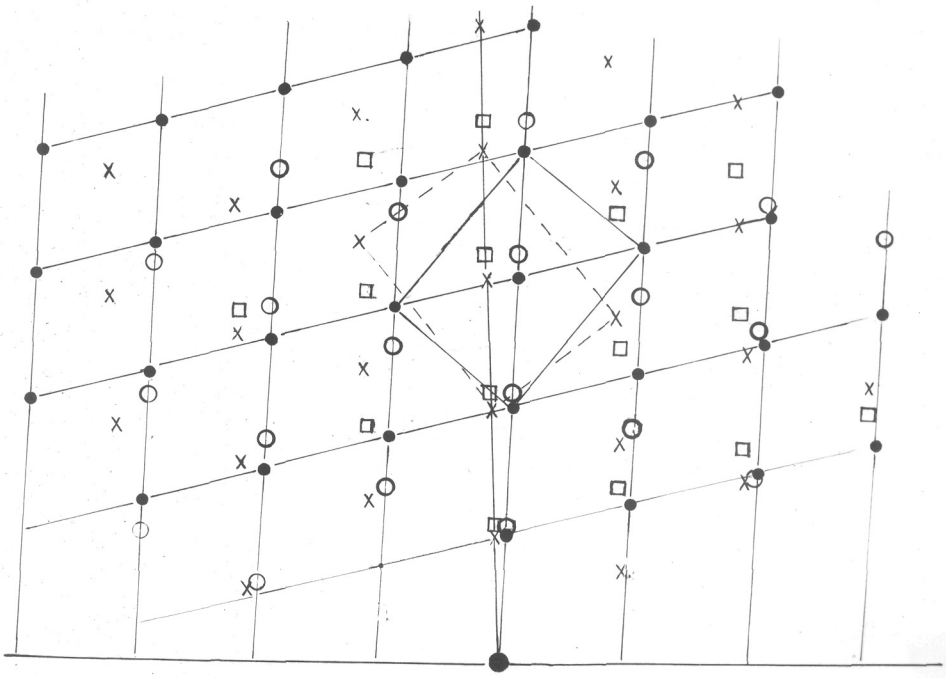

Fig 85. Spot positions in figure 80, showing component patterns.

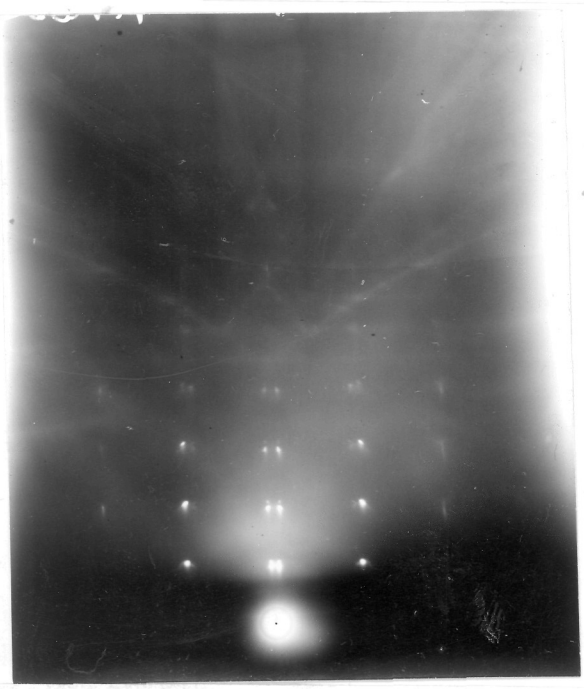

Fig 86. Beam near[110] ; α Fe pattern with spot groups due to {110} facets.

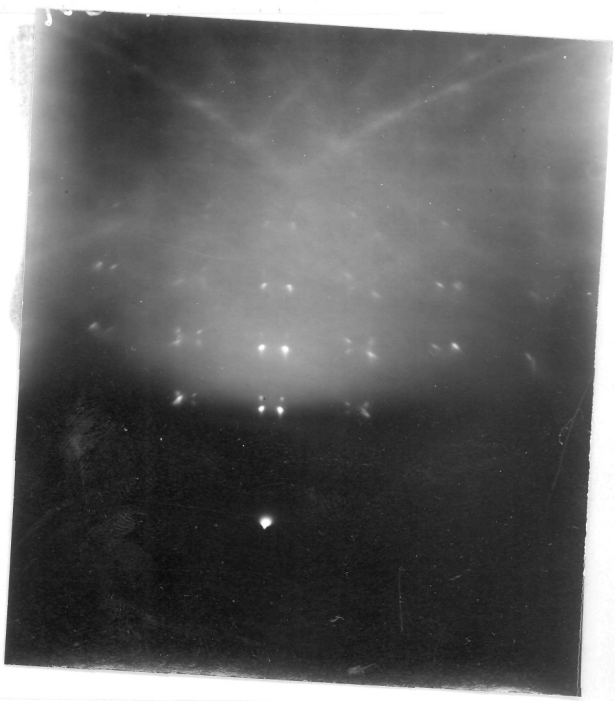

Fig 87. As figure 86 but larger grazing incidence angle.

four spots seen in figure 80, of which the upper two are weak. Similar groups of spots occur also in other parts of the pattern, but with more extensive modification in position due to the beam being in an azimuth 2° away from $[00\bar{1}]_{\alpha}$. As figure 85 shows, the pattern consists mainly of four component spot patterns of roughly centred-$\sqrt{2}$-rectangle type, corresponding to the γ-lattices having a $\{110\}$ plane not far from normal to the beam.

No spots corresponding to the second group of γ-iron lattices, derived from figure 84, were observed in figures 79, 80 or 81, although it is clear from figure 84 that some of the lattice points lie close to the Ewald sphere for these cases; hence it seems that no γ-iron lattices of this group were present in the specimen.

2. <u>The spot patterns from the α-iron surface exposed after etching away the γ iron.</u>

The pattern (figure 68) mentioned in Part 1(B), § 4 is best interpreted by considering figures 86 and 87, obtained when the beam was along $[1\bar{1}0]$. The initial crystal surface yielded figure 42 at this azimuth, the diffraction spots being in a $\sqrt{2}$-rectangular arrangement. Clearly, figures 86 and 87 are similar to figure 42 except that instead of each spot there is here a group of four spots, roughly symmetrically arranged relative to the position the normal spot would have occupied.

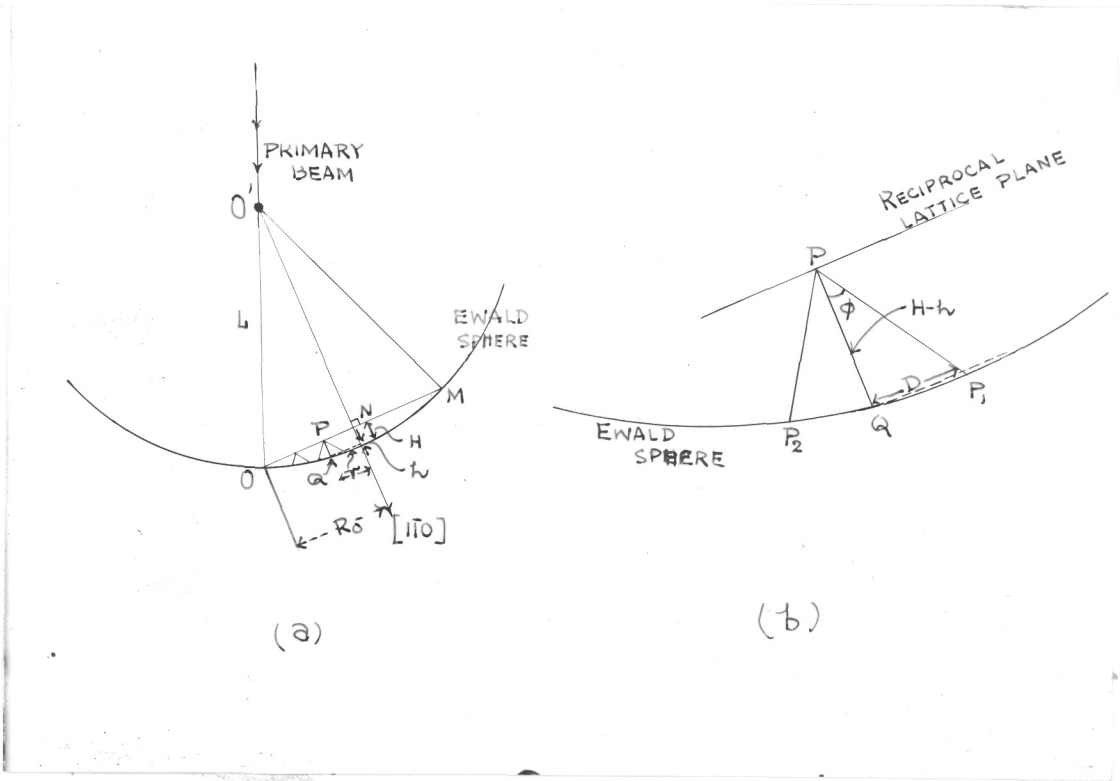

Fig 88. Diagram showing intersection of Ewald sphere by extension of reciprocal lattice intensity regions.

The distance apart of the spots of each group depends on the distance of the spot group from the zero-order circular Laue zone round the $[1\bar{1}0]$ axis. These groups of four spots are thus seen to correspond to the intersection of the Ewald sphere with four symmetrically directed extensions of the intensity regions round the reciprocal-lattice points. The spots are displaced from the normal spot positions, along the diagonals of the $\sqrt{2}$ rectangles at the corners of which the spots normally lie, hence the extensions of the intensity regions lie in the (111) and $(11\bar{1})$ planes. The inclination ϕ of the extensions to the $[1\bar{1}0]$ direction (which is nearly parallel to the electron beam) was calculated in the following way from the spot separation in appropriate spot groups.

In figure 88(a), O is the origin in the λL times enlarged reciprocal lattice, O' is the centre of the Ewald sphere (λL times enlarged but represented with exaggerated curvature in figure 88(a)), OM represents the $(1\bar{1}0)^*$ plane seen in section, O'N is the normal to OM and P represents a lattice point on the plane OM, having its intensity region extended along directions such as PP_1, (see figure 88(b)). PQ is normal to OM and P_1Q is normal to PQ and of length D. Thus $\tan\phi = P_1Q/PQ = D/(H-h)$, where with sufficient accuracy $H \simeq R_0^2/2L$ and $h \simeq r^2/2L$, in which L is the camera length, R_0 is the radius of the circular zero-order Laue zone round $[1\bar{1}0]$ *passing through the undeflected beam spot, and* r *is the radial*

distance from the point of intersection of $[1\bar{1}0]$ with the photographic plate to the centre of the spot group represented by P. In figure 86 the effectively circular zero-order Laue zone round the $[1\bar{1}0]$ row is centred on the plane of incidence (i.e. on the vertical line through the undeflected-beam spot) and has a radius R_0 of about 2.5 cms. In figure 86, obtained at the same azimuth but larger angle of grazing incidence, R_0 is about 3.85 cms., and in the centre of the zero-order circle the spots of each group are accordingly much further apart than in figure 86. From figure 86 calculation of ϕ from three spot groups centred on the plane of incidence gave values 60°6', 58°30', and 58°39', the mean being 59°5'. A graphical construction on a ten times enlarged scale also gave a mean ϕ of 59°.

Thus the four observed extensions of the intensity-regions are unequivocally found to be along $[101]^*$, $[10\bar{1}]^*$, $[0\bar{1}\bar{1}]^*$ and $[0\bar{1}1]^*$, while $[1\bar{1}0]^*$ extensions are absent. No spots would be expected at this crystal setting from $[110]^*$ extensions even if such were present. These observed extensions therefore indicate either surface planes parallel to (101), $(10\bar{1})$, $(0\bar{1}\bar{1})$ and $(0\bar{1}1)$, or thin lamellae parallel to these planes. This crystal form must have been caused by the abrasion of the crystal surface, because no such patterns were ever obtained from the initial surfaces, by electropolishing alone, or by chemical etching. It seems clear that these $\{110\}$

boundary faces of the α-iron surface must correspond to the interface between the unchanged α-iron crystal and the surface γ-iron regions. It has indeed been shown above in Part 2, §1, that the γ-iron lattices had a cube face parallel to one or other of these $\{110\}_\alpha$ planes, which thus supports this conclusion.

It may be noted that when the crystal was again resurfaced by about 6 minutes electropolishing, clear patterns of normal spots (elongated normal to the shadow edge) and sharp Kikuchi lines were again obtained, such as figure 42, from all parts of the surface. The crystal at this stage was about 0.5 mm. thick in the region which gave these patterns.

A further peculiarity of the spot pattern in figures 86 and 87 is that the four spots of each group have not all equal intensity. In the groups centred on the plane of incidence in figure 86, the lower two spots in each group are stronger than the upper two, while the next vertical row of spot groups on the left in the lower part of the pattern contains some groups having only the top left-hand spot strong; and in the corresponding row on the right of the plane of incidence it is the upper right spot which is strong. In figure 87, also, in the plane of incidence the lower pair of spots of each group are much stronger than the upper two, but in the next vertical rows on the left and right the four spots of each group are mainly about of equal intensity. In the next rows further

still to left and right it is the upper pair of spots of each group which are the stronger. At present these features have not been explained, but may possibly be a result of intensity variations along the ⟨110⟩ "intensity region" extensions of the type calculated by Laue and Riewe (1936) and illustrated by Rees and Spink (1950).

Although other patterns of the above type were also obtained at other azimuths, showing in general asymmetric groups of spots, these also corresponded to {110} boundary faces on the α-iron. It may further be emphasised that such patterns were observed in several abrasion experiments, independent of the direction in which the abrasion had been carried out.

IV. Discussion.

1. The nature of the lattice rotations observed in the surface regions.

The above results extend further those published by Evans, Layton and Wilman (1951). The only difference in these experiments was the use of a much lighter hand pressure and much slower speed to abrade the single crystal by a ten-inch single continuous stroke on 0000 emery paper flooded with benzene. In almost all cases large rotations occurred about a well-defined axis normal to a densely populated plane. Thus on the (107) face, abrasion along the "[$\bar{1}$10]", [$\bar{2}$10]" and [100]" azimuths respectively, led to rotations about the lattice directions [110], [120] and [010] respectively. On the nearly (110) face, abrasion along [$\bar{1}1\bar{2}$] and also along a direction 8° from this on the side towards [00$\bar{1}$], yielded rotation about [$1\bar{1}\bar{1}$].

Out of all these results, abrasion of the (107) face along "[$\bar{2}$10]" is the only case where the abrasion direction does not correspond to a direction parallel to the plane of symmetry. Here too, nevertheless, the observed rotation axis was normal to a densely populated net plane, (120), which was parallel to the abrasion direction. It seems difficult to account for this rotation by any translational slip system, even if it were possible to account for other cases as double

translational slip on two systems mirror symmetrical to each other across a plane of symmetry. However, all these results could most simply be interpreted by a coherent fragmentation having a rotational slip relationship of the lamellar fragments to each other and to the main crystal (cf. Wilman 1950, 1951, and Evans, Layton and Wilman 1951), this slip occurring on the planes normal to the rotation axis.

Apart from these simple cases of the observed rotation axis, however, two interesting and less simple cases were observed. When the (107) crystal face was abraded along "[$\bar{1}$00]" i.e. [$\bar{7}$01], this gave rise to rotations of (presumably) some parts of the surface regions about an axis along or close to [451] while others had rotated about an axis [45$\bar{1}$] symmetrically disposed to the (010) plane. The other case was the abrasion on the (110) face along [$\bar{1}$11], causing large rotation of the lamellae about an axis [$\bar{3}3\bar{4}$]. It seems most probable that the [451] axis of rotation could correspond to the flexure of ($\bar{2}$13) slip lamellae slipping over each other along [1$\bar{1}$1], i.e. the usual type of slip direction, but on the contrary, rotation about [$\bar{3}3\bar{4}$] could not correspond to flexural trahslational slip alone, in any of the types of slip along ⟨111⟩, the only observed slip direction of iron as observed by various workers (see Introduction §3(i)), because [$\bar{3}3\bar{4}$] is not perpendicular to any ⟨111⟩ row of the lattice. The [$\bar{3}3\bar{4}$] rotation could possibly represent a combination of initial rotational slip (on ($\bar{1}1\bar{1}$) or

$(\bar{1}1\bar{2})$) and subsequent translational slip within the lamellae, or might be a result of multiple translational slip alone.

The inhomogeneous nature of the deformation complicates the interpretation of the above results in terms of slip processe It seems that this kind of deformation corresponds to the abrasive particles exerting a high stress on the surface of the crystal (cf. Finch 1950, fig.5). They push away parts of the lattice in front of them, and exert as they pass, a tangential drag on the atoms at the sides and bottoms of the more or less deep channel-shaped scratches which they leave behind them (cf. Evans, Layton and Wilman, 1951).

An attempt was also made to study the nature of the initial deformation caused by mere pressure (similar to that used above) of the electropolished faces against the abrasive particles of the 0000 emery paper, without any tangential motion, but so far electron diffraction patterns did not show any clear signs of deformation, and optical micrographs (see figures 72 and 73) only showed minute dots corresponding to shallow indentations caused by the abrasive particles.

A large rise in temperature of the surface layers during abrasions is another factor which at present seems difficult to allow for, though it is quite evident that the formation of γ-iron was independent of the direction in which the abrasion had taken place, and the γ iron in the lower strata only occurred in orientations which corresponded to α to γ transformation

involving slip along those $\langle 111 \rangle_\alpha$ rows which lay parallel to the initial $(110)_\alpha$ surface of the crystal. It appears that at these levels below the original crystal surface, the abrasion had mainly caused the translational motion of $\{211\}_\alpha$ planes over each other along these particular usual slip directions $\langle 111 \rangle_\alpha$. It is also clear that the rise of temperature (to $> 900°C.$) due to abrasion apparently caused the shear to result in the formation of the γ iron which remained stable during the rapid cooling after the abrasion. This indicates that even at these temperatures, the preferred slip direction is still along $\langle 111 \rangle_\alpha$ ($= \langle 110 \rangle_\gamma$), which makes it unlikely that the observed rotation about $[\bar{3}3\bar{4}]$ could result from a flexural translational slip. The rotationally deformed upper layers, however, must reach still higher temperatures above 900°C., and there is no guarantee that $\langle 111 \rangle$ slip still occurs in iron at these temperatures. If the temperature had risen to above 1403°C., which is the temperature of transformation of γ iron to δ iron, it is unlikely that the orientation of the γ-iron resulting during the subsequent cooling would have been so sharply defined as was observed. Thus it appears unlikely that the temperature of the γ-iron layer rose as high as 1403°C.

The investigation of an abraded surface of polycrystalline mild steel, described in Part 1(D), did not show evidence of any formation of a γ-iron layer. The appreciable carbon content of mild steel may have hindered the formation of γ phase from the

α-phase. Further experiments would be desirable to elucidate this point.

2. The α - γ transformation in iron crystals.

When the ring patterns from the upper regions of the abraded iron crystals showed both α and γ ring patterns simultaneously measurements gave a value a_γ = 3.60 ± 0.01 Å. compared with a_α = 2.86 Å. The same value was also obtained from measurements of the spot separations in figure 79, obtained from the orientated γ iron layer in contact with the substrate crystal. This value is close to that of 3.57 Å. (extrapolated) quoted by Barrett (1953) for γ-iron at 20°C.

The presence of this γ-iron indicates that: (i) even in such light abrasion the metal surface reached a temperature of the order of 900°C. or more, at least locally, as is clearly to be expected in view of the results of Bowden and his collaborators (see Bowden and Tabor 1950) though they do not appear to have suggested the possibility of formation of γ-iron; (ii) the cooling of these regions was rapid enough to allow this γ-iron to retain its structure after cessation of the abrasion.

Courtel (1949, also see introduction 4 (iv)) noticed that the cubic variety of cobalt, formed under the effect of the energy received almost instantaneously due to mechanical abrasion, persists afterwards owing to the rapid cooling which

amounts to quenching. He also calculated, for example, that cooling of a surface layer of 1 μ thickness from 500° to 300°C. by simple conduction of heat from the surface into the body of the specimen which is at room temperature, does not take more than 10^{-7} second. In the case of martensite formation, Kurdjumov and Maksimova (1951) have discussed the kinetics of the transformation above room temperature.

In the present experiments the parallel abrasion furrows did not completely cover the surface, — thus it is possible that the γ-iron was located not so much in the lower strata below the surface, as in the intervening less deformed regions between the channels formed by abrasion scratches and was accessible to the electron beam only when the projecting edges of such furrows had been dissolved away. Optical micrographs (at 600 x) showed from this region where the orientated γ-iron occurred (at the stage after etching for 4 minutes and electro-polishing for 5 seconds) only occasional weak indications of narrow, elongated rectangular outlines which, however, could not be clearly correlated with the observed γ-iron orientations or α-iron $\{110\}$ surface form.

The γ-iron orientations relative to the α-iron crystal were of the type:- $(001)\gamma$ parallel to $(01\bar{1})\alpha$, which was evidently the interface between the two phases; and in this common plane $[\bar{1}10]\gamma$ was parallel to $[\bar{1}11]\alpha$ as shown in

figure 83. Of the set of geometrically equivalent γ-iron orientations of this type, only those were observed for which the common lattice row ($\langle 111 \rangle \alpha$ and $\langle 110 \rangle \gamma$) was parallel to the (110) surface of the initial α-iron crystal.

This orientation, in the low-carbon iron which was used, differs from the well-known conclusion of Kurdjumow and Sachs (1930; cf. also Sachs 1932) that quenching a single crystal of 1.4% carbon steel from the austenite (γ) phase gives α-iron lattices in orientations such that the two most densely-populated planes $\{111\}\gamma$ and $\{110\}\alpha$ were parallel, and that in these planes the two most densely populated rows $\langle 110 \rangle \gamma$ and $\langle 111 \rangle \alpha$ were parallel. It is also different from the type of orientation found by Nishiyama (1934) in the martensitic transformation occurring on cooling a 30:70% Ni-Fe crystal from the face-centred-cubic γ phase at room temperature by immersion in liquid air. The α phase was formed with $\{111\}\gamma$ parallel to $\{110\}\alpha$ but with $\langle 110 \rangle \gamma$ parallel to $\langle 001 \rangle \alpha$ in this common plane.

The Kurdjumow-Sachs orientation relationship was subseqeuntly confirmed for steel containing between 0.5 and 1.4% carbon, by Mehl, Barrett and Smith (1933), Wassermann (1935), Greninger and Troiano (1940) and Smith and Mehl (1942). No detailed results appear to have been obtained for very low carbon steel such as that used in the present experiments. In 30:70% Ni-Fe, the Nishiyama relationship has also been

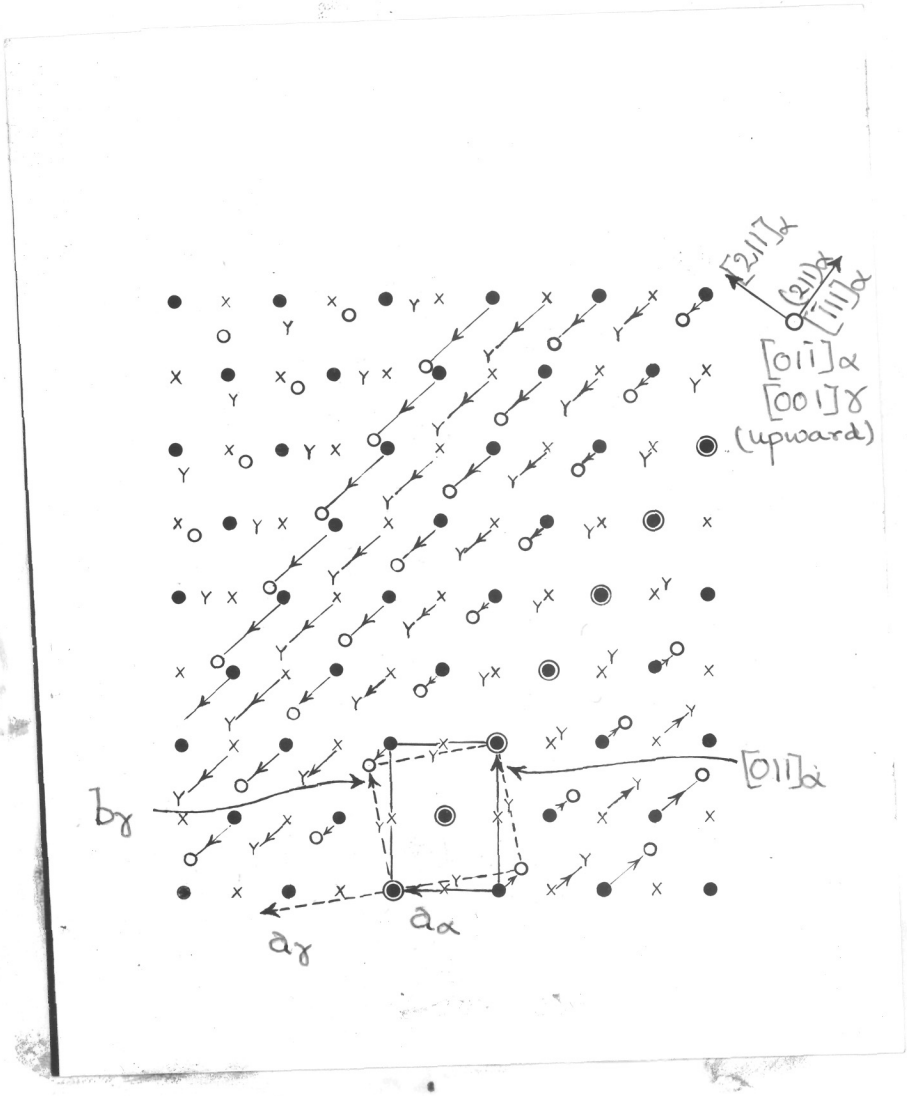

Fig 89. Net atomic movements during transformation from body centred-cubic α iron to face-centred cubic γ-iron, shown in a projection on $(01\bar{1})$;
● = atoms in iron at heights $\pm 0, 1, 2, 3, \ldots\ldots x\sqrt{2}a$, and
x = atoms at heights $\pm 1/2, 3/2, 5/2, \ldots\ldots x\sqrt{2}a$;
O and Y = atoms in iron at heights $0, 1, 2, 3, \ldots . xC_\gamma$ and $\pm 1/2, 3/2, 5/2, \ldots\ldots xC_\gamma$, respectively.

confirmed by Wassermann (1935), Greninger and Troiano (1940), and by Mehl and Derge (1937) who found the Kurdjumow-Sachs relationship above room temperature but the Nishiyama relationship below.

The mechanism of atomic motions in such transformations has been much discussed. Kurdjumow and Sachs (1930) suggested that the transformation from γ to α iron on cooling occurred by a shear on $(\bar{1}11)\gamma$ along $[\bar{1}\bar{1}2]\gamma$ followed by a second shear on $(1\bar{1}2)\alpha$ along $[\bar{1}11]\alpha$, with some further atomic readjustments. Nishiyama (1934) proposed that the transformation from γ to α phase in the 30:70% Ni-Fe occurred by a single shear on $(111)\gamma$ along $[\bar{1}\bar{1}2]\gamma$ as Kudjumow and Sachs had suggested, but then further lateral expansion causing the angle between the main rows in these planes to increase from 60° to 70°38', to lead to the required α lattice. These mechanisms are not now considered to account for all the observations of habit plane of the new phase and surface relief effects, and others have been proposed. Bowles and Barrett (1952) and Barrett (1953) have reviewed the various experimental results and theories, and Frank (1953) has provided further discussion of the transformation mechanism.

For the present experimental results, there is a simple and natural relationship between the γ and α iron structures, in that a $(01\bar{1})\alpha$ plane contains a centred-$\sqrt{2}$-rectangular atomic array in a $(001)\gamma$ plane, as in figure 89. The transformation

can be formally represented as equivalent to a homogeneous shear on $(211)\alpha$ planes along $[\bar{1}11]\alpha$ as in the normal $\{211\}$ twinning of α-iron, combined with a perpendicular homogeneous 6.0% extension along $[211]\alpha$ as in figure 89 (converting the rhombus of 93°22' angle to a square with 90° angle) and a homogeneous contraction of 13.4% along $[01\bar{1}]\alpha$, i.e. $[001]\gamma$. to convert the face-centred tetragonal lattice having $c/a = 2/\sqrt{3} = 1.155$ into the face-centred-cubic γ lattice. Although the atomic movements must actually be less linear than in this idealised representation (cf. Frank 1953). It is significant that the net motion is along $\langle 111\rangle\alpha$, i.e. $\langle 110\rangle\gamma$ rows, as in the normal translational slip in the body-centred-cubic α- and the face-centred-cubic γ-structures; and this mechanism can clearly lead to the observed $\{110\}\alpha$ - $\{001\}\gamma$ form of interface.

It is of particular interest to note, see figure 89, that as the result of a homogeneous shear on $(211)\alpha$ along $[\bar{1}11]\alpha$, adjacent $\langle 111\rangle\alpha$ rows in the plane of the diagram, i.e. $(01\bar{1})\alpha$ move past each other by a distance very nearly equal to one third of the slip translation, which is the interatomic spacing in these rows. Thus, every third row in the plane has moved along by practically a whole number of slip translations to a position similar to its initial position. This feature must therefore enable maintenance of a relatively stable fitting in of the atoms with the neighbouring $(01\bar{1})\alpha$ atomic sheet across the interface, during and after the shear.

V. General Conclusions.

The above results show that light unidirectional abrasion of the electropolished iron crystals caused large rotations of parts of the surface region of the crystal about a clearly defined axis which was usually normal to a densely populated plane lying parallel to the abrasion direction or nearly so and more or less steeply inclined to the surface. These results are similar to those of Evans, Layton and Wilman (1951), though the abrasion was very light as compared to theirs.

These results may correspond to fragmentation of the surface regions by lamellar rotational slip, such that the lamellae are normal to the observed rotation axis and still coherent with such neighbouring lamellae and still undistorted parts of the crystal. The microphotographs of the surface at all stages of etching show no clear evidence to indicate whether this is the kind of deformation occurring or whether the translational kind of slip is involved. The nature of the observed rotation seems, however, difficult to account for in terms of translational types of slip, especially when the observed rotation axis was not normal to a plane of symmetry of the lattice. Pressing the electropolished surfaces of the iron single crystals on to 0000 emery also did not result in any signs of deformation, though optical micrographs show minute indentation marks.

However, two unusual and interesting cases were observed. In one case of abrasion on the (107) face, rotation of some parts of the surface region took place about a [451] axis while rotation of others was about the [45̄1] axis symmetrically disposed to the previous axis. It seems most probable that this axis of rotation could correspond to the flexure of (2̄13) slip lamellae slipping over each other in the usual ⟨111⟩ type of slip direction. The second case showed a rotation about a [3̄34̄] axis which could not correspond to flexural translational slip, on any planes containing the usual ⟨111⟩ slip direction. It might be a combination of rotational slip and subsequent translational slip, or a result of multiple translational slip.

The presence of face-centred-cubic γ-iron in the disturbed surface layer indicates that the surface region must have reached 900°C. or more and that the cooling of the surface region was also sufficiently rapid to allow this γ-iron to retain its structure after the cessation of the abrasion.

From electron diffraction patterns of sharp spots obtained after etching away the rotationally disoriented regions, the presence of γ-iron strongly orientated relative to the main α-iron crystal was established. The observed orientation of the γ-iron, which was independent of the abrasion direction, differs from the well known conclusions of Kurdjumow and Sachs (1930) on the γ to α transformation in a 1.4% carbon steel

single crystal and also from those of Nishiyama (1934) on the γ to α transformation in 30-70% Ni-Fe.

A simple mechanism of the observed transformation in the present case is suggested and the indicated $\{110\}\alpha$ form of interface is well supported by the evidence that $\{110\}$ facets remained on the α-iron substrate after the layer of γ-iron had been dissolved away.

The abraded surface of polycrystalline mild steel did not show any formation of a γ-iron layer. The appreciable carbon content of the steel may have hindered the formation of the γ-phase from the α-phase.

The above results clearly show the complex nature of the deformation caused on a crystalline surface by abrasion, and have provided much evidence in the case of abrasion of iron crystals. More electron diffraction experiments are clearly desirable to clarify the nature of the process of abrasion still further.

Acknowledgements.

The author is most indebted to Dr.H.Wilman for his constant interest in the work and for many helpful discussions.

The author is also very grateful to Professor G.I.Finch, F.R.S., for his valued supervision during the early stages of this work, and for his many helpful suggestions.

Finally he wishes to thank Messrs C.C.Wakefield and Co., Ltd., for a scholarship during 1952-1953.

References.

Andrade, E.N.daC., and Hutching, P.J., Proc.Roy.Soc., A.152, 226, 1935.

Andrade, E.N.daC., and Roscoe, R., Proc.Phys. Soc., 49, 152, 1937.

Andrade, E.N.daC., and Tsien, L.C., Proc.Roy.Soc., A.163, 1, 1937.

Andrade, E.N.daC. and Chow, Y.S., Proc.Roy.Soc., A.175, 290, 1940.

Bakarian, P.W. and Mathewson, C.H., Trans.Amer.Inst.Min.Met.Eng. 152, 226, 1943.

Barrett, C.S., Trans.Amer.Inst.Min.Met.Eng., 135, 296, 1939.

Barrett, C.S., Ibid., 137, 128, 1940.

Barrett, C.S., "Cold Working of Metals", Cleveland, Ohio: Amer.Soc.Metals, p.65, 1949.

Barrett, C.S., "Structure of Metals", 2nd Ed., London:McGraw Hill 1953.

Barrett, C.S., Ansel, G. and Mehl, R.F., Trans.A.S.M., 25, 702, 1937.

Barrett, C.S. and Haller, C.T., Trans. A.I.M.E., 171, 246, 1947.

Barrett, C.S. and Levenson, L.H., Trans. A.I.M.E., 135, 327, 1939.

Barrett, C.S. and Levenson, L.H., Ibid., 137, 112, 1940.

Barrett, C.S. and Levenson, L.H., Ibid., 145, 281, 1941.

Benard, J. and Lacombe, P., Metaux et Corrosion, 21, 30, 1946.

Boas, W. and Schmid, E., Z.Physik, 71, 703, 1931.

Bowden, F.P. and Tabor, D., "The Friction and Lubrication of Solids" Oxford, Clarendon Press, 1950.

Bowles, J.S. and Barrett, C.S., Chapter I of Vol3 in Progress in Metal Physics (ed. by B.Chalmers) London: Pergamon Press. 1952.

Brick, R.M. and Williamson, M.A., Trans.A.I.M.E., 143, 84, 1941.

Brillantow, N.A. and Obreimow, I.W., Phys.Z.Sowjet. 6, 587, 1934

Brillantow, N.A. and Obreimow, I.W., Ibid., 12, 7, 1937.

Brown, A.F., Inst. of Metals Monograph and Report Series No.8, 103, 1950.

Buerger, M.J., Amer.Mineral., 15, 45, 174, 226, 1930.

Cahn, R.W., J.inst.Metals, 76, 121, 1949.

Cahn, R.W., J.Inst.Metals, 79, 129, 1951.

Cahn, R.W., Acta Crystallographica, 4, 470-1, 1951a.

Carapella, L.A. and Shaw, W.E., Trans.Amer.Soc.Met., 38, 1947.

Chen, N.K. and Maddin, R., J.Metals, 3, 937, 1951.

Clark, R., Craig, G.B. and Chalmers, B., Acta Crystallographica, 1950.

Collins, J.A. and Mathewson, C.H., Trans.A.I.M.E., 137, 150, 1940

Courtel, R., C.R.Acad.Sci. Paris, 226, 793-5, 1948.

Courtel, R., Ibid., 224, 2031-33, 1949

Courtel, R., Rev.met., 47, 700, 1950.

Courtel, R., Metaux et Corrosion, 25, 117, 1950; 145-55, 188-9, 1950.

Courtel, R., Proc.Roy.Soc., A.212, 459-62, 1952.

Crussard, C., Rev.met., 42, 286, 1945.

Crussard, C., Bull.Soc.Franc.Miner., 68, 174, 1949.

Czochralski, J., "Untwinning of Zinc Twins", Moderne Metallkunde, 1924.

Davidenkov, N.N., Kolesnikov, A.F. and Federov., K.V., J.exp. Phys., U.S.S.R., 3, 350-60, 1933.

Davisson and Germer, L.H., Phys.Rev., 30, 705, 1927.

Davisson, C.J., (mentioned by E.J.Armstrong in Bell.Sys.Tech.J. 25, 136, 1946.

Dorn,J.E. and Thomsen, E., Light Metal Age, 1, July, 1943.

Evans, D.M. and Wilman, H., Proc.Phys.Soc., A.63, 298, 1950

Evans, D.M., Layton, D.N. and Wilman, H., Proc.Roy.Soc., A.205, 17, 1951.

Exner, F., 'Untersuchungen uber die Harte an Kristallflachen' Preisschr. Akad.Wiss., Vienna, math-naturwiss.Kl. 1873.

Fahrenhost, W. and Schmid., Z.Phys., 78, 383, 1932.

Finch, G.I., Proc.Phys.Soc., B.63, 465, 1950.

Finch, G.I., Lewis, H.C. and Webbm D.P.D., Proc.Phys.Soc., B.66, 949, 1953.

Finch, G.I. and Wilman, H., Proc.Roy.Soc., A.115, 345, 1936.

Finch, G.I. and Wilman, H., Ergeb.exakt.Naturwiss., 16, 353, 1937.

Frank, F.C., Acta Metallurgica, 1, 15, 1953.

Frankenheim, M.L., 'De crystallorum cohaesions' Diss.inaug. Bratislava, 1829.

Franz, D.R., Pogg.Ann., 80, 37, 1850.

Friedel, G., Lecons de cristallographie. Paris: Berger-Levrault, 1926.

Gay, P., (Summarised proceedings of Confer. on high intensity X-ray beam, Lond., Phys.Soc. by A.E.De Barr and I.MacArthur in Brit.J.App.Phys., 1, 305-18, Dec. 1950.

Gay, P. and Hirsch, P.B., in Symposium on Properties of Metallic Surfaces, London, Institute of Metals, 1953.

Germer, L.H., Phys.Rev., 50, 659, 1936.

Goucher, F.S., Phil.Mag, 48, 229, 800, 1924.

Gough, H.J., Proc.Roy.Soc., A.118, 498, 1928.

Gough, H.J. and Cox, H.L., Proc.Roy.Soc., A.123, 1929.

Gough, H.J. and Cox, H.L., Ibid., A.127, 431, 1930.

Gough, H.J. and Cox, H.L., J.Inst.Met., 48, 227, 1932.

Grailich, J. and Pekarck, F., S-B.Akad.Wiss.Wein. math-naturwiss. Kl., 13, 410, 1854.

Greenland, K.M., Proc.Roy.Soc., A.163, 28, 1937.

Greninger, A.B., Trans.A.I.M.E., 117, 1935.

Greninger, A.B. and Troiano, A.R., Trans.A.I.M.E., 140, 307, 1940.

Guinier, A. and Tennevin, J., 'Progress in Metal Physics' Vol.2, London, Butterworth, 1950.

Hauy, R.J., 'Traite de mineralogie', Paris, 1801.

Heidenrich, R.D. and Shockley, W., 'Report of a conference on Strength of Solids' p.57, Physical Society, London. 1948.

Hess, J.B. and Barrett, C.S., Trans. A.I.M.E., 185, 599, 1949.

Hess, J.B. and Dietrich, R.L., Trans. A.I.M.E., 175, 564, 1948.

Honeycombe, R.W.K., Proc.Phys.Soc., A.63, 672, 1950a.

Honeycombe, R.W.K., Trans.A.I.M.E., 188, 1039, 1950b.

Honeycombe, R.W.K., J.Inst.Metals, 80, 45, 1951-2.

Jacquet, P.A., Metallurgist, p.39, June 30, 1939.

Jacquet, P.A., Metaux et Corrosion, 18, 1, 1943.

Jacquet, P.A., 2nd International Conf. on Electrodeposition, London: Electrodepositors Tech.Soc., 1947.

Jacquet, P.A. and Rocquet, P., C.R.Acad.Sci., Paris, 208, 1012, 1939.

Jannetax, P. and Goldberg, M., Z.Kristallogr., 28, 103, 1897.

Jillson, D.C., Trans.A.I.M.E., 188, 1009, 1950.

Joffe, A.F., 'The Physics of Crystals', New York, McGraw Hill, 1928.

Johnsen, A., Jahrb. Radioaktivitat u Elektronik, 11, 226, 1914.

King,R., Nature, 169, 543, 1952.

Kurdjumow, G. and Sachs, G., Z.Physik, 64, 325, 1930.

Kurdjumow, G. and Maksimova, O.P., Doklady Akademii Nank.U.S.S.R. 81, 565, 1951.

von Laue, M. and Riewe, K.H., Zeits.f.Krist., 95, 418, 1936.

Lippert, T.W., Iron Age, December, 23, 1940.

Maddin, R., Mathewson, C.H. and Hibbard, W.R., Jr., Trans. A.I.M.E., 175, 86, 1948.
T.P. 2676E., 1949a.
T.P. 2658E., 1949b.

Mark, H., Polanyi, M. and Schmid, E., Z.Physik, 12, 58, 1922.

Mason, W.P., McSkinin, H.J. and Shockley, W., Phys.Rev., 73, 1213 1948.

Mathewson, C.H., Trans.A.S.M., 32, 38, 1944.

Mehl, R.F., Barrett, C.S. and Smith, D.W., Trans.A.I.M.E., 105, 215, 1933.

Mehl, R.F. and Derge, G., Trans.A.I.M.E., 125, 482, 1937.

Merchant, M.E., Metal Progress, May, 1940.

Miller, R.F., Trans.A.I.M.E., 122, 176, 1936.

Mohs, F., 'Grundriss der Mineralogie', Dresden, 1822-24.

Mohs, F., 'Leichtflassliche Anfangsgrunde der Naturgeschichte des Mineralreichs', Vienna, 1832.

Mugge, O., Neues Jahrb.Mineral. Geol.Palaeont., 1, 71, 1898.

Nishiyama, Z., Sci.Rep.Tohoku Univ., 23, 638, 1934-5.

Orowan, E., Nature, 149, 643, 1942.

Orowan, E., 'Symposium on Internal Strains in Metals and Alloys' London: Inst. of Metals, p.47, 1947.

Osborne, F.F. and Adams, F.D., Econ.Geol., 26, 887, 1931.

Osmond, F. and Cartaud, G., Journ.Iron and Steel Inst., No.111, 1906.

Pfaff, F., S.B. Akad.Wiss., Munchen, 55, 1883.

Pfaff, F., S.B. Akad.Wiss., Munchen, 372, 1883.

Raether, H., Metaux et Corrosion, 22, 2, 1947.

Rees, A.L.G. and Spink, J.A., Acta Cryst., 3, No.4, 316, 1950.

Rosiwal, A., Anz. Akad.Wiss., Wien, Nr.12, 1893.

Rosiwal, A., Verh. geol.Reichsanst. Wien, 474, 1896.

Rosi, F.D. and Mathewson, G.H., J.Metals, 188, 1159, 1950.

Sachs, G., Z.Metallkunde, 24, 241, 1932.

Schmid, E. and Boas, W., 'Kristallplastizitat', Berlin:Springer, 1935.
English translation 'Plasticity of Crystals, London: Hughes.

Seebeck, A., Prufungs-Programm des Berliner Realgymnasiums, 1883.

Smith, G.V. and Mehl, R.F., Trans.A.I.M.E., 150, 211, 1942.

Taylor, G.I., Proc.Roy.Soc., A.118, 1, 1928.

Taylor, G.I. and Elam, C.F., Proc.Roy.Soc., A.112, 337-361,1926.

Tertsch, H., Z.Kristallogr., Mineral, Petrogr., Abt. A.89, 541, 1934.

Tertsch, H., Ibid., A.92, 39, 1935a.

Tertsch, H., Anz-Akad.Wiss., Wien, 17th Oct., 1935b.

Tertsch, H., Z.Kristallogr.Mineral, Petrogr., Abt. A.95, 296, 1936a.

Tertsch, H., Anz.Akad. Wiss. Wien, 15th Oct., 1936b.

Tertsch, H., Forsch.u.Fortschr., 12, 148, 1936c.

Tertsch, H., 'Die Festigkeitserscheinungen der Kristalle', Wien: Springer-Verlag. 1949.

Thomson, G.P., Nature 120, 802, 1927.

Tsien, L.C. and Chow, Y.S., Proc.Roy.Soc., A.163, 19, 1937.

Wassermann, G., Mitt.Kaiser-Wilhelm Inst. Eisenforsch., Dusseldorf, 17, 149, 1935.

Werner, A., Von der ausserlichen Kennzeichen der Fossilien, Leipzig, 1774.

Wernick, S., 'Electrolytic Polishing and Bright Plating of Metals', London: Alvin Redman., 1948.

Wilks, E.M., Phil.Mag., 43, 1140-45, 1952.

Wilman, H., Proc.Phys.Soc., 60, 341, 1948a.

Wilman, H., Ibid., 61, 416, 1948b.

Wilman, H., Nature, 165, 321, 1950.

Wilman, H., Proc.Phys.Soc., A.64, 329, 1951.

Wilman, H., Acta Crystall., 5, 782, 1952.

Yakoleva, E.S. and Yakutovich, M.V., J.exp.theor.Phys., U.S.S.R. 10, 1146-50, 1950.

Young, C.B.F. and Brytoznk, W.L., Metal.Fin., 40, 237-41, 306-12 1942.